Sea ice motion within the Beaufort Sea

By

Dave Babb

A Thesis submitted to the Faculty of Graduate Studies of

The University of Manitoba

In partial fulfilment of the requirements of the degree of

MASTER OF SCIENCE

Department of Environment and Geography

University of Manitoba

Winnipeg

ABSTRACT

Sea ice drift and associated forcing mechanisms within the Beaufort Sea are examined within the context of a mechanically weakening Arctic ice pack. Extensive *in situ* observations of ice drift, ice mass balance and surface winds are supplemented by remotely sensed and modeled data to analyse the forcing of sea ice motion. First we analyse the anomalous export of 13.4 x 10^3 km^2 of sea ice through the Bering Strait during winter 2011-2012. The event highlights a tendency towards increased ice transport through the Bering Strait since 2008 as a result of climate induced weakening of the arctic ice pack. Secondly, as part of the Beaufort Regional Environmental Assessment we analyse the seasonal evolution of ice drift in the Beaufort Sea during Spring as the ice pack transitions from mechanically strong conditions in late winter to weak summer conditions that foster free drift and thus increased ice drift speeds.

ACKNOWLEDGEMENTS

I would like to thank my supervisor Dr. David Barber and my graduate committee members, Drs. Tim Papakyriakou, Paul Cooley and Jennifer Lukovich for their support, contributions of knowledge and guidance in this research endeavour.

I would like to give special thanks to Drs. Ryan Galley and Matthew Asplin for their support, collaboration and friendship during this research endeavour.

I would like to thank the Captains and crew of the CCGS Amundsen for their support and expertise in the field. Thanks to the department of Aboriginal Affairs and Northern Development Canada and their Beaufort Regional Environmental Assessment (BREA) program.

I would also like to thank the following organizations for their financial support: the ArcticNet program of the Network of Centres of Excellence, the Arctic Science Partnership, the Northern Science Training Program and industrial partners at Imperial Oil Ltd. and BP.

To my friends, family and my partner Julie, I thank you for your constant encouragement and support throughout this endeavour.

"*Ancient peoples understood: when you kick Mother Earth, she kicks back. She does not roll over and submit to her own death*"

Thom Hartman

The Last Hours of Ancient Sunlight

DEDICATION

This thesis is dedicated to the memory of Dr. Klaus Hochheim, Cpt. Marc Thibault and Pilot Daniel Dubé who tragically passed away in September 2013 while conducting research in the Canadian Arctic. All three will forever be remembered for their passion and dedication to Arctic research.

TABLE OF CONTENTS

LIST OF TABLES

LIST OF FIGURES

LIST OF COPYRIGHTED MATERIAL

CHAPTER ONE: INTRODUCTION

This thesis presents a detailed analysis of ice drift and ice transport within the Beaufort Sea. Using a combination of *in situ*, satellite based and modeled data we analyse ice drift, ice transport and the forcing mechanisms of these processes.

1.1 Rationale and context

Arctic sea ice is a thin, porous plate that separates the ocean and atmosphere, and limits the exchange of energy, materials and momentum between the two mediums. Due to the exchange of momentum the ice pack remains in near constant motion and typically drifts at 2% of the speed and 30° to the right of surface winds [*Thorndike and Colony,* 1982]. Ice drift is further influenced by oceanic forcing, the Coriolis force and internal stresses within the ice pack. These factors dictate the large scale patterns of ice drift, the small scale variability of ice drift, the export of sea ice and the annual cycle in ice drift speeds. Under anthropogenic influences the Arctic has warmed, causing large scale reductions in the arctic ice pack and changes in the dynamic behavior of sea ice. These changes have manifested themselves through increased ice drift speeds [*Rampal et al.,* 2009; *Spreen et al.,* 2011; *Kwok et al.,* 2013], increased dynamic activity [*Rampal et al.,* 2009] and increased ice export [*Kwok et al.,* 2010; *Howell et al.,* 2013].

Understanding the effect of a warming arctic and deteriorating ice pack on the dynamic nature of sea ice is of significant interest to both the scientific and industrial communities. The economic development of offshore resources and transportation corridors through the Arctic, particularly the Canadian Arctic, has become increasingly feasible over recent years as the ice pack continues to decline and seasonally reveal known resource rich areas. This along with the Canadian government's support of industrial activity has spurred progress towards the development of offshore resources. Particularly in the Beaufort Sea where current estimates

predict there are 1.7 x 10^9 m^3 of recoverable oil resources and 1.6 x 10^{12} m^3 of marketable gas resources [BREA 2012]. Though the Beaufort ice pack has deteriorated considerably it continues to pose a serious threat to offshore activity [*Galley et al.,* 2013; *Barber et al.,* 2014]. Therefore a greater understanding of the Beaufort ice pack and its dynamic nature must be attained in order to minimize the potential risks.

1.2 Thesis Objectives

The overall purpose of this study is to improve the scientific communities understanding of ice drift and its related forcing mechanisms in the Beaufort Sea. Specifically how decadal changes to the Arctic ice pack influence ice transport and how ice drift responds to external forcing mechanisms during the spring transition from late winter to early summer sea ice conditions. Overall the objectives of my research are two-fold:

1) To analyze the export of multiyear sea ice through the Bering Strait during winter 2011-2012 and assess the forcing that caused this event. Subsequently, set the 34 year historical context of ice transport through the Bering Strait and the atmospheric forcing that drove this event.
2) To quantitatively analyze the seasonal evolution of ice drift and its response to external forcing mechanisms in the Beaufort Sea during the spring transition. Specifically highlighting how the dynamic nature changes as the ice pack transforms from a compact ice pack in late winter to a mechanically weak ice pack in early summer.

1.3 Thesis Outline

This thesis is composed of five chapters. The first chapter introduces the rationale and outline for the thesis. The second chapter provides a comprehensive literature review on the field of sea ice motion and sea ice dynamics.

Chapter three answers the first thesis objective and contains a manuscript published by Babb et al., [2013], entitled *Multiyear sea ice export through the Bering Strait during winter 2011-2012*, that has been published in the **Journal of Geophysical Research – Oceans**. This paper presents *in situ* observations of multiyear sea ice export through the Bering Strait as part of a larger export event during the winter of 2011-2012. Using 34 years of ice beacon data and satellite derived fields of ice motion we set the historical context of this event and show that this was a truly anomalous event that is reflective of changes in the Arctic that are fostering an increasingly mobile ice pack. Using *in situ* coastal based winds and re-analyzed fields of sea level pressure we describe the forcing mechanisms that drove this event and analyze these in the context of the past 34 years as well.

Chapter four answers the second thesis objective and contains a second manuscript written by Babb et al., [2014], entitled *The seasonal evolution of sea ice motion and forcing mechanisms in the Beaufort Sea*, which will be submitted to the **Journal of Geophysical Research – Oceans**. The paper uses a spatially and temporally coincident dataset of *in situ* ice drift, surface wind and ocean current observations to quantitatively analyze the seasonal evolution of ice motion and forcing mechanisms through the spring transition of the Beaufort ice pack. During spring the ice pack declines from a late winter consolidated ice pack to a mechanically weak ice pack during summer in which individual floes enter a state of free drift and become increasingly responsive to winds. This work was completed as part of the Canadian Government's Beaufort Regional Environmental Assessment (BREA) that used a multidisciplinary approach to provide background knowledge and baseline studies of the Beaufort Sea prior to the impending development of offshore activity in the area.

Conclusions and recommendations for future work on the subject of sea ice dynamics in the Beaufort Sea are presented in chapter five. Implications of this research for both scientific and industrial applications are also discussed.

Literature Cited

Barber, D.G., G.M. McCullough, D.G. Babb, A.S. Komarov, L.M. Candlish, J.V. Lukovich, M. Asplin, S. Prinsenberg, I . Dmitrenko and S. Rysgaard (2014), Climate change and ice hazards in the Beaufort Sea, *Elementa*, 2:000025, doi:10.12952/journal.elementa.000025.

Galley, R.J., B.G.T. Else, S.J. Prinsenberg, D. Babb, D.G. Barber (2013), Sea ice concentration, extent, age, motion and thickness in regions of proposed offshore oil and gas development near the Mackenzie Delta – Canadian Beaufort Sea, *Arctic*, 66(1), 105-116.

Howell, S.E.L, T. Wohlleben, M. Dabboor, C. Derksen, A. Komarov and L. Pizzolato (2013), Recent changes in the exchange of sea ice between the Arctic Ocean and the Canadian Arctic Archipelago, *J. Geophys. Research*, 118, 1-13, doi:10.1002/jgrc.20265.

Kwok, R., G. Spreen and S. Pang (2013), Arctic sea ice circulation and drift speed: Decadal trends and ocean currents, *J. Geophys. Res. Oceans*, 118, 2408-2452, doi: 10.1002/jgrc.20191.

Rampal, P., J. Weiss and D. Marsan (2009), Positive trend in the mean speed and deformation rate of arctic sea ice, 1979-2007, *J. Geophys. Research*, 114, C05013, doi: 10.1029/2008JC005066.

Spreen, G., R. Kwok and D. Menemenlis (2011), Trends in Arctic sea ice drift and role of wind forcing: 1992-2009, *Geophys. Res. Letters*, 38, L19501, doi: 10.1029/2011GL048970.

Thorndike, A.S. and R. Colony (1982), Sea Ice Motion in Response to Geostrophic Winds, *J. Geophys. Research*, 87(C8), 5845-5852.

CHAPTER TWO: BACKGROUND AND LITERATURE REVIEW

Norwegian explorer/scientist Fridtjof Nansen collected the first observations of ice drift when in 1893 he froze his ship, *Fram*, into the pack ice north of the East Siberian Islands and let her and her crew drift for several years in the Arctic ice pack [*Greve* 1994; *Weeks* 2010]. Nansen proposed that *Fram* would drift with the ice, under the influence of strong ocean currents, from the Eastern Arctic across the North Pole and towards the strait between Greenland and Svalbard that is now known as Fram Strait [*Greve* 1994]. Nansen developed his theory when the *Jeanette*, an American ship that unintentionally entered the ice pack north of Alaska was abandoned in 1879 and discovered in the ice pack near Greenland in 1884 [*Gordienko* 1958; *Greve* 1994; *Weeks* 2010]. Nansen's story is a remarkable one, and includes a last ditch effort to reach the North Pole on skis when it was determined *Fram* had reached a peak latitude of 86°N and was not going to drift across the pole. Between September 1893 when she entered the ice and August 1895, when Nansen and the *Fram* returned to Norway (separately), the crew collected various oceanographic and atmospheric data while collecting extensive observations on the sea ice [*Gordienko* 1958]. Specifically Nansen noted the strong relation between surface winds and the resulting ice motion which lead him to postulate that sea ice drifts at 2% of and 30 - 45° to the right of surface winds [*Nansen* 1902; *Thorndike and Colony 1982*]. *Gordienko* [1958] stated that Nansen's drift across the pole "opened a new epoch in polar oceanography".

2.1 Equation of motion

Sea ice motion is the realization of five forces acting on an ice floe. The exchange of momentum across the ocean-sea ice-atmosphere (OSA) system is represented by the following equation,

$$\mathrm{M}\, a = \tau_a + \tau_w + F_c + F_i + F_t \qquad (1)$$

where the ice floe mass (M) times the acceleration (a) is equal to the sum of the air drag (τ_a), water drag (τ_w), Coriolis force (F_c), internal ice stress (F_i) and the force due to sea surface tilt (F_t) [*Wadhams,* 2000]. A schematic of the external forcing from the wind (τ_a), ocean currents (τ_w), and internal stresses (σ; F_i in equation 1) on an ice floe is provided in Figure 2.1. Surface winds are the dominant forcing factor whereas ocean currents can either exert an accelerative or decelerative force [*Leppäranta,* 2005]. The Coriolis force is the result of the earth's rotation and deflects ice floes to the right of the surface wind direction. Internal stresses within the ice pack arise due to floe-floe interactions which oppose motion and dampen ice drift speeds. When internal stresses are absent sea ice enters a state of free drift, in which ice drift is controlled by the atmospheric, oceanic and Coriolis forces, with the latter creating inertial oscillations along the ice floes trajectory [*McPhee,* 1978]. *Leppäranta* [2005] defines three states of ice drift according to the level of internal stresses; free drift, drift in the presence of internal stresses and stationary ice, with the latter representing a compact, mechanically strong ice pack in which internal forces oppose all external forcing. The sea surface height force arises due to horizontal gradients in sea surface height, however this term is negligible on short time scales [*Hibler and Tucker* 1979; *Thorndike and Colony*, 1982; *Wadhams*, 2000].

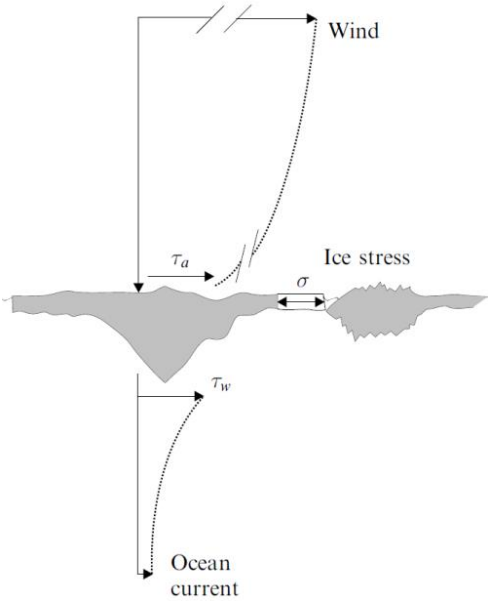

Figure 2.1: Schematic of air stress (t_a) from winds, water stress (t_w) from ocean currents and internal ice stress (o). From Leppäranta 2005.

2.1.1 Air drag

Air stress is one of the most important OSA interactions that occur in high latitude marine environments, affecting ice drift, upper ocean currents, sea surface tilt and physical characteristics of the ice pack [*Guest et al*., 1995]. The transfer of momentum across the atmosphere-sea ice interface is dependent on surface roughness, which is represented by a surface drag coefficient (C_a) that represents both the skin drag (small scale roughness) and form drag (large scale roughness; e.g. ridges) [*Wadhams,* 2000; *Leppäranta,* 2005]. Air stress (τ_a) (Figure 2.1) is defined as:

$$\tau_a = \rho_a C_a |U_a - U_i| (U_a - U_i) \quad (2)$$

where ρ_a is the air density, C_a is the drag coefficient, U_a is the wind velocity measured at the anemometer height (10m) and U_i is the velocity of the ice surface. *In situ* winds must be corrected for ice motion so the stress is determined from the relative wind [*Wadhams,* 2000]. C_a is dependent on age and the deformation state of the ice pack, which determines the roughness of both large scale and small scale surface features [*Guest and Davidson,* 1991]. Large scale features such as ridges, which range in size on the scale of meters and in length on the scale of kilometers, comprise the form drag of a surface and increase C_a as the size and frequency of ridges increases [*Wadhams,* 2000]. Large ridges are referred to as 'sails', as they increase momentum transfer from surface winds to sea ice. Small-scale features are analyzed on scales of millimeters and meters, and comprise the skin friction drag over undeformed sea ice [*Wadhams,* 2000]. The unitless C_a varies between 8.0×10^{-3} for rough multiyear ice (MYI) and 0.7×10^{-3} for grease ice (thin frazil ice), but is generally parameterized between 1.4 to 2.1 $\times 10^{-3}$ [Wadhams, 2000]. The C_a of MYI is greater than that of first year ice (FYI) which itself is greater than young ice types (grease, nilas and pancake) which dampen surface waves and therefore have a lower C_a than open water [*Wadhams,* 2000]. Seasonally C_a increases as the ice pack breaks up

through spring, thereby exposing sides of ice floes that increase the form drag of the ice floe as well as the skin drag by increasing turbulence within the near surface wind field [*Wadhams,* 2000]. C_a is dependent on ice concentration, with a maximum value at 80% ice concentration [*Anderson,* 1987]. Traditionally C_a is determined by measuring the shape of the atmospheric boundary layer with several anemometers deployed at different heights on a mast on an ice floe [*Leppäranta,* 2005]. Alternatively measurements of air stress over sea ice have also been collected from ships [*Andreas et al*., 1984; 1993], aircraft [*Overland,* 1985], buoys [*Reynolds et al.,* 1985] and drift stations [*Overland and Colony,* 1994].

A general rule of thumb for sea ice drift in the northern hemisphere is what is known as the 'Nansen-Ekman ice drift law' [*Nansen* 1902] which states that ice drifts at 2% of the surface wind speed with a turning angle of 30° – 45° to the right of the surface winds [*Thorndike and Colony* 1982; *Colony and Thorndike,* 1984, *Wadhams* 2000; *Rigor et al.,* 2002]. Sea ice drift can also be described by the 'isobaric drift law' which states that sea ice drifts with a speed of 1% of and 5° to the right of geostrophic winds along sea level pressure contours (isobars) [*Zubov,* 1945; *Thorndike and Colony,* 1982; e.g. *Kwok,* 1998; *Rigor et al.,* 2002; *Vihma et al.,* 2012]. Periods when ice drift varies from the isobars or surface winds are ascribed to either the increased role of ocean currents [*Rigor et al.,* 2002] or a local increase of internal stress in a compact ice field [*Kimura and Wakatsuchi,* 2000; *Vihma et al.,* 2012]. A good example of this is along the western coast of the Canadian Arctic Archipelago where variability in sea ice drift is ascribed to internal stresses which are greatest in this region of the Arctic [*Bourke and Garrett,* 1987; *Melling,* 2002].

Thorndike and Colony [1982] describe the relationship between ice velocity (u) and geostrophic winds (G) with equation 3,

$$u = AG + c + \varepsilon \quad (3)$$

where A is a complex constant that represents the linear response of the ice velocity to geostrophic winds, c is the long term constant part of the ice velocity that is attributed to currents and internal ice stress, and ε represents the portion of ice velocity which is due to the variability in currents and internal stresses that are neither constant nor a linear function of the geostrophic winds [*Thorndike and Colony*, 1982; *Thomas* 1999]. A is a complex coefficient that involves a scaling factor ($|A|$) and turning angle (θ) which is represented by the following equation,

$$A = |A|e^{-i\theta} \quad (4)$$

positive θ indicates ice drift to the right of the direction of surface winds, whereas negative θ indicates ice drift to the left of winds. Using ice drift and sea level pressure (SLP) data from ice beacons *Thorndike and Colony* [1982] determined that overall $|A| = 0.008$ θ = 8° and that the geostrophic winds explained 70% of the variability in ice velocity. This means that ice drifted at 0.8% of the speed and 8° to the right of geostrophic winds. *Thorndike and Colony* [1982] note a high degree of seasonal variability in both $|A|$ and θ with typical values of 0.0077 and 5° during winter and spring, 0.0105 and 18° during summer and 0.0080 and 6° during fall. This represents a summer increase of 35% in $|A|$ and 6° in θ which they attribute to a seasonal decrease in internal stresses within the ice pack. *Thomas* [1999] used 15 years of ice beacon data to show that both $|A|$ and θ peaked during August and September (0.011 and 18°) and declined through fall and winter to annual minimums in February and March (0.007 and 0°).

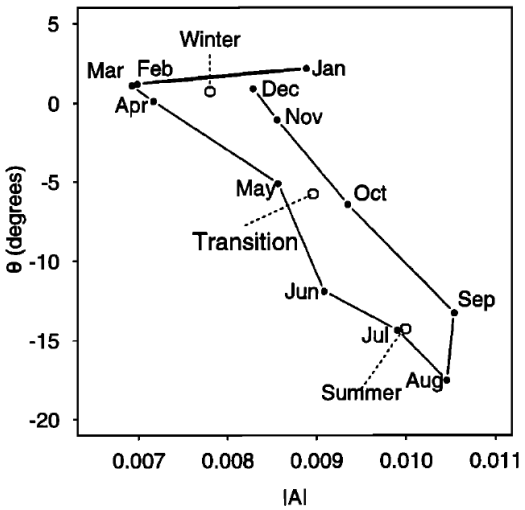

Figure 2.2: The seasonality of $|A|$ versus θ, (used with permission from Thomas [1999])

Kwok et al., [2013] expanded on this analysis using passive microwave derived fields of ice motion and SLP fields from the National Center for Environmental Prediction (NCEP) reanalysis, and found a summer increase of 10% in $|A|$ and 9° in θ. The seasonality of $|A|$ and θ is presented in Figure 2.2 where ice drift between November and April is clearly different from ice drift June and September, with two transitional months of May and October. Note that in Figure 2.2 that *Thomas* [1999] uses the opposite sign convention for turning angles. The seasonality of $|A|$ and its relation to internal stresses was further confirmed by *Steele et al.*, [1997] and *Kimura and Wakatsuchi* [2000]. *Thorndike and Colony* [1982] found no evidence of spatial variability in $|A|$, though this is attributed to their limited dataset of preliminary ice beacon data and a few drift studies. More recent studies, using enhanced datasets have proven that $|A|$ is subject to a high degree of spatial variability that is inherently related to internal stresses [*Steele et al.*, 1997; *Kimura and Wakatsuchi*, 2000; *Kwok et al.*, 2013]. $|A|$ is lower (0.008) near the north coast of Ellesmere Island and Greenland where internal stresses are greatest [*Bourke and Garrett*, 1987; *Melling*, 2002] and higher (0.020) in peripheral seas (e.g. Bering, Okhotsk and Barents Seas) where internal stresses are reduced [*Kimura and Wakatsuchi*, 2000]. *Thomas* [1999] notes that even if each ice floe responds 100% linearly to the winds, differences in mass, surface roughness and

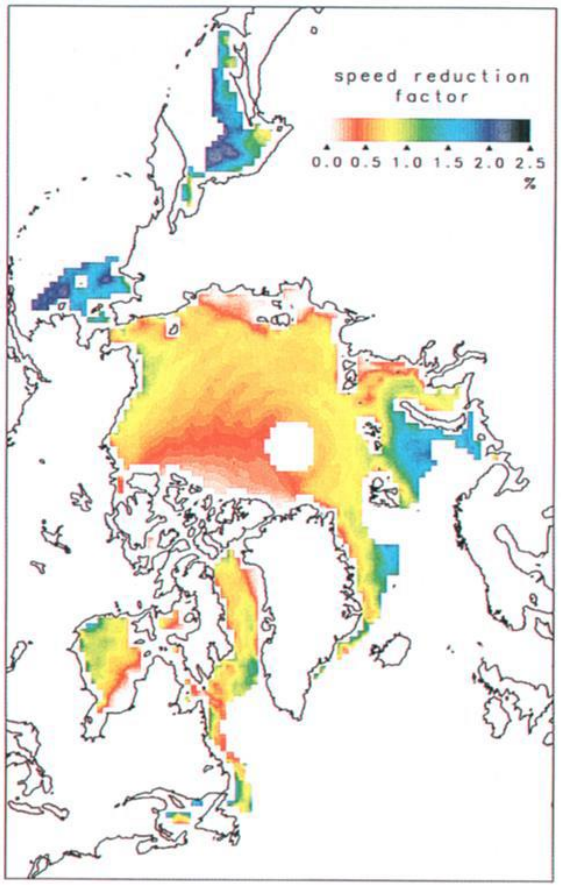

Figure 2.3: Spatial distribution of the speed reduction factor (used with permission from Kimura and Wakatsuchi, 2000).

currents will cause each floe to drift differently and this is what gives rise to differential motion within the ice pack.

2.1.2 Water drag

Water stress occurs across the ocean-sea ice boundary on the underside of an ice floe. Just like air stress, the transfer of momentum across the ocean-ice boundary is represented by a drag coefficient (C_w) which is highly dependent on surface roughness and required to calculate the water stress (τ_w) (Figure 2.1) using the following equation:

$$\tau_w = \rho_w C_w |U_w - U_i| (U_w - U_i) \quad (7)$$

where ρ_w is the water density, C_w is the drag coefficient, U_w is the water velocity measured 1-2m below the sea ice (e.g. *McPhee* 1979, *Wadhams* 2000) and U_i is the velocity of the ice surface. *McPhee* [1979] and *Reynolds et al.,* [1985] determined that $C_w = 0.0054$, though many dynamic models (e.g. *Hibler* 1979, *Koberle and Gerdes* 2003, *Yang* 2009) use $C_w = 0.0055$. There is great spatial and temporal variability in the C_w term according to surface roughness, ice type and season [*McPhee* 1979; *Wadhams* 2000]. *Wadhams* [2000] states that form drag, from sails and keels is a greater component of C_w than of C_a due to the height/depth of these features relative to the overall thickness of the atmospheric and oceanic boundary layer. Directly below the ice is a strong shear zone in which the top few meters of water moves with the ice. Below this layer, stress is transmitted down through the layers of the water column as the Coriolis force causes each subsequent layer further to the right. This layer is called the Ekman layer and through a process called Ekman pumping drives the accumulation of freshwater within the Beaufort Gyre [*Yang,* 2009; *Giles et al.,* 2012].

Seasonally C_w decreases as melt water increases the density stratification of the oceanic boundary layer which reduces vertical momentum transfer and reduces drag by creating ‘slippery

ice' [*McPhee,* 1979; *Wadhams,* 2000]. Theoretically the seasonal decline of C_w is compounded by the preferential melt of keels by the turbulent ocean heat flux [*Wadhams,* 1992; S*chramm et al.,* 2000] which reduces the form drag of the ice pack.

2.1.3 Internal stresses

Internal stresses within the ice pack arise due to floe-floe interactions which oppose motion and dampen ice drift speeds. Internal stresses are dependent on the local ice state, which is a reflection of the concentration and thickness of the local ice pack [*Hibler,* 1979]. Given that internal stresses oppose ice drift, there is an inverse relationship between ice drift speeds and the ice state that is fostered by internal stresses. This relationship explains the annual cycle in ice drift speeds that is characterized by a maximum during the annual September sea ice minimum, and a minimum during the March/April sea ice maximum [*Rampal et al.,* 2009; *Spreen et al.,* 2011]. This relationship has also fostered positive multi-decadal trends in ice drift speeds as a result of negative multi-decadal trends in the mechanical strength of the Arctic ice pack [*Spreen et al.,* 2009; *Kwok et al.,* 2013]. *Kwok et al.* [2013] state that 90% of the Arctic Ocean has positive trends in ice drift speeds and negative trends in multiyear sea ice coverage. The authors ascribe increasing ice drift speeds to the transition towards a younger ice pack that is inherently thinner and weaker, making it increasingly responsive to atmospheric forcing. *Zhang et al.,* [2012] compared model runs from 1979-2006 to 2007-2011 and found a 33% reduction in sea ice volume that resulted in a 37% decline in ice mechanical strength and 31% decline in internal stresses. These reductions fostered a 13% increase in ice drift speeds.

When internal stresses are absent sea ice enters a state of free drift, in which ice drift is controlled by the atmospheric, oceanic and Coriolis forces, with the latter creating inertial oscillations along the ice floes trajectory [*McPhee,* 1978]. *Leppäranta* [2005] defines three states

of ice drift according to increasing levels of internal stress; free drift, drift in the presence of internal stresses and stationary ice. The latter indicates a compact, mechanically strong ice pack in which internal forces oppose all external forcing and lock up the ice pack [*Steele et al.*, 1997].

2.1.4 The Coriolis force

The Coriolis force arises due to the rotation of the earth and acts on every body of mass on the earth's surface. The force is negligible on the human scale but is important in terms of ice drift, surface winds and ocean currents [*Wadhams*, 2000]. In the northern hemisphere the force acts 90° to the right of the direction of motion, conversely the force acts 90° to the left in the southern hemisphere. The magnitude of the Coriolis force (F_c) is given by:

$$F_c = 2\, m\, \omega\, U_i \sin\phi \qquad (8)$$

where m is the mass of the body, ω is the angular velocity of Earth (ω = 7.272 x 10^{-5} rad s^{-1}), U_i is the ice velocity and ϕ is the latitude. The Coriolis force is greatest near the poles and zero at the equator. Because the force is dependent on mass the Coriolis force is much more important for the motion of heavier bodies such as icebergs and ice islands than for the motion of relatively thin sea ice floes [*Wadhams* 2000]. The Coriolis force may be dampened by internal stresses within the ice pack, but when an ice floe enters a state of free drift the Coriolis force gives rise to inertial oscillations along the trajectory of ice drift [*Wadhams*, 2000; *Gimbert et al.*, 2012].

2.1.5 Sea surface height

The stress due to sea surface tilt arises because the sea surface does not always correspond directly to the geoid. The geoid is defined as the idealized surface over which the gravitational potential is constant. Variations in sea surface height can be caused geologically by the distribution of ocean and continental crust and mid-ocean ridges, or atmospherically by uneven heating, evaporation and precipitation processes [*Wadhams* 2000]. Under these forces water

tends to pile up in some places and be depressed in other areas, collectively these create a horizontal gradient of sea surface height which drives circulation and ice drift from high to low. However, observations and models have shown this value to be insignificant in ice motion on the scale of days [*Hibler and Tucker* 1979; *Thorndike and Colony*, 1982], but more important on time scales of months [*Wadhams* 2000].

2.1.6 Free drift conditions

Free drift is defined as the drift of an ice floe in the absence of internal stresses, in which the ice drifts under the influence of atmospheric, oceanic and Coriolis forces [*Leppäranta*, 2005]. *McPhee* [1978] coined the term when he noted a change in drift conditions for individual, separate ice floes or ice fields with low compactness, less than 0.8. Free drift conditions can be identified by ice drift at the inertial frequency, which is typically opposed and dampened by internal stresses [*McPhee,* 1978; *Gimbert et al.,* 2012]. Therefore inertial oscillations along the trajectory of an ice floe reveal free drift conditions. Free drift occurs seasonally during the summer and is spatially restricted to marginal ice zones or areas of reduced (< 0.8) ice concentrations [*Gimbert et al.,* 2012]. *Geiger and Perovich* [2008] observed an increase in inertial motion during the spring breakup of the Antarctic ice pack. In response to the multi-decadal mechanical weakening of the Arctic ice pack, *Gimbert et al.,* [2012] found an increase in the magnitude of inertial oscillations that reveals an increasingly dynamic and mobile Arctic ice pack.

Wadhams [2000] visually presents inertial oscillations of an idealized ice floe with no water stress (Figure 2.4A) and with water stress (Figure 2.4B). The idealized floe in Figure 2.4A is under the influence of a northerly wind and the Coriolis force (F_c). From its initial position (‘0’) the floe accelerates from rest, as it accelerates F_c begins to act 90° to the right of its

heading, thereby causing the ice floe to turn to the right. So long as the floe retains a velocity component parallel to the wind it will continue to accelerate, which causes F_c to increase as well. Eventually the floe will reach the '2/4' position of its inertial oscillation and experience equal and opposite forces from the wind and F_c at which point the floe will slow down but continue to drift under its own momentum and come to rest exactly due east of its initial location. At this point the floe has completed one inertial oscillation with a time equal to its inertial period. The inertial period is dependent on latitude and ranges from 12 hours at the poles to infinity at the equator where F_c is equal to zero.

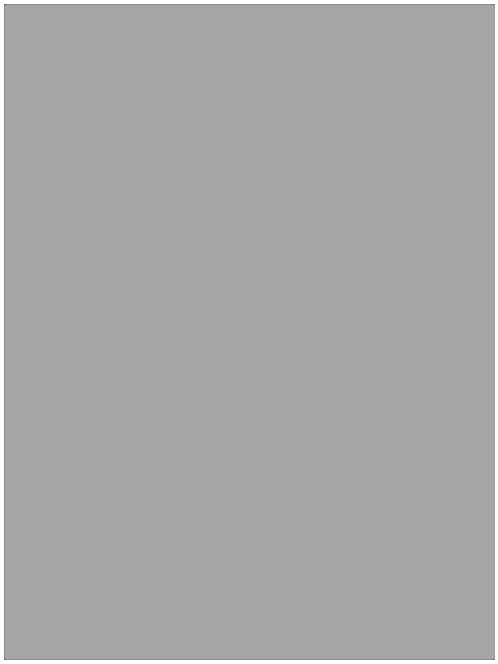

Figure 2.4: A) Idealized drift of an ice floe through an inertial oscillation, under the force of surface wind and the Coriolis force. B) Same settings with a water stress term applied to the ice floe. From Wadhams (2000) Figure 4.1.

In Figure 2.4B the same idealized floe is forced by the same northerly wind, except now the ice floe is subject to water stress which opposes motion. With a resistive force the ice floe slows faster than in the previous example, causing it to come to rest quicker and therefore complete a shortened inertial oscillation. The net trajectory of the floe will be 45° to the right though inertial oscillations will continue until the forces come to equilibrium and oscillations disappear. In the natural system forces are not steady, so equilibrium is rarely if ever achieved and inertial oscillations will persist so long as the internal stresses remain absent.

2.2 Methods of observing ice drift

Historically observations of ice motion were difficult to obtain as they could only be collected by drifting ships and ice camps, both of which lacked sufficient spatial and temporal

resolution [*Colony and Thorndike* 1980; *Fowler et al.,* 2013; *Comiso,* 2010]. Early methods provided preliminary, rough maps of mean ice circulation [*Nansen,* 1902; *Gordienko,* 1958; *Colony and Thorndike,* 1984], and began to unveil the complexity in small scale ice drift and its high degree of variability [*Colony and Thorndike,* 1980]. This section will outline the two ways that ice drift is currently observed by: ice beacons (2.2.1), spaceborne platforms (2.2.2). An important note is on the frame of reference of each dataset. Ice beacons look at the fluid motion of a particle (ice floe) through space and time in a lagrangian frame of reference. Alternatively other methods look at the fluid motion of particles (ice floes) through a particular space over time in a eularian frame of reference.

2.2.1 Ice Beacons

Ice beacons are comprised of GPS and Satellite antennae, a battery pack, modem and processor; all of which is enclosed within a weather/waterproof case. Ice beacons are deployed in a 12” deep auger hole (diameter 8”) on ice floes and rely on satellite based communication to transmit their location and any peripheral information (e.g. air pressure, air temperature) back to the user. The frequency of transmissions is variable and can be defined by the user, though it does affect the power consumption which limits the lifespan of the unit. High frequency data (e.g. 15 minutes – 1 hour) is necessary for capturing the small scale variability of ice motion and tracking inertial oscillations, whereas low frequency data (e.g. 6 hours) may provide a longer record that is useful for tracking large scale patterns of sea ice drift over long temporal scales. Frequency should be defined according to the objectives of the dataset.

Ice beacons have been in use since the 1970’s when the autonomous ice beacon was developed [Colony and Thorndike, 1980]. The development of the ice beacon tracking system led to the creation of the International Arctic Buoy Program (IABP), run out of the University of

Washington. The IABP is mandated "to maintain a network of drifting buoys in the Arctic Ocean to provide meteorological and oceanographic data for real-time operational requirements and research purposes including support to the World Climate Research Programme and the World Weather Watch Programme" (IABP website). The first map of Arctic ice drift from the IABP 1980 annual report is presented in Figure 2.5. In this map we see several characteristics of large scale patterns of Arctic ice drift such as the Beaufort Gyre and the Transpolar Drift Stream. To this day the IABP continues to coordinate beacon deployments throughout the Arctic and maintains an historic ice beacon dataset (1979-present) which is freely available through their website (http://iabp.apl.washington.edu/).

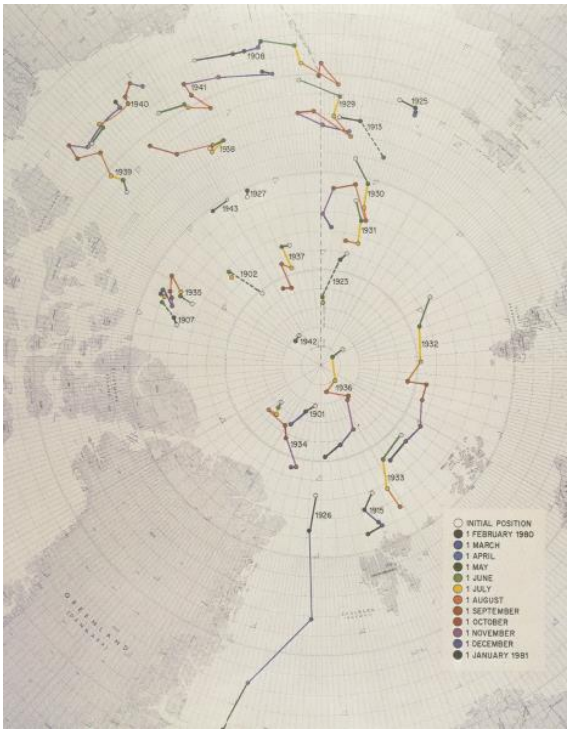

Figure 2.5: IABP map of arctic ice drift in 1980.

2.2.2 Satellite based methods

The study of ice motion was revolutionized with the advent of polar orbiting satellites which provided regular coverage of the polar regions and provided new opportunities to estimate sea ice motion [*Fowler et al*., 2001; *Comiso* 2010]. Using satellite based sensors, a series of visible, infra-red or radar images could be used to track ice floes and determine their displacement between image pairs [*Emery et al.,* 1991]. Manual ice tracking between two sequential images was performed at first [e.g. *Laviolette and Hubertz,* 1975] and proved useful but the process was labor intensive, subject to interpretation errors and was highly subjective [*Emery et al*., 1991]. An automated technique for calculating ice motion from sequential images

in the visible spectrum from the Advanced Very High Resolution Radiometer (AVHRR) was developed by *Ninnis et al.,* (1986). The technique expanded on previous work on tracking clouds in satellite imagery [*Leese et al*., 1971], and provided 'reasonable' maps of sea ice motion for the Beaufort Sea region [*Ninnis et al.,* 1986]. However images in the visible spectrum were obscured by cloud cover and limited by light conditions, which is critical in the Arctic, therefore subsequent studies applied this technique to radar image pairs [*Fily and Rothrock* 1987; *Vesecky et al.,* 1988; *Collins and Emery*, 1988]. Radar data collected from spaceborne synthetic aperture radar (SAR) sensors provided increased spatial resolution (10 to 100m), were not affected by cloud cover and were not limited by light conditions; making the SAR approach much more feasible. *Kwok et al.,* [1990] developed an operational system of extracting ice motion from SAR imagery at the Alaska SAR facility at the University of Alaska Fairbanks using the European ERS-1, Japanese ERS-1 and Canadian Radarsat sensors. This system, now known as the Radarsat Geophysical Processor System (RGPS) is still in use to this day and provides high resolution information on sea ice drift and deformation [e.g. *Kwok et al.,* 2008; *Kwok and Cunningham,* 2012]. SAR derived ice motion fields had proven useful for small scale local phenomena but impractical for large, basin scale ice drift [*Liu and Cavalieri* 1998]. This issue was resolved in the late 1990's when a process for extracting daily pan arctic fields of ice motion from spaceborne passive microwave sensors, in operation since 1978, was developed [*Liu and Cavalieri*, 1998; *Fowler et al.,* 2001]. Using archived data from the Scanning Multi-channel Microwave Radiometer (SMMR) (1978 to 1987) and the Special Sensor Microwave Imager (SSM/I) (1987 to present) a 34+ year record of daily sea ice motion vectors with 25 km resolution is available from the NSIDC [*Fowler et al.,* 2013; NSIDC online FTP]. *Liu and Cavalieri* [1998] note that passive microwave sensors, even with a coarser resolution of 12.5km,

could still track the opening and closing of leads, track large ice floes, observe polynyas and large flaw leads in the Laptev and East Siberian Seas.

2.2.2.1 Active microwave

Spaceborne Synthetic Aperture Radar (SAR) is a powerful research tool that captures the radar backscatter of surface and near surface features irrespective of weather and light conditions. SAR captures high resolution imagery by exploiting the along track motion of the sensor and using range and doppler shift of multiple return pulses to synthesize a large antenna and increase the spatial resolution to metres or tens of metres [*Massom,* 2009]. SAR data has several applications in the polar regions, including, ice type classification, discrimination of leads and polynyas, lead opening and closing, ice motion, ice deformation, ice surface roughness, landfast ice extent, wave-ice interactions, seasonal melt/freezeup detection, detailed ice edge characterisation, wind speed and direction, and ice berg and ice island detection and tracking [*Massom,* 2009]. *Massom* [2009] described SAR as "the most suitable and preferred sensor for regional sea ice mapping and monitoring". The advantages of SAR are its high spatial resolution, variable swath width, all weather capabilities, operation regardless of light conditions, increased available detail through different polarization modes, its continuous record in the C-band since 1991 and with newer systems the steerable beam allows for more frequent image acquisition over a region of interest [*Massom,* 2009]. A limitation of SAR is its low repeat coverage time, generally on the order of 24 hours which makes sub daily variability impossible to identify. Though this issue may soon be resolved by the proposed European Space Agency's Sentinel constellation [*Berger and Asbacher,* 2012] and the Canadian Space Agency's Radarsat constellation mission [*Flett et al.,* 2009] that will provide sub daily coverage and thus sub daily fields of ice motion. In a paper outlining preliminary objectives of the Sentinel constellation,

Malenovsky et al., [2012] outlined sea ice motion as a 'high importance – top priority' variable which the Sentinel SAR sensors will be used to study.

The specific use of SAR for detecting ice motion in the polar regions was developed in the 1980's using SAR data collected during the short, 106 day, Seasat mission [e.g. *Hall and Rothrock,* 1981; *Leberl et al.,* 1983; *Currlander et al.,* 1985; *Carsey & Holt,* 1987]. These early studies relied on manual feature matching between image pairs which was labour intensive and subject to interpretation errors. *Hall and Rothrock* [1981] were able to observe one ice displacement vector every 7.89 km^2, though no vectors could be retrieved from several large expanses of featureless ice. Subsequently, digital image processing replaced film processing and *Curlander et al.,* [1985] extract one displacement vector every 3.4 km^2, and reduced processing time for an image pair down to 10 hours. *Leberl et al*., [1983] concluded that "sequential satellite SAR sea ice mapping is the best way to measure mesoscale ice motion and deformation in polar regions".

The limited Seasat dataset proved the feasibility of ice tracking with spaceborne SAR platforms, but the methods were labour intensive and remained subject to human interpretation errors. Subsequently automated tracking techniques were developed that provided faster image analysis, made the process repeatable, could handle the increasing availability of SAR data and removed human interpretation errors [*Massom,* 2009]. NASA developed the Geophysical Processor System (GPS) which ran an automated ice tracking algorithm that used both feature based and area based feature tracking methods to provide a uniformly sampled grid (3-5 km resolution) for image pairs [*Kwok et al.,* 1990]. With the launch of Radarsat in 1996 a new Radarsat GPS (RGPS) was developed which took advantage of lower repeat coverage times and increased swath widths [*Kwok,* 1998]. Radarsat provided complete coverage of the Arctic in 72

hours and would do so every week allowing weekly fields of important sea ice properties to be available [*Kwok et al.,* 2008]. The use of pan-Arctic fields of a particular variable made the RGPS much more effective than the single snap shot products (100 km^2) that the former GPS provided. The RGPS monitored five key sea ice parameters, 1) sea ice motion, 2) ice age/thickness, 3) date of melt onset/freeze-up, 4) open water fraction and 5) histograms of backscatter [*Kwok,* 1998]. In terms of sea ice motion the RGPS used the same hybrid feature and area tracking system used in the former GPS. The main difference between the GPS and RGPS ice tracking systems was based on the repeat coverage times afforded by the new Radarsat sensor. This allowed the RGPS to track the same features for extended periods of time which provides a beacon-like dataset in the Lagrangian frame of reference.

The ice motion data products available from both the GPS and RGPS systems have proven to be very useful in the Arctic. The data sets have been utilised in studies of sea ice deformation [*Lindsay,* 2002], relating ice dynamics to *in situ* measurements of internal ice stresses [*Richter-Menge et al.,* 2002], quantifying the spatial hierarchy of sea ice dynamics between multifloe scales (2-10 km) and the aggregate scale (10-75 km) [*McNutt and Overland* 2003] and quantifying the seasonal evolution of spatial scaling on sea ice dynamics [*Stern and Lindsay,* 2009]. Dr. R. Kwok, as one of the developers of the GPS and RGPS systems [*Kwok* 1990; *Kwok* 1998], has been heavily involved in the implementation of its data. Specifically on work dealing with sea ice deformation [*Kwok et al.,* 2003; *Kwok,* 2006b; *Kwok and Cunningham,* 2012], export [*Kwok et al.,* 2004; *Kwok,* 2005; *Kwok,* 2006a; *Kwok et al.,* 2010] and MYI coverage [*Kwok,* 2004]. *Kwok et al.,* [2008] used RGPS ice motion datasets to validate ice drift within dynamic sea ice models. The authors state "In contrast to buoy drift, the density and extent of

the RGPS coverage allows a more extensive assessment and understanding of model simulations at spatial scales from ~10km to near basin scales and from days to seasonal timescales."

The RGPS system continues to operate on Radarsat-1 data, however new ice tracking methods have been developed for Radarsat-2, which was launched in 2007. Radarsat-2 has a cross polarization mode, which *Komarov and Barber* [2012] found to significantly improve the accuracy and effectiveness of SAR based ice tracking algorithms.

The ultimate goal of spaceborne SAR ice tracking methods is to provide an operational system in which ice motion fields and the drift of extreme ice features can be relayed to vessels operating in the area. An operational system is of interest and possibly of necessity for companies looking to develop offshore resources and maritime shipping corridors through the Arctic, specifically the Canadian Arctic. A current limitation to ice tracking systems is the lack of frequent imagery which can be used to discern sub daily motion fields. Current spaceborne SAR platforms provide daily fields of ice motion (e.g. *Komarov and Barber* 2012), but with the European Space Agency's Sentinel constellation [*Berger and Asbacher,* 2012] and the Canadian Space Agency's Radarsat Constellation Mission [*Flett et al.,* 2009] coming to fruition, the possibility of regular sub daily ice motion fields may become a reality in the not so distant future.

2.2.2.2 Passive microwave

Spaceborne passive microwave radiometers are heavily relied upon in the polar regions due to their long temporal scale (continuous since 1978), high repeat coverage (daily fields available), ability to see through clouds and their ability to operate in the dark. Satellite based radiometers are integral for monitoring sea ice concentration, extent, type and large scale drift [*Massom,* 2009]. Presently the SSM/I and Advanced Microwave Scanning Radiometer EOS 2 (AMSR-E2) are operating, with the latter acting as a replacement for AMSR-E which failed

unexpectedly in October 2011. Passive microwave radiometers measure the thermal emission of electromagnetic radiation in the range of millimetre to centimetre wavelengths from the surface [*Massom,* 2009]. This range is characterized by a strong difference between the emissivity of FYI, MYI and open water as well as large variation between horizontal and vertical polarizations [*Massom,* 2009].

The 85GHz and 37GHz channels of the SSM/I sensors and the 35 GHz channel of its predecessor SMMR, are used to derive sea ice motion [e.g. *Liu and Cavalieri,* 1998; *Emery et al.,* 1997; *Martin and Augstein,* 2000; *Fowler et al.,* 2001; *Fowler et al.,* 2013]. Other studies have used AMSR-E and its 18GHz channel to measure sea ice motion [*Kwok,* 2008] but since AMSR-E failed those records have been relying on SSM/I derived ice motion vectors. Inherent to passive microwave sensors is low spatial resolution (12.5km-25km) which is attributed to the sensors large swath widths which affords daily coverage of the polar regions.

The National Snow and Ice Data Center (NSIDC) provides the Polar Pathfinder 25km EASE grid ice motion dataset that uses spaceborne passive microwave sensors and ice beacons to provide daily ice motion fields from 1978 to present for both polar regions (available online at http://nsidc.org/data/docs/daac/nsidc0116_icemotion.gd.html) [*Fowler,* 2013]. The dataset uses an automated procedure of spatial autocorrelation that calculates ice motion vectors from passive microwave data from the Advanced Very High Resolution Radiometer (AVHRR), Special Sensor Microwave/Imager (SSM/I) and Scanning Multichannel Microwave Radiometer (SMMR) [*Fowler,* 2013]. After this, ice motion fields from the passive microwave sensors are integrated with the ice motion fields from the IABP through an optimal interpolation procedure described in the metadata (available online http://nsidc.org/data/docs/daac/nsidc 0116_icemotion /gridded.html).

2.3. Pan Arctic patterns of ice drift

Ice drift within the Arctic Ocean is highly variable on intervals of days and over small spatial scales, while over longer intervals and larger spatial scales it is well defined with a characteristic mean field of motion. Two predominant features of the mean field of motion are the Beaufort Gyre (BG) and the Transpolar Drift Stream (TDS). The BG is an anticyclonic circulation pattern centered in the Canada Basin that transports ice throughout the western Arctic. The TDS is a near linear feature that transports ice from the Eastern Arctic across the North Pole towards Fram Strait where the ice is exported from the Arctic into the North Atlantic. Within the mean field of motion exists an area of convergent ice motion along the north coast of Greenland and the Canadian Arctic Archipelago (CAA) which contains the thickest sea ice in the world [*Bourke and Garrett* 1987; *Melling,* 2002] and provides the last refuge of the oldest ice types [*Maslanik et al.,* 2011; *Comiso,* 2012].

Nansen and the drift of the *Fram* provided the first glimpse into the large scale pattern of ice motion, as the ship drifted from the eastern Arctic through what is now known as Fram Strait along what is now known as the TDS. This led to further exploration of the Arctic with embedded ships and drifting ice camps (e.g. the Russian NP station program). *Gordienko* [1958] gathered ice drift data from these various platforms and presented the first map of arctic ice drift patterns (Figure 2.6). *Gordienko* [1958] discussed the "anticyclonic ring of ice drift in the section of ocean adjacent to Canada and Alaska" (The BG) and the movement of ice towards the Strait between Greenland and Svalbard (TDS; Fram Strait). He attributed the latter pattern to the basin wide flow of upper ocean currents towards the Strait where water masses and sea ice exit the Arctic into the North Atlantic. *Gordienko* [1958] ascribed the drift of sea ice to surface winds but

outlined that this forcing takes place against the 'background' forcing of upper ocean currents which he described as constant currents.

Figure 2.6: Preliminary map of arctic ice drift from Gordienko [1958] (Figure 7).

Subsequently *Gudkovich* [1961] (available in *Rigor et al.,* 2002) and *Sokolov* [1961] (available in *Proshutinsky and Johnson* 1997) presented two different regimes of the mean pattern of ice motion in which the key features (BG and TDS) varied in size and extent (Figure 2.7). These two regimes were later defined by *Proshutinsky and Johnson* [1997] as the anticyclonic and cyclonic patterns of circulation which *Rigor et al.,* [2002] ascribed to variations in SLP patterns described by the Arctic Oscillation. Regime A [*Gudkovich* 1961; *Sokolov* 1962] or the anticyclonic circulation pattern [*Proshutinsky and Johnson* 1997] was characterized by a large BG centered in the Canada Basin with the TDS located in the eastern Arctic, transferring ice from the Russian marginal seas (i.e. East Siberian, Laptev and Kara Seas) over the pole towards Fram Strait. Regime B [*Gudkovich* 1961; *Sokolov* 1962] or the cyclonic circulation

pattern [*Proshutinsky and Johnson* 1997] was characterized by a smaller BG shifted into the southern Canada Basin with a stronger and broader TDS that transports ice not only from the Eastern Arctic but from the Chukchi Sea as well towards Fram Strait. Generally the two regimes differ in the size and extent of the BG and TDS which has significant implications for ice transport [*Rigor et al.,* 2002], ice export [*Kwok,* 2009] and the physical oceanography of the Arctic Ocean [*Proshutinsky and Johnson* 1997].

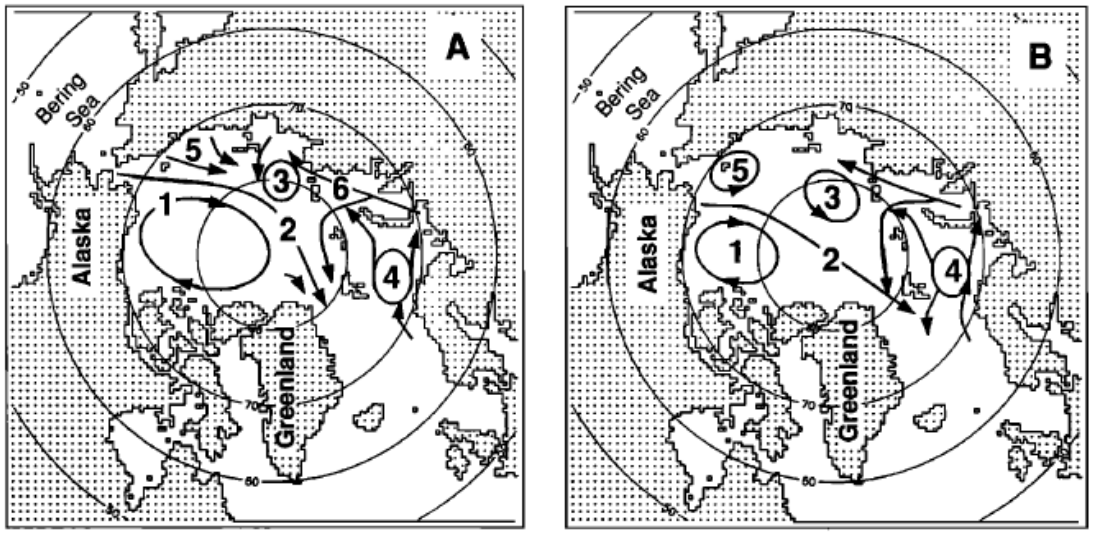

Figure 2.7: Two regimes of Arctic ice drift identified by Sokolov [1962]. Used with permission from Proshutinsky and Johnson [1997] who later defined them as Anticyclonic and Cyclonic patterns of ice drift.

Rigor et al., [2002] use the IABP archive of ice beacon data from 1979 to 1998 to characterize how ice drift varied between high and low phases of the Arctic Oscillation (AO). The AO is an index defined by the leading principal component of the SLP pattern of the Northern Hemisphere, specifically the opposing pressure patterns of the middle and high latitudes [*Thompson and Wallace,* 1998]. The AO in its low phase is characterized by high pressure over the polar region and low pressure in the mid-latitudes, while the opposite is true under a high AO index. Through wind forcing, changes in the AO have significant impact on the large scale patterns of sea ice drift throughout the Arctic [*Kwok,* 2000; *Rigor et al.,* 2002].

Changes in patterns of ice drift directly affect key properties such as ice export, extent, transport and dynamics [*Kwok,* 2000] which further affect the atmospheric and oceanographic properties of the Arctic. Encompassed within the AO is the North Atlantic Oscillation (NAO) [*Thompson and Wallace,* 1998; *Kwok and Rothrock,* 1999] which defines the SLP variation between the mid-latitude Azores High and the polar Icelandic Low [*Hurrell,* 1995]. The NAO is shown to act in phase with the AO and exerts more of an effect on ice motion in the Atlantic sector of the Arctic which is influenced by the Icelandic Low [*Kwok,* 2000]. The Icelandic Low influences the SLP gradient across Fram Strait, thus *Kwok* [2004] found a strong correlation (R^2 = 0.62) between Fram Strait ice area export and the NAO.

A high AO index is reflective of lower pressure over the Arctic with a weaker Beaufort High over the Beaufort Sea and deeper Icelandic Low over the North Atlantic that extends beyond Greenland into the Arctic [*Rigor et al.,* 2002]. Throughout the Arctic, SLP is lower by 3-5 hPa during a high AO than during a low AO. In terms of ice drift, a high AO (Figure 2.8D) causes the BG to weaken and retreat towards Alaska [*Zhang, et al.,* 2000; *Rigor et al.,* 2002], increased ice export through Fram Strait, increased ice import from the Barents and Kara Seas into the central Arctic, and a broader but weaker TDS [*Kwok,* 2000]. The AO entered a high phase in 1989 that persisted until 1996 and caused a large outflow of old arctic sea ice during the late 1980's [*Rigor and Wallace,* 2004]. *Lindsay and Zhang* [2005] refer to this flushing of old ice as the 'trigger' that set about large scale feedback processes that continue to drive the decline of arctic sea ice.

A low AO (Figure 2.8B) is reflective of high pressure over the Arctic with a strong Beaufort High that dominates the Arctic and precludes the Icelandic Low from entering the Arctic Basin. A large Beaufort High drives the anticyclonic BG to expand beyond the Canada

Basin into the Eastern Arctic and northwards along the coast of the Canadian Arctic Archipelago (CAA). By expanding into the eastern Arctic the BG transports more sea ice from its southern pass into the TDS which then transports this ice towards Fram Strait [*Rigor et al.,* 2002]. However, by expanding northwards along the CAA the BG recirculates and entrains more old ice from the High Arctic. The AO was in a low phase between 1979 and 1988. During this low phase ice could recirculate within the BG for over 10 years, allowing ice to survive for several melt seasons and age to the point where MYI covered 80% of the Arctic [*Rigor and Wallace,* 2004]. The TDS under a low AO transports ice towards Fram Strait much faster and hence from much further away than it does under a positive AO [*Rigor et al.,* 2002]. Under a low AO ice from The East Siberian Sea will exit Fram Strait in roughly four years, whereas under a high AO this same ice may take greater than five years to exit Fram Strait [*Rigor et al.,* 2002].

Figure 2.8: Comparison of the two ice drift regimes (a and b) identified by Gudkovich [1961] compared to ice drift regimes during High and Low AO indices (c and d) identified by Rigor et al., [2002] Figure 10

2.3.1 The Beaufort Gyre

The Beaufort Gyre (BG) is an anticyclonic feature of the western Arctic manifested in both the upper ocean currents and the drift of sea ice. The BG is driven by the Beaufort High which is a semi-permanent feature in the sea level pressure pattern of the Arctic [*Overland,* 2009]. The Beaufort High is present in both the fall and winter pressure patterns [*Overland,* 2009] as well as the annual mean sea level pressure patterns [*Serreze and Barrett,* 2011]. Under the influence of the Beaufort High sea ice is transported southward out of the High Arctic along the western edge of the CAA into the Beaufort Sea, from which ice circulates westward through the Beaufort, Chukchi and East Siberian Seas before returning to the High Arctic. At this point ice can either recirculate within the BG or enter the TDS which will transport the ice towards Fram Strait, where it will exit the Arctic and enter the north Atlantic [*Pfirman et al.,* 2004; *Martin and Martin 2006*]. The loss of ice from the BG into the TDS is dependent on the shape and extent of the BG, both of which are variable, and affects the age of arctic sea ice and the ice volume export through Fram Strait [*Rigor et al.,* 2002; *Martin and Martin* 2006]. Historically sea ice has recirculated in the BG for between 7 [*Rigor et al.,* 2002] and 10 years [*Rigor and Wallace,* 2004], though ice island T-3 drifted in the BG for over 27 years [*Jeffries* 1992]. However recently due to increasing sea ice melt (e.g. *Perovich et al.,* 2008) an increasing proportion of sea ice does not survive summer in the marginal seas, thereby cutting off the potential for sea ice to age as it recirculates within the BG [*Maslanik et al.,* 2007]. Recently, *Stroeve et al.,* [2011] showed the complete loss of all multiyear sea ice in the Beaufort Sea during summer 2010, essentially ending the recirculation and aging of ice through the BG.

The BG has historically been called one of the most hostile and inaccessible areas of the globe because of its long dark winters, harsh climate and thick drifting sea ice [*Proshutinsky et*

al., 2009]. *Proshutinsky et al.,* [2009] describe the BG as a "unique phenomenon comprising a set of specific atmospheric, sea ice and oceanic conditions that have significant influence on the Arctic climate". *Proshutinsky et al.,* [2009b] compare the ocean-ice-atmosphere system within the BG as a flywheel in which each medium stores and exchanges mass and energy differently during different climate regimes. A result of the anticyclonic rotation of sea ice and surface currents within the BG is large scale Ekman pumping which leads to upwelling along the Alaskan coast and downwelling in the interior BG [*Proshutinsky et al.,* 2009a; *Yang et al.,* 2009]. As a result the BG stores freshwater [*Proshutinsky et al.,* 2002; 2009a; 2009b; *Carmack et al.,* 2008; *Yang,* 2009; *McLaughlin and Carmack,* 2010; *McLaughlin et al.,* 2011] which causes sea surface heights to crown across the BG as freshwater is accumulated [*Giles et al.,* 2012; *Morison et al.,* 2012]. *McPhee et al.,* [2009] refer to the BG as the largest storage feature of freshwater in the Arctic. Recently sea surface heights and therefore freshwater storage have been increasing throughout the BG indicating a 'spin up′ of the BG [*Giles et al.,* 2012]. *Yang et al.,* [2009], *McPhee et al.,* [2009] and *Giles et al.,* [2012] attribute this 'spin up' to a reduction in the mechanical strength of sea ice resulting in increased ice drift speeds that transfer more momentum through the sea ice thereby driving increased Ekman pumping. *Martin et al.,* [2014] used a model to demonstrate how a decreasing ice pack has led to increased momentum transfer in the upper ocean currents, stating that ocean surface stress increased by 20% between 1979 and 2012. Ekman pumping retains freshwater within the BG, but if the BG weakens or temporarily reverses it can release freshwater. A large release of freshwater in the 1960's and 70's has been cited as the cause of the great salinity anomaly in the Greenland Sea [*Serreze et al.,* 1992].

Reversals of the BG were briefly discussed by *Hibler* [1980] and said to last one week. *McLaren et al.,* [1987] expanded upon this work and used ice drift and sea level pressure data

collected by ice beacons to show the presence of a recurring late summer reversal of the BG that was driven by changes in the atmospheric forcing and caused divergent ice motion. *McLaren et al.,* [1987] note a particularly strong reversal in 1980, which they attribute to "an extensive area of reduced ice concentration". The authors do not explicitly relate this to a reduction in internal stresses associated with reduced ice concentration, but given the results of subsequent work (e.g. *Steele et al.,* 1997) we assume the reduction in internal stresses allowed the ice pack to respond to cyclonic winds and create an above average reversal event. Subsequently, using the same IABP data, *Serreze et al.,* [1989] confirmed the existence of reversal events in response to cyclonic atmospheric forcing during late summer to early fall and stated that reversals can persist for up to 30 days. More recently *Lukovich and Barber* [2006] showed that reversal events are highly variable in strength and timing, that they are most common during August and September and that they occasionally occur during winter. *Asplin et al.,* [2009] found high correlations between cyclonic activity in the surface pressure patterns and BG reversals, while also predicting an increase in the occurrence of reversal events due to large scale declines in the arctic ice pack affecting the mobility and increasing the momentum transfer to sea ice.

2.3.2 The Transpolar Drift Stream

As indicated earlier, the other significant feature of the mean pattern of ice motion in the Arctic is the TDS which transports ice from the Eastern Arctic across the pole towards Fram Strait and into the North Atlantic [*Hibler,* 1980; *Colony and Thorndike,* 1984]. The TDS provided the basis for Nansen's theory of drifting the *Fram* across the North Pole and out of the Arctic through Fram Strait. The TDS has been a major feature of all maps showing the mean large scale pattern of ice motion in the Arctic [*Gordienko,* 1958; *Gudkovich,* 1961; *Sokolov,* 1962], however its variability in size, location and source region were not captured in these

preliminary studies. *Serreze et al.,* [1989] showed that the long term mean pattern of ice drift is towards Fram Strait, but that the TDS can reverse during summer for periods as long as 30 days. *Rigor et al.,* [2002] showed that under a high AO index the TDS increases in size, extends further into the western Arctic, exports more ice from the Russian marginal seas (increasing production of thin ice) and increases ice drift speeds through Fram Strait thereby increasing the areal flux of sea ice through Fram Strait by 10%. Under a low AO index the TDS is smaller, slower and confined to the eastern Arctic, though a greater proportion of it is comprised of thicker and older ice originating from the BG. Because of this the volume export through Fram Strait is higher under a low AO whereas the areal export is greater under a high AO [*Rigor et al.,* 2002].

2.3.3 Ice drift in the switchyard and Canadian Arctic

The region north of the CAA and Greenland is referred to as the switchyard region, it is home to the thickest and most dynamically active sea ice in the world [*Bourke and Garrett* 1987; *Melling,* 2002] and provides the last refuge of old multiyear sea ice [*Maslanik et al.,* 2011; *Comiso,* 2012]. The BG and TDS converge against the existing ice pack in this region, which is constrained against the coast of the CAA and northern Greenland, creating great internal stresses that reduce ice drift and encourage dynamic activity. Every year a portion of the ice from the switchyard region drifts south through Nares Strait (between Ellesmere Island and Northern Greenland) into Baffin Bay while some enters the CAA, but generally ice remains within the switchyard region for up to several years allowing it to age and dynamically thicken.

Ice from the switchyard region enters the Queen Elizabeth Islands (QEI) of the CAA during summer when a portion of the typically landfast ice in the interisland straits becomes mobile [*Melling,* 2002; *Howell et al.,* 2013]. Two thirds of the 315km of the interisland straits

that border the Arctic Ocean are locked up with landfast ice from October to July, while the remaining third remains locked up with ice arches through summer [*Howell et al.,* 2013]. Historically ice within the QEI is MYI that has either aged within the QEI or been dynamically imported from the Arctic Ocean [*Melling,* 2002; *Howell et al.,* 2008a; 2008b; 2013]. The amount of MYI dynamically imported from the Arctic Ocean began increasing in 1994 and continues to increase as interisland ice arches that prevent ice motion have weakened and are now less resilient to an increasingly long summer melt season (+7 days decade^{-1}) [*Alt et al.,* 2006; *Howell et al.,* 2009]. A longer melt season creates more open water which reduces both the internal stresses of the ice pack and the strength of ice arches. Due to reductions in the strength of ice arches and an increasing presence of open water, ice within the CAA has become more mobile and ice drift from the Arctic Ocean into the CAA has increased as a result [*Howell et al.,* 2008a; 2008b; 2013]. *Kwok* [2006] quantified the ice import/export between the CAA and the Arctic Ocean through gates in the QEI, across M'clure Strait and across Amundsen Gulf. Roughly 8 x 10^3 km^2 yr^{-1} was imported through the QEI while 85 x10^3 and 20 x 10^3 km^2 yr^{-1} were exported into the Beaufort Sea by the two southern gates respectively. *Howell et al.,* [2013] expanded on this work with Radarsat derived fields of ice motion and noted a strong seasonality in the ice fluxes, with negligible ice fluxes between November and May in M'Clure Strait and October to July in the more northern QEI flux gates. The authors note that CAA ice fluxes are predominantly driven by SLP patterns and the resulting atmospheric forcing, but that weak ice conditions and open water must be present in order for ice to drift into the QEI. The authors find considerable interannual variability with no trend across M'Clure Strait, but find near continuous inflow into the CAA across the QEI gates with an increasing trend since 2005 which they

attribute to the increasing presence of open water. *Howell et al.,* [2013] note that 60% of the ice that enters the CAA through the QEI is MYI that came from the switchyard region.

2.3.4 Ice export

Changes in the ice mass balance of the Arctic are a result of thermodynamics (melt) or dynamics (export) or a combination of both. Therefore to better understand the recent decrease in sea ice volume it is important to understand both processes and their contribution towards observed trends in the arctic ice pack. Though increasing air and water temperatures are driving increased melt rates throughout the Arctic [e.g. *Perovich et al.,* 2008] and significantly contributing to the loss of arctic sea ice, we cannot ignore changes to the dynamic nature of the ice pack that may contribute to this loss or foster further reductions. A possible dynamic contribution to the dwindling ice pack is increased ice export. Ice area fluxes (F_i) (km^2) are used to quantify ice export and transport, and are calculated by the following equation,

$$F_i = \sum c_i u_i \, \Delta x \qquad (1)$$

where, c_i is sea ice concentration, u_i is the velocity component normal to the gate and Δx is the size of the pixel (i.e. 25km). The ice area flux can be scaled up to an ice volume flux (km^3) if ice thickness data exists along the flux gate for the period of time analyzed. The Norwegian Polar Institute has operated moorings with upward looking sonars in Fram Strait continually since 1991. When combined with satellite derived field of ice motion and concentration ice volume fluxes through Fram Strait can be calculated (e.g. *Vinje et al.,* 1998; *Kwok et al.,* 2004; *Spreen et al.,* 2014).

Fram Strait is located between the northeast coast of Greenland and Svalbard, Norway. Roughly 10% of the arctic sea ice mass balance is exported annually through the ~400 km wide strait into the North Atlantic where the input of freshwater plays a considerable role in the

convective overturning of the global ocean thermohaline circulation pattern [*Kwok,* 2004]. As much as 94% of all ice exported from the Arctic passes through Fram Strait [*Arfeuille et al.,* 2000] with an average volume of 2200 km^3 yr^{-1}. [*Kwok et al.,* 2004; *Kwok,* 2009]. On average Fram Strait exports 706 x 10^3 km^2 yr^{-1} of sea ice with a maximum of 1002 x 10^3 km^2 yr^{-1} during 1994-1995, which was characterized by a high AO, and a minimum of 516 x 103 km^2 yr^{-1} during 1984-1985, which was characterized by a low AO [*Kwok,* 2009]. Around 87% of the export through Fram Strait occurs during winter (October to May) with a peak in March of roughly 90 x 10^3 km^2 yr^{-1} [*Kwok,* 2009]. Ice export through Fram Strait has a high degree of interannual variability that is dependent on ice drift speeds and the source region of the ice exported. *Kwok* [2009] used passive microwave derived fields of ice motion to track the source region of ice exported through Fram Strait during one year and found a high degree of variability in TDS location, breadth and size. A key result was the relation between source region and type of ice that is exported. When the source region was in the western Arctic, thicker/older ice from the Beaufort Sea and North Greenland was exported. Conversely when the source region was in the Eastern Arctic, younger/thinner ice was exported. On average ice drifted 1100 (270) km in one year before passing through Fram Strait, and came from a spatial area of 676 (169) x 10^3 km^2, which correlates well (R = 0.58) with the mean area outflow of 706 x 10^3 km^2 [*Kwok,* 2009]. Source regions were furthest from Fram Strait during the late 1980's and 1990's during a prolonged period of high AO indices when the TDS was larger and drifted faster. *Kwok* [2009] found a positive trend in the SLP gradient across Fram Strait, which theoretically should result in increased drift speeds and therefore increased export. However there was no trend in the Fram Strait export due to a negative trend in sea ice concentration in Fram Strait throughout the annual cycle (1979-2007 annual average of -3.33% $decade^{-1}$). More Recently, *Spreen et al.,* [2014]

analyzed the Norwegian Polar Institutes 20 year record of ice thickness across Fram Strait and found a significant negative trend in ice volume exported through Fram Strait between 1992 and 2011. The authors found ice thickness has declined at a rate of 3 cm yr^{-1} since 1992 with an increasingly negative trend since 2003. The authors attribute the negative trend in volume export to the reduced ice thickness as the ice area export did not change significantly during this time [*Spreen et al.,* 2014].

Large episodic export events from the TDS through Fram Strait occurred in 2005 and again in 2007 when an atmospheric dipole formed over the TDS and drove a phenomenon referred to as the 'Polar Express' [*Nghiem et al.,* 2007; 2011]. Under the forcing of an atmospheric low over the Barents Sea and high over the Beaufort Sea the TDS accelerated and forced ice southwards through Fram Strait. Historically the TDS and Fram Strait were composed mostly of MYI (up to 84% in Fram Strait [*Gow and Tucker,* 1987]) however with recent declines in MYI throughout the Arctic and reducing survival rates of MYI in the BG there has been a trend towards younger ice within the TDS [*Comiso,* 2012]. A younger TDS means thinner ice which will theoretically drift faster and behave more dynamically will be advected towards Fram Strait, having implications for ice export and delivery of freshwater into the North Atlantic Ocean.

Ice export through Nares Strait into Baffin Bay is limited seasonally by ice arches that form during late fall/early winter when MYI from the Lincoln Sea converges within the Strait [*Kwok,* 2005]. Ice is forced southwards through Nares Strait by a sea level pressure gradient from the Lincoln Sea to Baffin Bay [*Gudmandsen,* 2000; *Samelson et al.,* 2006]. Typically ice arches immobilize ice within Nares Strait between November and March. However the duration of this period is highly variable, with a maximum of 220 days in 2000 and a minimum of 80 days in 1998. Between 1996 and 2002 an average of 33 x 10^3 km^2 yr^{-1} or 130 km^3 yr^{-1} (assuming a

mean thickness of 4m) of sea ice was exported southwards through Nares Strait [*Kwok,* 2005]. However in 2007 during the sea ice minimum the ice arch never formed and ice continuously drifted through Nares Strait, exporting 87 x 10^3 km^2 or 254 km^3 of sea ice. Ice export was again above average in 2008, thus *Kwok et al.,* [2010] updated the average Nares Strait ice export to 42 x 10^3 km^2 yr^{-1} for the period from 1997 to 2009. *Kwok et al.,* [2010] predict that if warming temperatures continue to cause weaker sea ice conditions the ice arch may no longer form, hence causing sea ice, specifically MYI from the switchyard region, to be exported year round into Baffin Bay.

Ice transport through the 85 km wide and 50 m deep Bering Strait is considered negligible [*Gow and Tucker,* 1987]. *Aagard and Carmack* [1989], citing personal communication with C. Pease, stated the Bering Strait imports 30 km^3 of sea ice into the Arctic annually, though it has been shown that sea ice can be episodically exported through the Bering Strait into the Bering Sea [*Pease,* 1980]. These export events occur once or twice a year and are correlated with reversals in ocean currents of the Bering Strait [*Pease,* 1980], which flow predominantly northward [*Woodgate et al.,* 2006]. However, *Overland and Pease* [1982] clarified that southward sea ice export through the Bering Strait is driven by northerly surface winds resulting from the presence of the Siberian High, which is a strong atmospheric high pressure system situated north of the Bering Strait. Ice export through the Bering Strait is limited because it is a converging channel in which ice arches may form during winter and impede ice drift [*Sodhi,* 1977], much in the same way they seasonally preclude ice drift through Nares Strait [*Kwok,* 2005; *Kwok et al.,* 2010] and interisland straits of the CAA [*Howell et al.,* 2008*a*; 2008*b*; 2013]. Ice arch formation is dependent on the channel width, ice shear strength and the wind velocity [*Kubat et al.,* 2006; *Hibler et al.,* 2006]. For the Bering Strait *Sodhi* [1977] calculated a critical

wind speed of 5.6 m s^{-1} above which ice arches cannot form and ice can move freely through the channel.

2.4. Ice drift in a changing Arctic

The relation between ice state and ice drift has been well developed, as the two are inversely related through the mechanical strength of the ice pack which determines the internal stresses that act to dampen ice drift. The relation between ice state and ice drift varies through an annual cycle as well as on longer decadal scales. The annual cycle is well established with a peak in ice drift speeds during the September sea ice minimum and a minimum in ice drift speeds during the March/April sea ice maximum [*Spreen et al.,* 2011]. In terms of decadal trends, between 1982 and 2009 in response to a mechanical weakening of the arctic ice pack ice drift speeds increased at a rate of 6.15 and 3.60% $decade^{-1}$ during winter and summer, respectively [*Kwok et al.,* 2013]. When the analysis is limited to the period from 2001 to 2009 the rates increase by 76% and 80% to 23.55 and 17.71% $decade^{-1}$, respectively [*Kwok et al.,* 2013]. *Kwok et al.* [2013] also note that over 90% of the Arctic Ocean displays a positive trend in ice drift speeds and a negative trend in MYI coverage. A transition towards a seasonal ice cover through the loss of MYI is a key indicator of climate induced change in the Arctic [*Nghiem et al.,* 2007; *Kwok et al.,* 2009; *Maslanik et al.,* 2011; *Comiso,* 2012; *Parkinson and Comiso,* 2013]. *Stroeve et al.,* [2014] note that in the mid-1980s MYI accounted for 70% of the total winter ice extent, whereas by the end of 2012 this value had dropped to 20%. Coincidentally the oldest ice types of 5+ year old ice have declined from 50% of the MYI pack in the 1980s to less than 10% in 2011, with reductions now occurring within the central Arctic ice pack [*Maslanik et al.,* 2011]. Concurrent reductions in sea ice extent (1919-2013: -14% $decade^{-1}$ [*Stroeve et al.,* 2014]), sea ice thickness (-0.08 to -0.20 m yr^{-1} [*Kwok and Rothrock,* 2009]) and melt season length (5 days

decade^{-1} [*Stroeve et al.,* 2014]) have culminated in a trend of -2.8 x 10^3 km^3 decade^{-1} in sea ice volume [*Schweiger et al.,* 2011]. Using a model *Zhang et al.,* [2012] found that between the two periods from 1979-2006 and 2007-2011, arctic ice volume declined by 33% which caused a 37% decrease in the mechanical strength and 31% decrease in internal stresses of the ice pack. This change culminated in a 13% increase in ice drift speeds and 17% increase in deformation rates. Beyond increased ice drift speeds and deformation rates, the mechanical weakening of the ice pack has increased the transport of ice through the Bering Strait [*Babb et al.,* 2013], the interisland straits of the Canadian Arctic Archipelago [*Howell et al.,* 2013] and Nares Strait [*Kwok et al.,* 2010].

Evidence for changes in the arctic ice pack are perhaps best represented by the drift of the French schooner *Tara* during the 2007-2008 International Polar Year. Following in Fridtjof Nansen's footsteps the ship and her 8 man crew entered the ice pack near the East Siberian Islands and drifted with the TDS towards Fram Strait, collecting oceanographic, meteorological and geophysical observations during the drift. A mere 15 months later the *Tara* emerged through Fram Strait, roughly three times faster than it had taken the Fram 115 years prior [*Gascard et al.,* 2008]. The drift of the *Tara* provides tangible evidence of a changing Arctic in which the arctic ice pack has become increasingly mobile and is now drifting at greater speeds.

Literature cited:

Aagaard, K. and E.C. Carmack (1989), The role of sea ice and other fresh water in the Arctic Circulation, *J. Geophys. Research*, 94, C10, 14,485-14,498.

Alt, B., K. Wilson and T. Carrieres (2006) A case study of old-ice import and export through Peary and Sverdrup Channels in the Canadian Arctic Archipelago: 1998-2005, *Annals of Glaciology*, 44, 329-338.

Andersen, R.J. (1987), Wind stress measurements over rough ice during the 1984 Marginal Ice Zone Experiment, *J. Geophys. Res.*, 92 (C7), 6933-6941, doi:10.1029/JC092iC07p06933.

Andreas, E., W.B. Tucker and S.F. Ackley (1984), Atmospheric Boundary Layer Modification, Drag Coefficient and Surface Heat Flux in the Antarctic Marginal Ice Zone, *J. Geophys. Res.* 89, C1, 649-661.

Andreas, E.L., M.A. Lange, S.F. Ackley and P. Wadhams (1993), Roughness of WEddel Sea ice and estimates of the air ice drag coefficient, *J. Geophys. Res.*, 98 (C7), 12,439-12,452.

Arfeuille, G., L.A. Mysak and L.-B. Tremblay (2000), Simulation of the interannual variability of the wind driven Arctic sea-ice cover during 1958-1998, *Climate Dynamics*, 16, 107-121.

Asplin, M.G., J.V. Lukovich and D.G. Barber (2009), Atmospheric forcing of the Beaufort Sea ice gyre: Surface pressure climatology and sea ice motion, *J. Geophys. Res.* 114, C00A06, doi: 10.1029/2008JC005127.

Asplin, M.G., R. Galley, D.G. Barber and S. Prinsenberg (2012), Fracture of summer perennial sea ice by ocean swell as a result of Arctic storms, *J. Geophys. Res. Oceans*, 117, C06025, doi: 10.1029/2011JC007221.

Barber, D.G., G.M. McCullough, D.G. Babb, A.S. Komarov, L.M. Candlish, J.V. Lukovich, M. Asplin, S. Prinsenberg, I . Dmitrenko and S. Rysgaard (2014), Climate change and ice hazards in the Beaufort Sea, *Elementa*, 2:000025, doi:10.12952/journal.elementa.000025.

Berger, M. and J. Asbacher (2012), preface The sentinel missions new opportunites for science, *Remote Sensing of the Environment*, 120, 1-2.

Bourke, R.H., and R.P. Garrett (1987), Sea ice thickness distribution in the Arctic Ocean, *Cold Regions Science and Technology*, 13, 259-280.

Carmack, E., F. McLaughlin, M. Yamamoto-Kawai, M. Itoh, K. Shimada,R. Krishfield, and A. Proshutinsky (2008), Freshwater storage in theNorthern Ocean and the special role of the Beaufort Gyre, in Arctic-Subarctic Ocean Fluxes: Defining the Role of the Northern Seas in Climate, edited by R. R. Dickson et al., pp. 145 – 169, Springer,New York.

Carsey, F and B Holt (1987), Beaufort-Chukchi ice margin data from Seasat: Ice Motion, *J. Geophys. Res.*, 92 (C7), 7163-7172.

Collins, M.J. and W.J. Emery (1988), A computational method for estimating sea ice motion in sequential Seasat synthetic aperture radar imagery by matched filtering, *J. Geophys. Res.*, 93 (8), 9241 – 9251.

Colony, R. and A.S. Thorndike (1980), The Horizontal Coherency of the motion of Summer Arctic Sea Ice, *J. of Physical Oceanography*, 10, 1281-1289.

Colony, R. and A.S. Thorndike (1984), An Estimate of the Mean Field of Arctic Sea Ice Motion, *J. Geophys. Research*, 89(C6), 10,623-10,629.

Comiso, J. (2010), Polar Oceans from Space, Atmospheric and Oceanographic Sciences Library Vol. 41, Springer, New York.

Comiso, J.C. (2012), Large Decadal Decline of the Arctic Multiyear Ice Cover, *J. Climate*, 25, 1176-1193.

Currlander, J.C., B. Holt and K.J. Hussy (1985), Determination of Sea Ice Motion Using digital SAR imagery, *IEEE J. of Ocean Engineering*, OE-10 (4).

Emery, W.J., C.W. Fowler, J. Hawkins and R.H. Preller (1991), Fram Strait Satellite Image-Derived Ice Motions, *J. Geophys. Res.*, 96 (C3), 4751-4768.

Emery, W.J., C. Fowler, J. Maslanik and S. Pfirman (1997), New Satellite Derived Sea Ice Motion Tracks Arctic Contamination, *Marine Pollution Bulletin*, 35 (7-12), 345-352.

Fily, M. and D.A. Rothrock (1987), Quantitative use of satellite SAR imagery of sea ice, *Advances in Space Research*, 7(11), 323-326.

Flett, D., Y. Creview and R. Girard (2009), The RADARSAT constellation mission Meeting the government of Canada's needs and requirements, *International Geoscience and Remote Sensing Symposium*, 2, 5418303, II910-II912.

Fowler, C., W. Emery, and M. Tschudi. (2013) Polar Pathfinder Daily 25 km EASE-Grid Sea Ice Motion Vectors V2, Boulder, Colorado USA: NASA DAAC at the National Snow and Ice Data Center.

Fowler, C., W.J. Emery and J. Maslanik (2004), Satellite-Derived Evolution of Arctic Sea Ice Age: October 1978 to March 2003, *IEEE Geoscience and Remote Sensing Letters*, 1(2), 71-74.

Gascard, J.C., et al. (2008), Exploring Arctic Transpolar Drift During Dramatic Sea Ice Retreat, *EOS*, 89 (3), 21-22.

Geiger, C.A. and D.K. Perovich (2008), Springtime ice motion in the western Antarctic Peninsula, *Deep-Sea Research II*, 55, 338-350.

Giles, K.A., S.W. Laxon, A.L. Ridout, D.J. Wingham and S. Bacon (2013), Western Arctic Ocean freshwater storage increased by wind-driven spin up of the Beaufort Gyre, *Nature*, 5, doi:10.1038/NGE01379.

Gimbert F., D. Marsan, J. Weiss, N.C. Jourdain and B. Barnier (2012), Sea ice inertial oscillations in the Arctic Basin (2012), *The Cryosphere*, 6, 1187-1201, doi: 10.5194/tc-6-1187-2012

Greve, M. (1994), Fridtjof Nansen (english translation by M.E. Davies), Aschehoug, 56pp, accessed online at www.frammuseum.no on Setember 6th, 2012.

Gordienko, P.A. (1958), Arctic drift ice, in *Proceedings on the Conference of sea ice, Publ. 598*, edited by R.W. Thurston, pp 210-222, National Research Council, National Academy of Sciences, Washington D.C.

Gow, A.J. and W.B. Tucker III (1987), Physical Properties of Sea ice discharged from Fram Strait, *Science*, 236 (4800), 436-439.

Gudmandsen, P. (2000), A remote sensing study of Lincoln sea, paper presented at ERS-ENVISAT Symposium, Eur. Space Agency, Gothenburg, Sweden.

Guest, P.S., J.W. Glendening and K.L. Davidson (1995), An observational and numerical study of wind stress variations within marginal ice zones, *J. Geophys. Res.*, 100 (C6), 10 887-10 904.

Guest, P.S. and K.L. Davidson (1991), The aerodynamic Roughness of Different Types of Sea Ice, *J. Geophys. Res*., 96 (C3), 4709-4721.

Hakinen, S., A. Proshutinsky and I. Ashik (2008), Sea ice drift in the Arctic since the 1950s, *Geophys. Res. Lett.*, 35, L19704, doi:10.1029/2008GL034791.

Hall, R.T. and D.A. Rothrock (1981), Sea ice displacement from Seasat Synthetic Aperture Radar, *J. Geophys. Res.*, 86)C11) 11,078-11,082.

Hibler, W.D. (1979), A Dynamic Thermodynamic Sea Ice Model,*J. Physical Oceanography*, 9, 815-847.

Hibler, W.D. III (1980), Sea ice growth, drift and decay, in Dynamics of Snow and Ice Masses, edited by S.C. Colbeck, pp. 141-209, Acedemi Press, New York.

Hibler, W.D. and W.B. Tucker (1979), Some results from linear-viscous model of the Arctic ice cover, *J. Glaciology*, 22 (87), 293-304.

Hibler, W.D., J.K. Hutchings and C.F. Ip (2006), Sea-icea arching and multiple flow states of Arctic pack ice, *Annals of Glaciology*, 44, 339-345

Howell, S.E.L., A. Tivy, J.J. Yackel, B.G.T. Else and C.R. Duguay (2008a), Changing sea ice melt parameters in the Canadian Arctic Archipelago: Implications for the future presence of multiyear ice, *J. Geophys. Research*, 113, C09030, doi:10.1029/2008JC004730.

Howell, S.E.L., A. Tivy, J.J. Yackel and S. McCourt (2008b), Multiyear sea ice conditions in the western Canadian arctic archipelago region of the northwest passage: 1968-2006, *Atmosphere-Ocean*, 46(2), 229-242.

Howell, S.E.L., C.R. Duguay and T. Markus (2009), Sea ice conditions and melt season duration variability within the Canadian Arctic Archipelago: 1979-2008, *Geophys. Res. Lett.*, 36, L10502, doi: 10.1029/2009GL037681.

Howell, S.E.L, T. Wohlleben, M. Dabboor, C. Derksen, A. Komarov and L. Pizzolato (2013), Recent changes in the exchange of sea ice between the Arctic Ocean and the Canadian Arctic Archipelago, *J. Geophys. Research*, 118, 1-13, doi:10.1002/jgrc.20265.

Hurrell, J.W. (1995), Decadal trends in the north Atlantic Oscillation: Regional temperatures and precipitation, *Science*, 269 (5224), 676-679.

Jeffries, M.O. (1992) Arctic ice shelves and ice islands: origin, growth and disintegration, physical characteristics, structural-stratigraphic variability, and dynamics, *Reviews of Geophysics*, 30(3), 245-267.

Koberle, C. and R. Gerdes (2003), Mechanisms determining the variability of Arctic Sea Ice Conditions and Export, *J. Climate*, 16, 2843-2858.

Komarov, A. and D.G. Barber (2012), Detection of sea ice motion from co- and cross-polarization RADARSAT-2 images, *International Geoscience and Remote Sensing Symposium*, 6350604, 33277-3280.

Kimura, N. and M. Wakatsuchi (2000), Relationship between sea-ice motion and geostrophic wind in the Northern Hemisphere, *Geophys. Res. Letters*, 27(22), 3735-3738.

Kubat, I., M. Sayed, S.B. Savage and T. Carrieres (2006), Flow of ice through converging channels, *International Journal of Offshore and Polar Engineering*, 16 (4), 268-273.

Kwok, R. (1998), The RADARSAT Geophysical Processor System, in Analysis of SAR data of the Polar Oceans: Recent Advances edited by C. Tsatsoulis, and R. Kwok, pp. 235-258, Springer, Berlin.

Kwok, R. (2000), Recent changes in Arctic Ocean Sea Ice Motion Associated with the North Atlantic Oscillation, *Geophys. Res. Lett.*, 27 (6), 775-778.

Kwok, R. (2004), Annual cycles of multiyear sea ice coverage of the Arctic Ocean: 1999-2003, *J. Geophys. Res.*, 109, C110044, doi:10.1029/2003JC002238.

Kwok, R. (2005), Variability of Nares Strait ice flux, *Geophys. Res. Lett.*, 32 (24), 1-4.

Kwok, R. (2006a), Contrasts in sea ice deformation and production in the Arctic seasonal and perennial ice zones, *J. Geophys. Res.*, 111, C11S22, doi: 10.1029/2005JC003246.

Kwok, R. (2006b), Exchange of sea ice between the Arctic Ocean and the Canadian Arctic Archipelago, *Geophys. Res. Lett.*, 33, L16501, doi:10.1029/2006GL027094.

Kwok, R. (2009), Outflow of Arctic Ocean Sea Ice into the Greenland and Barents Seas: 1979-2007, *J. of Climate*, 22, 2438-2457.

Kwok, R., J.C. Curlander, R. McConnell and S.S. Pang (1990), An ice motion tracking system at the Alaska SAR facility, *IEEE J. of Oceanic Engineering*, 15 (1), 44-54

Kwok, R. and D.A. Rothrock (1999), Variability of Fram Strait ice flux and North Atlantic Oscillation, *J. Geophys. Res.* 104 (C3), 5177-5189.

Kwok, R., G.F. Cunningham and W.D. Hibler (2003), Sub-daily sea ice motion deformation from RADARSAT observations, *Geophys. Res. Lett.*, 30 (23) doi: 10.1029/2003GL018723.

Kwok, R, G.F. Cunningham and S.S. Pang (2004), Fram Strait sea ice outflow, *J. Geophys. Research*, 109, C01009, doi: 10.1029/2003JC001785.

Kwok, R, W. Maslowski and S.W. Laxon (2005), On large outflows of Arctic sea ice into the Barents Sea, *Geophys. Res. Lett.* 32 (22), L22503, 1-5.

Kwok, R., E.C. Hunke, W. Maslowski, D. Menemenlis and J. Zhang (2008), Variability of sea ice simulations assessed with RGPS kinematics, *J. Geophys. Res.* 113, C11012, doi: 10.1029/2008JC004783.

Kwok, R., and D.A. Rothrock (2009) Decline in Arctic sea ice thickness from submarine and ICESat records: 1958-2008, *Geophysical Research Letters*, 36, L15501, doi:10.1029/2009GL039035.

Kwok, R. and G.F. Cunningham (2010), Contribution of melt in the Beaufort Sea to the decline in Arctic multiyear sea ice coverage: 1993-2009, *Geophys. Res. Letters*, 37, L20501, doi:10.1029/2010GL044678.

Kwok, R. and G.F. Cunningham (2012), Deformation of the Arctic Ocean ice cover after the 2007 record minimum in summer sea ice extent, *Cold Regions Science and Technology*, 76-77, 17-23.

Kwok, R., G. Spreen and S. Pang (2013), Arctic sea ice circulation and drift speed: Decadal trends and ocean currents, *J. Geophys. Res. Oceans*, 118, 2408-2452, doi: 10.1002/jgrc.20191.

LaViolette, P.E. and J.M. Hubertz (1975). Surface circulation patterns off the East Coast of Greenland as deduced from satellite photographs of ice floes. *Geophysical Research Letters* 2. doi: 10.1029/GL002i009p00400.

Leberl, F., J. Raggam, C. Elachi and W.J. Campbell (1983), Sea ice motion measurements from SEASAT SAR images, *J. Geophys. Res.* 88 (C3), 1915-1928.

Leese, J.A., C.S. Novak and B.B. Clark (1971), Automated technique for obtaining cloud motion from geosynchronous satellite data using cross correlation, *J. Applied Meteorology*, 10 (1), 118-132.

Leppäranta, M. (2005), The drift of sea ice, Springer, Chichester, UK, pp 261.

Lindsay, R.W. (2002), Ice deformation near SHEBA, *J. Geophys. Res.*, 107 (C10), doi: 10.1029/2000JC000445.

Lindsay R.W. and J. Zhang (2005), The thinning of arctic sea ice, 1988-2003: have we passed a tipping point?, *J. Climate*, 18, 4879-4894.

Liu, A.K. and D.J. Cavalieri (1998), On sea ice drift from the wavelet analysis of the Defense Meteorological Satellite Program (DMSP) Special Sensor Microwave Imager (SSM/I) data, *International J. of Remote Sensing*, 19 (7), 1415-1423.

Lukovich, J., and D. Barber (2006), Atmospheric controls on sea ice motion in the Southern Beaufort Sea, *J. Geophys. Research*, 111, D18103, doi: 10.1029/2005JD006408.

Malenovsky, Z., et al. (2012), Sentinels for science: potential of sentinel-1, -2 and 03 missions for scientific observations of ocean, cryosphere and land, *Remote Sensing of Environment*, 120, 91-101.

Maslanik, J.A., C. Fowler, J. Stroeve, S. Drobot, J. Zwally, D. Yi and W. Emery (2007), A younger thinner arctic ice cover, Increased potential for rapid extensive sea ice loss, *Geophys. Res. Lett*, 34, L24501, doi: 10.1029/2007GL032043.

Maslanik, J., J. Stroeve, C. Fowler and W. Emery (2011), Distribution and trends in Arctic sea ice age through spring 2011, *Geophys. Res. Letters*, 38, L13502, doi: 10.1029/2011GL047735.

Massom, R.A. (2009), Principal Uses of Remote Sensing in Sea Ice Field Research, in Field Techniques for Sea Ice Research edited by H. Eicken, R. Gradinger, M. Salganek, K. Shirasawa, D. Perovich and M. Leppäranta, pp. 405-466 University of Alaska Press, Fairbanks.

Martin, T. and E. Augstein (2000), Large scale drift of arctic sea ice retrieved from passive microwave satellite data, *J. Geophys. Res.*, 105 (C4), 8775-8788.

Martin, T. and T. Martin (2006), Anomalies of sea ice transport in the Arctic, *Annals of Glaciology*, 44, 310-316.

Martin, T., M. Steele and J. Zhang (2014), Seasonality and long term trend of Arctic Ocean surface stress in a model, *J. Geophys. Res. – Oceans*, 119, doi: 10.1002/2013JC009425.

McLaren, A.S., M.C. Serreze and R.G. Barry (1987), Seasonal variations of sea ice motion in the Canada basin and their implications, *Geophys. Res. Lett.*, 14 (11), 1123-1126.

McLaughlin, F., E. Carmack, A. Proshutinsky, R.A. Krishfield, C. Guay, M. Yamamoto-Kawai, J.M. Jackson, and B. Williams. 2011. The rapid response of the Canada Basin to climate forcing: From bellwether to alarm bells. *Oceanography* 24(3):146–159.

McLaughlin, F.A. and E.C. Carmack (2010), Deepening of the nutricline and chlorophyll maximum in the Canada Basin interior, 2003-2009, *Geophys. Res. Lett.*, 37, L24602, doi: 10.1029/2010GL045459.

McNutt, S.L. and J.E. Overland (2003), spatial hierarchy in Arctic sea ice dynamics, *Tellus*, 55A, 181-191.

McPhee, M.G. (1978), A simulation of inertial oscillations in drifting pack ice, *Dynamics of Atmospheres and Oceans*, 2, 107-122.

McPhee, M.G. (1979), The effect of the Oceanic Boundary Layer on the Mean Drift of Pack Ice: Application of a Simple Model, *J. Physical Oceanography*, 9, 388- 400.

McPhee, M.G., A. Proshutinsky, J.H. Morison, M. Steele and M.B. Alkire (2009), Rapid change in freshwater content of the Arctic Ocean, *Geophys. Res. Lett.*, 36, L10602, doi: 10.1029/2009GL037525.

Melling, H. (2002), Sea ice of the northern Canadian Arctic Archipelago, *J. Geophys. Research*, 107, C11, doi: 10.1029/2001JC001102.

Morison, J., R. Kwok, C. Peralta-Ferriz, M. Alkire, I. Rigor, R. Andersen and M. Steele (2012), Changing Arctic Ocean freshwater pathways, *Nature*, 481, doi: 10.1038/nature10705.

Nansen, F. (1902), Norwegian North Polar Expedition 1893-1896, Scientific Results, vol. 3, The Oceanography of the North Polar Basin, 427 pp., Longmans, Green, London.

Nghiem, S.V., I.G. Rigor, D.K. Perovich, P. Clemente-Colon, J.W. Weatherly and G. Neumann (2007), Rapid reduction of Arctic perennial sea ice, *Geophys. Res. Lett.* 34, L19504, doi: 10.1029/2007GL031138

Nghiem, S.V., G. Neumann, P. Clemente-Colon, I.G. Rigor and D.K. Perovich (2011), Arctic perennial sea ice crash of the 2000s and its impacts, *BIONATURE 2011: The second international conference on bioenvironment, biodiversity and renewable energies*, 38-42.

Ninnis, R.M., W.J. Emery and M.J. Collins (1986), Automated extraction of pack ice motion from advanced very high resolution radiometer imagery. *Journal of Geophysical Research* 91: doi: 10.1029/JC091iC09p10725.

Overland, J.E., and C.H. Pease (1982), Cyclone Climatology of the Bering Sea and Its Relation to Sea Ice Extent, *Mon Wea. Rev.*, 110, 5-13.

Overland, J.E. (1985), Atmospheric boundary layer structure and drag coefficients over sea ice, *J. Geophys. Res.*, 90 (C5), 9029-9049.

Overland, J.E. and R.L. Colony (1994), Geostrophic drag coefficients for the central Arctic derived from soviet drifting station data, *Tellus*, 46A, 75-85.

Overland, J.E. (2009), Meteorology of the Beaufort Sea, *J. Geophys. Research*, 114, C00A07, doi: 10.1029/2008JC004861.

Parkinson, C.L. and J.C. Comiso (2013), On the 2012 record low Arctic sea ice cover: Combined impact of preconditioning and an August Storm, *Geophys. Res. Letters*, 40, 1-6, doi:10.1002/grl.50349.

Pease, C.H. (1980), Eastern Bering Sea Ice Processes, *Mon. Wea. Rev.*, 108, 2015-2023.

Perovich, D.K., Richter-Menge, J.A., Jones, K.F., and Light, B. (2008), Sunlight, water and ice: Extreme Arctic sea ice melt during the summer of 2007, *Geophys. Res. Letters,* 35, L11501, doi: 10.1029/2008GL034007.

Pfirman, S., W.F. Haxby, R. Colony and I. Rigor (2004), Variability in Arctic ice drift, *Geophys. Res. Lett.,* 31, L16402, doi:10.1029/2004GL020063.

Proshutinsky, A. and M.A. Johnson (1997), Two circulation regimes of the wind driven Arctic Ocean, *J. Geophys. Res.,* 102 (C6), 12,493-12,514.

Proshutinsky, A., R.H. Bourke and F.A. McLaughlin (2002), The role of the Beaufort Gyre in Arctic climate variability: Seasonal to decadal climate scales, *Geophys. Res. Lett.,* 29 (23), doi:10.1029/2002GL015847.

Proshutinsky, A., R. Krishfield and D. Barber (2009a), Preface to special section on Beaufort Gyre Climate System Exploration Studies: Documenting key parameters to understand environmental variability, *J. Geophys. Res.,* 114, C00A08, doi: 10.1029/2008JC005162.

Proshutinsky, A., et al. (2009b), Beaufort Gyre freshwater reservoir: State and variability from observations, *J. Geophys. Res.,* 114, C00A10, doi: 10.1029/2008JC005104.

Rampal, P., J. Weiss and D. Marsan (2009), Positive trend in the mean speed and deformation rate of arctic sea ice, 1979-2007, *J. Geophys. Research,* 114, C05013, doi: 10.1029/2008JC005066.

Reynolds, M., C.h. Pease and J.E. Overland (1985), Ice drift and regional meteorology in the southern Bering Sea: Results from MIZEX west, *J. Geophys. Res.* 90 (C6) 11,967-11,981.

Richter-Menge, J.A., S.L. McNutt, J.E. Overland and R. Kwok (2002), Relating arctic pack ice stress and deformation under winter conditions, *J. Geophys. Res.* 107 (C10), doi:10.1029/2000JC000477.

Rigor, I., J.M. Wallace and R. Colony (2002), Response of Sea Ice to the Arctic Oscillation, *J. of Climate,* 15, 2648-2663.

Rigor, I.G. and J.M. Wallace (2004), Variations in the age of Arctic sea ice and summer sea ice extent, *Geophys. Res. Lett.* 31, L09401, doi:10.1029/2004GL019492.

Samelson, R.M., T. Agnew, H. Melling, and A. Munchow (2006), Evidence for atmospheric control of sea-ice motion through Nares Strait, Geophysical Research Letters, 33, L02506, doi:10.1029/2005GL025016.

Schramm, J.L., G.M. Flato and J.A. Curry (2000), Toward the modeling of enhanced basal melting in ridge keels, *J. Geophys. Res. – Oceans,*105 (C6) 14081-14092.

Schweiger, A., r. Lindsay, J. Zhang, M. Steele, H Stern and R. Kwok (2011), Uncertainty in modeled Arctic sea ice volume, *J. Geophys. Res.* 116, C00D06, doi: 10.1029/2011JC007084.

Serreze, M.C., R.G. Barry and A.S. McLaren (1989), Seasonal variations in sea ice motion and effects on sea ice concentration in the Canada basin, *J. Geophys Res.* 94 (c8), 10,955-10,970.

Serreze, M.C., J.A. Maslanik, r.G. Barry and T.L. Demaris (1992), Winter atmospheric circulation in the arctic basin and possible relationships to the great salinity anomaly in the northern north atlantic, *Geophys. Res. Lett*, 19 (3), 293-296.

Serreze, M.C. and A.P. Barrett (2011), Characteristics of the Beaufort Sea High, *J. Climate*, 24, 159-182, doi: 10.1175/2010JCLI3636.1.

Sodhi, D.S. (1977), Ice arching and the drift of pack ice through restricted channels, Report 77-18, Cold Regions Research and Engineering Laboratory, Hanover, New Hampshire.

Sokolov,A . L. (1961), Drift of ice in the Arctic Basin and changes in ice conditions o ver the northern sea route, Probl.A rct. Antarct.,E ngl. Transl., 11, 1-20.

Steele, M., J. Zhang, D. Rothrock and H. Stern (1997), The force balance of sea ice in a numerical model of the Arctic Ocean, *J. Geophys. Research*, 102(C9), 21,061-21,079.

Stroeve, J.C., J. Maslanik, M.C. Serreze, I. Rigor, W. Meier and C. Fowler (2011), Sea ice response to an extreme negative phase of the Arctic Oscillation during winter 2009/2010, *Geophys. Res. Letters*, 38, L02502, doi: 10.1029/2010GL045662.

Stroeve, J.C., T. Markus, L. Boisvert, J. Miller and A. Barrett (2014), Changes in Arctic melt season and implications for sea ice loss, *Geophys. Res. Lett.*, 41, doi: 10.1002/2013GL058951.

Spreen, G., R. Kwok and D. Menemenlis (2011), Trends in Arctic sea ice drift and role of wind forcing: 1992-2009, *Geophys. Res. Letters*, 38, L19501, doi: 10.1029/2011GL048970.

Spreen, G., E. Hansen, R. Kwok, J. King and S. Gerland (2014), Changes in Fram Strait sea-ice volume export between 1992 and 2012 observed in combined ULS and satellite data, Presented at the International Glaciological Society – Sea Ice Symposium, Hobart, Australia, March 9-14, 2014.

Stern, H. L. and R.W. Lindsay (2009), Spatial scaling of Arctic sea ice deformation, *J. Geophys. Res.*, 114, C10017, doi: 10.1029/2009JC005380.

Thomas, D. (1999), The quality of sea ice velocity estimates, *J. Geophys. Res.* 104 (C6), 13,627-13,652.

Thompson, D.W.J. and J.M. Wallace (1998), The Arctic Oscillation signature in the wintertime geopotential height and temperature fields, *Geophys. Res. Lett*, 25 (9), 1297-1300.

Thorndike, A.S. and R. Colony (1982), Sea Ice Motion in Response to Geostrophic Winds, *J. Geophys. Research*, 87(C8), 5845-5852.

Vesecky, J.F., R. Samadani, M.P. Smith and J.M. Daida (1988), Observations of sea-ice dynamics using synthetic aperture radar images: Automated analysis, *IEEE transaction on Geoscience and Remote Sensing*, 26 (1), 38-47.

Vihma, T., P. Tisler and P. Uotila (2012), Atmospheric forcing on the drift of Arctic sea ice in 1989-2009, *Geophysical Research Letters*, 39, L02501, doi:10.1029/2011GL050118.

Vinje, T., N. Nordlund and A. Kvambekk (1998), Monitoring ice thickness in Fram Strait, *J. Geophys. Res.*, 103(C5), 10,437-10,449.

Wadhams, P. (1992), Sea ice thickness distribution in the Greenland Sea and Eurasian Basin, *J. Geophys. Research*, 97, 5331-5348.

Wadhams, P. (2000), Ice in the Ocean, Gordon and Breach Science Publishers, London UK, pp 351.

Weeks,W.F. (2010), On Sea Ice, University of Alaska Press, Fairbanks.

Woodgate, R.A., K. Aagaard and T.J. Weingartner (2006), Interannual changes in the Bering Strait fluxes of volume, heat and freshwater between 1991 and 2004, *Geophys. Res. Letters*, 33, L15609, doi: 10.1029/2006GL026931.

Yang, J. (2009), Seasonal and interannual variability of downwelling in the Beaufort Sea, *J. Geophys. Res.*, 114, C00A14, doi:10.1029/2008JC005084.

Zhang, J., D. Rothrock and M. Steele (2000), Recent Changes in Arctic Sea Ice: The interplay between Ice Dynamics and Thermodynamics, *J. Climate*, 13, 3099-3114.

Zhang, J., R. Lindsay, A. Schweiger and I. Rigor (2012), Recent changes in the dynamic properties of declining Arctic sea ice: A model study, *Geophys. Res. Lett.*39, L20503, doi:10.1029/GL053545.

Zubov, N.N (1945), Arctic Ice, English Translation: U.S. Naval Oceanographic Office (1963), 506 pp.

CHAPTER THREE: MULTIYEAR SEA ICE EXPORT THROUGH THE BERING STRAIT DURING WINTER 2011-2012

This paper has been published in the *Journal of Geophysical Research – Oceans*. The work represents a core chapter of my thesis that was conceived, analyzed and reported by me as the senior author.

Babb, D.G. R.J. Galley, M.G. Asplin, J.V. Lukovich and D.G. Barber (2013), Multiyear sea ice export through the Bering Strait during winter 2011-2012, *Journal of Geophysical Research – Oceans*, 118, 5489-5503, doi:10.1002/jgrc.20383.

Abstract:

Six ice beacons deployed in the Beaufort Sea during August 2011 tracked the anomalous export of multiyear sea ice from the Chukchi Sea through the Bering Strait to the Bering Sea between November 2011 and May 2012. These are the first observations in 34 years of ice beacon export through the Bering Strait. Using 34 years of passive microwave derived ice motion fields we find that during 2011-2012 southward ice motion in the Chukchi Sea persisted for a record six of seven months and that sea ice speeds were significantly faster than the long term mean. The combination of increased ice speeds and reduced likelihood of ice arch development through the strait culminated in the record export of 13.5 x 10^3 km^2 of sea ice through the Bering Strait. Monthly sea level pressure fields, dominated by an Aleutian Low and Siberian High, show anomalies in December and January played a role in initiating this event and forced multiyear ice into the southern Chukchi Sea. However these variations were small and typical of this area, yet we find no evidence of a similar export event in the last 34 years even though the forcing was similar to the climatology. This leads us to attribute this event to a change in the responsiveness of the Arctic ice pack to typical forcing mechanisms.

3.1 Introduction:

Arctic sea ice has undergone a dramatic transformation in recent years from an icescape dominated by multiyear sea ice (MYI) to one dominated by first year sea ice [*Nghiem et al.,* 2007; *Kwok et al.,* 2009; *Maslanik et al.,* 2011; *Comiso,* 2012; *Parkinson and Comiso,* 2013]. Inherent to this change is a thinner ice pack [*Comiso,* 2012] which in combination with recent reductions in sea ice extent [*Stroeve et al.,* 2011] has made the Arctic ice pack more mobile [*Rampal et al.,* 2009; *Spreen et al.,* 2011; *Galley et al.,* 2013; *Kwok et al.,* 2013]. Changes in ice thickness and an overall reduction in the mechanical strength of sea ice are cited as the primary driver of increasing ice motion velocities, with slightly increased wind velocities playing a smaller role [*Rampal et al.* 2009; *Spreen et al.* 2011; *Kwok et al.* 2013].

The summertime reduction of MYI extent is most significant in Arctic marginal seas, particularly in the Beaufort and Chukchi Seas [*Kwok and Cunningham,* 2010; *Comiso,* 2012]. Historically, 93% of MYI survived the summer melt in the Beaufort Sea, between 2006 and 2010 due to warming trends and anomalous sea ice melt [e.g. *Perovich et al.,* 2008] only 73% of MYI within the Beaufort Sea survived the summer [*Maslanik et al.,* 2011]. More recently, *Stroeve et al.,* [2011] showed that nearly all MYI in the Beaufort Sea during spring 2010 melted out that summer. However, the Beaufort Sea continues to receive MYI from the High Arctic along the western edge of the Canadian Arctic Archipelago (CAA) as part of the large scale anticyclonic sea ice circulation pattern known as the Beaufort sea ice gyre (BG) [*Lukovich and Barber,* 2006; *Kwok,* 2009; *Maslanik et al.,* 2011; *Galley et al.,* 2013]. As part of the BG sea ice in the Beaufort and Chukchi Seas drifts westward into the East Siberian Sea and Eastern Arctic [*Rigor et al.,* 2002; *Rigor and Wallace,* 2004; *Hutchings and Rigor,* 2012] where it is either recirculated in the BG or entrained in the Transpolar Drift Stream and exported south through Fram Strait

[*Gordienko,* 1958; *Rigor et al.,* 2002]. As much as 94% of all ice exported from the Arctic passes through Fram Strait [*Arfeuille et al.,* 2000] with an average areal extent of 706 x 10^3 km^2 yr^{-1} [*Kwok,* 2009].

Sea ice is also exported from the Arctic through Nares Strait, the CAA, the Barents Sea and the Bering Strait [*Aagaard and Carmack,* 1987]. The Barents Sea exports less than 1% of total ice export [*Alekseev et al.,* 1997] whereas between 5% [*Alekseev et al.,* 1997] and 20% [*Melling,* 1999] of total ice export passes through the CAA. Sea ice export through the CAA may be increasing as ice barriers that have historically impeded ice motion are weakening under a warmer atmosphere and increasing the mobility of sea ice within the CAA [*Howell et al.,* 2008; 2010]. Nares Strait exported an average of 33 x10^3 km^2 of sea ice between 1996 and 2002, most of which was thick multiyear sea ice from the northern coast of the CAA and Greenland, with a minimum ice flux during winter when ice arches impede ice drift [*Kwok,* 2005]. Under a warming climate and weakening ice pack these ice arches are less likely to form, allowing ice export to reach record levels of 87 and 77 x 10^3 km^2 in 2007 and 2008 [*Kwok,* 2010].

Gow and Tucker [1987] refer to the Bering Strait as a region of negligible ice export from the Arctic Ocean. *Aagaard and Carmack* [1989], citing personal communication with C. Pease, stated the Bering Strait imports 30 km^3 of ice into the Arctic annually, though sea ice can episodically pass south through the Bering Strait and enter the Bering Sea [*Pease,* 1980]. These export events occur once or twice a year and are correlated with reversals in ocean currents of the Bering Strait [*Pease* 1980], which flow predominantly northward [*Woodgate et al.,* 2006]. However, *Overland and Pease* [1982] clarified that southward sea ice export through the Bering Strait is driven by northerly surface winds resulting from the presence of the Siberian High, a strong atmospheric high pressure system situated north of the Bering Strait. Ice export through

the Bering Strait is limited because it is a converging channel in which ice arches may form during winter, impeding ice drift [*Sodhi,* 1977]. Ice arch formation is dependent on the channel width, ice shear strength and the wind velocity [*Kubat et al.,* 2006; *Hibler et al.,* 2006]. For the Bering Strait *Sodhi* [1977] calculated a critical wind speed of 5.6 m s^{-1} above which ice arches cannot form and ice can move freely through the channel.

The Siberian High is a typical atmospheric feature located to the north of the Bering Strait during fall and winter, developing over Siberia during fall and extending across the Pacific Arctic through winter [*Pickart et al.,* 2009] before transitioning into the Beaufort High during spring [*Overland,* 2009; *Serreze and Barrett,* 2011]. Opposing the Siberian High is the Aleutian Low, a typical atmospheric feature south of the Bering Strait that is highly variable, a reflection of Pacific cyclones that originate along the Asian coast and intensify across the North Pacific toward the Bering Sea and the Gulf of Alaska [*Pickart et al.,* 2009].

There are two typical wintertime configurations of mean sea level pressure (MSLP) patterns in the Bering Sea region: Type A means a deep Aleutian Low in the Gulf of Alaska with a Siberian High to the northwest with an associated ridge of high pressure extending east across the Pacific Arctic into the CAA. Type B means an Aleutian Low approaching a blocking high in the Gulf of Alaska with the Siberian High located over Siberia [*Pickart et al.,* 2009]. The blocking high is blocked in by the coastal mountain ranges of Alaska and Canada and subsequently forces Pacific cyclones and therefore the Aleutian Low to the north or south [*Pickart et al.,* 2009]. When deflected north, the Aleutian Low moves over the Bering Strait and Alaska, changing the orientation of the isobars, MSLP gradients and thus altering the wind patterns over the region.

MSLP patterns and the associated pressure gradients create surface winds which in the polar regions are a dominant factor in the forcing of sea ice motion [*Thorndike and Colony,* 1982; *Colony and Thorndike,* 1984; *Rigor et al.,* 2002]. During fall, winter and spring surface winds in conjunction with surface currents and internal stresses determine the speed and direction at which sea ice drifts [*Steele et al.,* 1997]. Surface winds and ocean currents contribute equally to sea ice motion on timescales longer than one year and drive the large-scale patterns of motion (e.g. BG and Transpolar Drift Stream) but on timescales of less than a year sea ice motion is variable and reflective of surface winds [*Thorndike and Colony,* 1982; *Colony and Thorndike,* 1984; *Rigor et al.,* 2002]. Ice motion is further complicated near coastlines where coastal influences increase turning angles and affect the ice momentum balance. A general rule of thumb is that sea ice in the northern hemisphere drifts at 2% of the speed and with a turning angle of 45^{o} to the right of surface winds [*Nansen,* 1902; *Colony and Thorndike,* 1982]. Sea ice drift can also be described by the 'isobaric drift law' which states that sea ice drifts along MSLP contours (isobars) [*Zubov,* 1945; *Thorndike and Colony,* 1982; e.g. *Kwok,* 1998; *Rigor et al.,* 2002; *Vihma et al.,* 2012]. Variations in MSLP which affect the orientation and gradient of the isobars alter the surface winds and therefore affect ice motion. Periods when ice motion does not follow the isobars are ascribed to either the increased role of ocean currents [*Rigor et al.,* 2002] or a local increase of internal stress in a compact ice field [*Kimura and Wakatsuchi,* 2000; *Vihma et al.,* 2012], such as along the western coast of the CAA where internal stress is greatest in the Arctic [*Bourke and Garrett,* 1987; *Steele et al.,* 1997; *Melling,* 2002].

The Bering Sea has experienced decreasing trends in sea ice concentration, thickness, duration and extent during recent years due to increases in air and water temperatures [*Overland and Stabeno,* 2004; *Grebmeier et al.,* 2006; *Parkinson and Cavalieri,* 2008]. Sea ice motion in

the Bering Sea has been described as a 'conveyor belt' [e.g. *Pease,* 1980; *Overland and Pease,* 1982; *Clement et al.,* 2004] which under northerly winds transport thin first year sea ice from the north to the southern edge of the ice pack where the ice encounters warmer Pacific surface waters and melts at its thermodynamic limit [*Pease,* 1980]. Maximum sea ice extent within the Bering Sea has an inherently high level of interannual and intra-annual variability [*Pease,* 1980; *Cavalieri and Parkinson,* 1987; *Clement et al.,* 2004; *Stabeno et al.,* 2007; *Parkinson and Cavalieri,* 2008] which is ascribed to the influence of Pacific cyclones [*Overland and Pease,* 1982; *Cavalieri and Parkinson,* 1987] and makes the slightly negative trend in sea ice extent non-significant [*Parkinson and Cavalieri,* 2008]. Due to the intra-annual variability within the Bering Sea the maximum extent of sea ice can be observed as early as January or as late as May [*Stabeno et al.,* 2007] with a mean of March 11th at a mean latitude of 58.1°N [*Francis and Hunter,* 2007]. *Overland and Pease* [1982] and subsequently *Clement et al.* [2004], define high ice years as years during which ice reaches St. Paul Island (57.3°N, 170.3°W) and low ice years as years during which ice only reaches St. Matthew Island (60.7°W, 166.5°W). During the winter of 2011-2012 sea ice extended past St. Paul Island and the Bering Sea experienced its second highest sea ice extent in the satellite record which interrupted winter fishing operations and fuel re-supply missions to northern Alaskan towns [*NSIDC* 2012].

We present ice beacon data from September 2011 to May 2012 that showed MYI export from the Arctic through the Bering Strait into the Bering Sea. Satellite-derived ice motion fields show persistent southward motion through the Bering Strait occurred between November 2011 and May 2012, exporting 17 x 10^3 km^2 of sea ice into the Bering Sea. MSLP observations indicate that this event occurred under typical atmospheric winter conditions for this region. We then set the historical context of this export using 34 years of historic ice beacon and space-borne

passive microwave derived ice motion data. Lastly, we compare the monthly MSLP patterns of 2011-2012 to the 34-year MSLP climatology of the study region to determine if anomalous MSLP during 2011-2012 drove the export event.

3.2 Methods:

From 11 to 26 August 2011 a multidisciplinary cruise took place in the Southeastern Beaufort Sea aboard the Canadian research icebreaker *CCGS Amundsen* as part of a collaborative project between ArcticNet and industry partners at Imperial Oil Research Ventures Ltd. We identified large MYI floes within the high (8-9+/10) concentration MYI summer sea ice tongue at about 74°N, 127°W [e.g. *Hutchings and Rigor* 2012; *Galley et al.,* 2013] to which we moored the ship and proceeded to instrument (Figure 3.1). Primary site 1 (S1) was a vast MYI floe measuring roughly 3km x 1km and primary site 2 (S2) was a big MYI floe measuring 1km x 0.4km. Several similarly sized secondary sites surrounding the primary sites were also visited and sampled. Sea ice temperature, thickness and salinity were measured by coring samples at each primary and secondary site and an ice beacon (Canatec Associates Ice Beacon, 15 minute GPS location interval, iridium transmission) was deployed at each site. Of the 15 ice beacons deployed, nine failed during September and October, while the remaining six drifted towards the Chukchi Sea and provide the motivation for this paper.

Ice beacons are housed in a weather/waterproof cylinder and deployed in an auger (8" diameter) hole drilled 18" deep into the ice in order to keep the Iridium and GPS antennae facing upwards. Autonomous ice beacons have been used to study sea ice dynamics in the Arctic since the 1970's [e.g. *Colony and Thorndike,* 1984; *Rampal et al.,* 2009]. The International Arctic Buoy Program (IABP) has an historical archive that consists of 3 hourly positions from 1978 to December 2001 and 12 hourly positions from January 2002 to present (available online at

ftp://iabp.apl.washington.edu.pub.IABP/C) [*Rampal et al.*, 2009]. We use this archived dataset to provide the historical context of ice export through the Bering Strait.

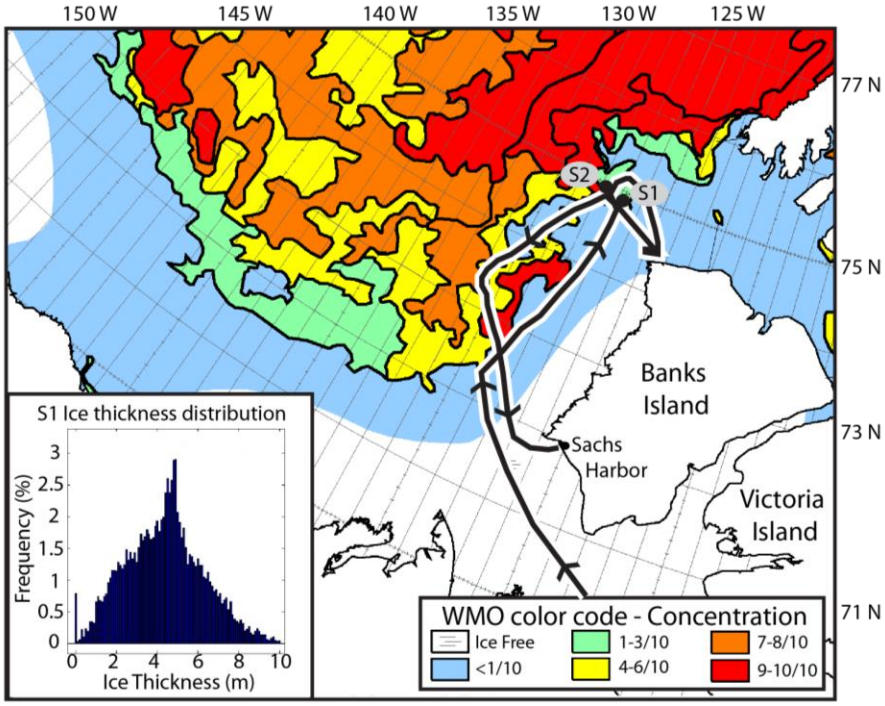

Figure 3.1: Canadian Ice Service Western Arctic ice chart for August 15th, 2011. The ship track (black line) of the CCGS Amundsen is overlaid on the ice chart along with primary study sites S1 and S2. The inset provides the ice thickness distribution from S1 which was collected using the HEMI system

Ice thickness measurements were made via aerial surveys using a helicopter-mounted electromagnetic induction system (HEMI) [*Peterson et al.*, 2008; e.g. *Barber et al.*, 2009; *Galley et al.*, 2013], and point samples of ice thickness on the primary sites and secondary sites were obtained by manual measurements with a measuring tape through auger (2" diameter) holes.

To expand our ice beacon data spatially, Polar Pathfinder daily 25km EASE-GRID sea ice motion vectors derived from a combination of data from the IABP, passive microwave (Scanning Multichannel Microwave Radiometer and Special Sensor Microwave/Imager) and optical remote sensing platforms (Advanced Very High Resolution Radiometer) [*Fowler*, 2010] were provided by the National Snow and Ice Data Center (NSIDC). M. Tschudi at NSIDC provided the updated dataset of *Fowler* [2010] up to June 2012. Mean monthly fields of ice motion for the area

surrounding the Bering Strait were calculated for September 2011 to May 2012. Monthly mean heading (°) and ice drift velocity (cm s^{-1}) were derived from a region of interest (ROI) located in the southern Chukchi Sea (black box in Figure 3.2). We define southward motion as any month with a mean heading between 135° and 225° (dotted lines in the ROI in Figure 3.2). The ice motion fields were also used to calculate ice area fluxes into and out of the Chukchi Sea through three gates (dot-dash lines in Figure 2), 1) the Bering Strait (75 km in length, 3 samples), 2) The Chukchi Sea between Pt. Barrow and Wrangel Island (625km in length, 25 samples), and 3) the De Long Strait between Wrangel Island and Siberia (106km in length, 3 samples). Gates 2 and 3 were summed to provide a total ice flux between the Chukchi Sea and the Arctic Ocean. Following *Kwok,* [2009] the monthly mean ice flux (F) (km^2 month^{-1}) was calculated using the following equation:

$$F = \sum c_i u_i \, \Delta x \qquad (1)$$

where, c_i is the monthly mean sea ice concentration, u_i is the monthly mean velocity component normal to the gate and Δx is the size of the pixel (i.e. 25km). Monthly mean ice concentrations were extracted from the NSIDC dataset Sea Ice Concentrations from Nimbus-7 SMMR and DMSP SSM/I-SSMIS Passive Microwave Data [*Cavalieri et al.,* 1996 updated 2013]. Positive fluxes represent positive meridional (northward) ice transport into the Chukchi Sea from the Bering Sea and into the Arctic Ocean from the Chukchi Sea. Negative fluxes represent negative meridional (southward) ice transport out of the Arctic Ocean into the Chukchi Sea and into the Bering Sea from the Chukchi Sea. Following *Kwok* [2009] the error in ice flux (σ_f) calculations is determined using the following equation:

$$\sigma_f = \sigma_e L/\sqrt{N} \qquad (2)$$

where, σ_e is the error in ice drift velocities with a maximum value of 0.412 cm s^{-1} (0.356 km d^{-1}) [*Fowler,* 2010], *L* is the gate width (km) and *N* is the number of samples across the gate. The uncertainty in ice flux calculations for the Bering Strait, Chukchi Sea and De Long Strait gates are approximately ±15, ±128 and ±22 km^2 d^{-1}, respectively. The summed error for the period of November 1 to May 31 across the Bering Strait is approximately ±3.1 x 10^3 km^2, while the daily errors from the other two gates sum to a total error of ±31.6 x 10^3 km^2 for the total November to May ice flux between the Chukchi Sea and Arctic Ocean. Due to the interpolation process used to derive the *Fowler* [2010] ice motion dataset errors may exist within pixels near coastlines. The ice drift vectors within the Bering Strait are noted as being within 25km of the coast and are therefore subject to errors associated with coastal influences [*Fowler,* 2010]. Analysis from both the ROI ice drift and ice flux gates are used to assess the historical context of ice motion and transport during winter 2011-2012 against the 1979-2011 historical record.

MSLP data were acquired from the National Oceanic and Atmospheric Administration's (NOAA) National Center for Environmental Prediction's (NCEP) re-analysis 2 dataset [*Kalnay et al.,* 1996; *Kanamitsu et al.,* 2002]. Monthly means for the period of September 2011 to May 2012 for the region encompassing the Beaufort, Chukchi, East Siberian and Bering Seas were calculated. MSLP climatology of the same region was created from 34 years (1979-2012) of the NCEP re-analysis 2 dataset and used to determine monthly MSLP anomalies during our study period.

The Alaska State Climate Center provided hourly wind data from the NOAA weather stations located at Gambell (63.78°N, 171,73°W) and Pt. Hope (68.35°N, 166.8°W) (Figure 3.2) from which we calculated monthly mean wind vectors derived from a 3-cup anemometer at a height of 10m.

3.3 Results

3.3.1 2011-2012 Ice export event

The Canadian Ice Service ice chart for the western Arctic from 15 August 2011 encapsulates the general conditions in the Beaufort Sea in mid-August 2011 (Figure 3.1). Helicopter-based ice thickness measurements performed within a 25km radius of our sites S1 (3km x 1km) and S2 (1km x 0.4km) provided mean thicknesses of 6.49m and 6.69m, respectively. A sample of the ice thickness distribution for S1 and its surrounding ice are provided (Figure 3.1: inset). The ice thickness distribution shows a modal thickness of 5.0m with a mean of 4.36m and a long right-hand tail extending to the HEMI's maximum reading of 10m indicative of thick MYI.

Six ice beacons (named A-F) deployed on MYI in the Beaufort Sea during August 2011 tracked the anomalous export of MYI from the Chukchi Sea through the Bering Strait during the winter of 2011-2012 (Figure 3.2 and Table 3.1). The beacon tracks in Figure 3.2 are not continuous due to periods during which beacon transmissions were not received (Table 3.1). We highlight Beacon E (Figure 3.2), which ceased communication in November near Pt. Barrow, but began communicating in May in the western Bering Sea as it drifted towards the Kamchatka Peninsula where it ceased transmitting. During high ice years thin first year sea ice from the Bering Sea may drift along the Kamchatka Peninsula [*Polyakova,* 2007], but there is no evidence of MYI from the Arctic Ocean drifting along Kamchatka. Beacon A (Figure 3.2) drifted at speeds up to 10 cm s^{-1} during December before slowing down to ~2 cm s^{-1} during January, February and March as it drifted south through the Bering Strait. Beacon A was the only ice beacon to transmit continuously as it passed southwards through the Bering Strait, but three

beacons (A, B and E) deployed on MYI in the Beaufort Sea during August 2011 were exported through the Bering Strait during the winter and spring of 2012.

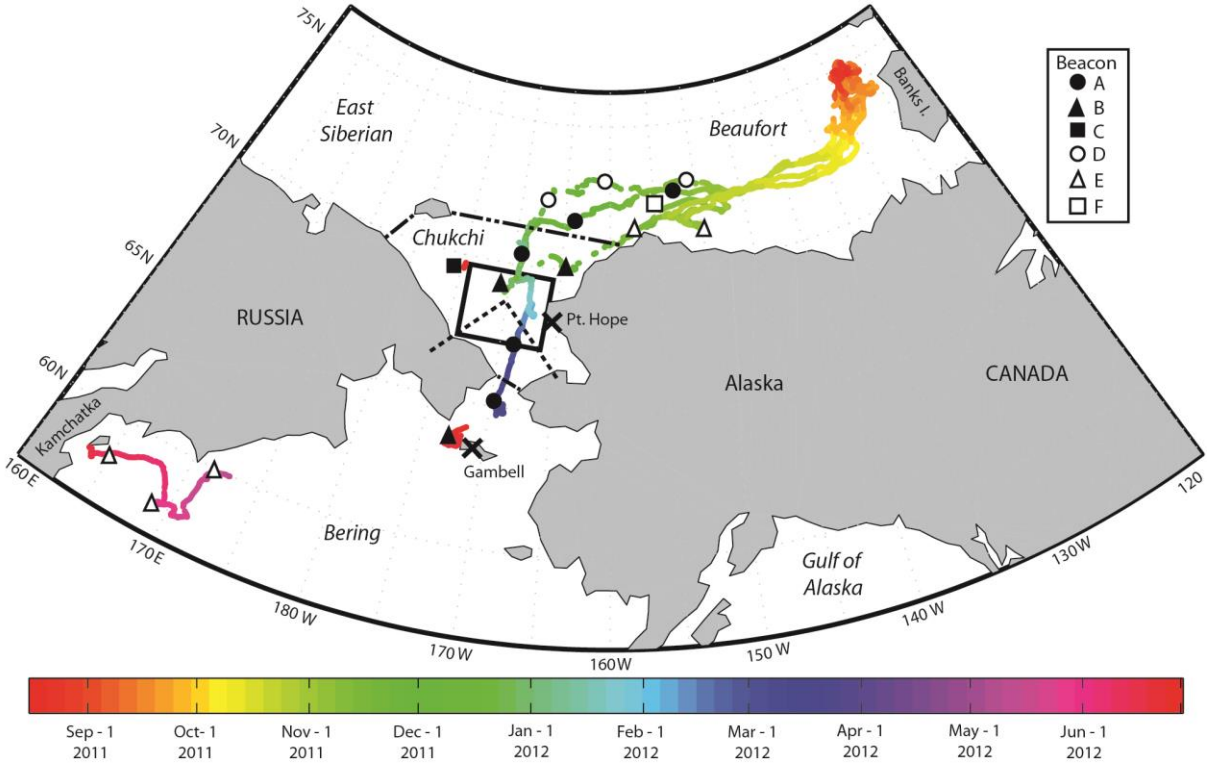

Figure 3.2: Ice beacon tracks color-coded by date from their initial location in the Beaufort Sea in August 2011, to their final locations in the Chukchi and Bering Seas. The black box north of the Bering Strait represents the region of interest (ROI) used to define monthly mean speed and direction of ice in the analysis of satellite derived ice motion fields for 2011-2012 and the historic 34-year record. Short dashed black lines from the ROI define the 135° and 225° (clockwise from 0° North) limits which we use to define southward ice motion. NOAA weather station data was used from Pt. Hope and Gambell, Alaska. Long dashed black lines represent the three ice flux gates 1) Bering Strait, 2) Chukchi Sea and 3) De Long Strait; the latter two are summed to represent ice flux between the Chukchi Sea and the Arctic Ocean.

Table 3.1: Summary of six ice beacons (A-F) and the dates (MM/DD/YY) during which they transmitted

	Deployed	Ceased Transmitting	Back on-line	Failed
A	8/15/12	3/30/13	----------	----------
B	8/18/12	12/20/12	6/19/13	7/15/13
C	8/18/12	10/18/12	6/25/13	7/01/13
D	8/18/12	1/12/13	----------	----------
E	8/18/12	11/15/12	5/13/13	7/05/13
F	8/16/12	1/01/13	----------	----------

The ice beacon data coincide with the general regional ice motion pattern shown in basin scale monthly mean fields of ice motion from September 2011 to May 2012 (Figure 3.3 and Table 3.2). In the Beaufort Sea during September (Figure 3.3A) and October (Figure 3.3B) sea ice drifted southwest from west of Banks Island (Figure 3.1) towards the Chukchi Sea. *Hutchings and Rigor* [2012] showed this southwestward motion is typical of the southern Beaufort Sea, and acts to pull the MYI tongue into the Chukchi Sea. In November (Figure 3.3C) 7.6 x 10^3 km^2 of sea ice entered the southern Chukchi Sea from the Arctic Ocean, drifting southwards through the ROI (225° at 0.83 cm s^{-1}) (Table 3.2) as the export event of 2011-2012 began with 0.4 x 10^3 km^2 of sea ice passing through the Bering Strait into the Bering Sea. In December (Figure 3.3D) sea ice within the Chukchi Sea drifted southwards at high speeds (up to 10 cm s^{-1}), driving the largest ice fluxes of 2011-2012 into the Chukchi Sea (94 x 10^3 km^2) and into the Bering Sea (4.0 x 10^3 km^2). January (Figure 3.3E) was characterized by a reduction in drift speeds but southward ice motion persisted (135° at 2.47 cm s^{-1}) as 41 x 10^3 km^2 of sea ice entered the Chukchi Sea from the East Siberian Sea, and 1.5 x 10^3 km^2 of sea ice drifted southwards into the Bering Sea. The imbalance of input and output across the two gates suggests that the ice pack within the Chukchi Sea was "locked up" [after *Steele et al.,* 1997] and was thus subject to high internal stresses and was dynamically active. In February (Figure 3.3F) and March (Figure 3.3G) southward ice motion through the ROI (1.75 and 1.35 cm s^{-1}) and ice export into the Bering Sea (2.7 x 10^3 and 3.6 x 10^3 km^2, respectively) persisted for a fourth and fifth straight month. Although slower wind speeds prevailed during these months (Figure 3.4) we attribute the reduction in ice speed to high internal stresses that result from the imbalance of sea ice entering and exiting the Chukchi Sea. April (Figure 3.3H) was the first month of winter 2011-2012 that ice in the ROI did not drift south (277° at 0.45 cm s^{-1}) (Table 3.2) and that ice was imported into

the Arctic Ocean from the Chukchi Sea (16 x 10^3 km^2), though for the sixth straight month ice was exported through the Bering Strait (0.3 x 10^3 km^2). During May (Figure 3.3I), ice within the ROI returned to a southern heading (214° at 0.72cm s^{-1}) as 0.9 x 10^3 km^2 of sea ice was exported into the Bering Sea. Between November 2011 and May 2012 159 x 10^3 km^2 of sea ice was exported from the Arctic Ocean into the Chukchi Sea and 13.5 x 10^3 km^2 of sea ice was exported through the Bering Strait into the Bering Sea. The Bering Strait exported roughly 20% as much sea ice as was exported through Nares Strait during its maximum in 2007 [*Kwok,* 2010] and 2.4% of the mean ice export through Fram Strait [*Kwok,* 2009]. During June and July (not shown) the ice edge melted and retreated north into the Arctic Ocean en route to a record minimum sea ice extent in September 2012.

Mean monthly plots of MSLP over the region encompassing the Beaufort, Chukchi, Bering and East Siberian Seas are presented in Figure 3.4. Overlaid on these plots are observed 10-m winds collected by NOAA weather stations north of the Bering Strait at Pt. Hope, Alaska and south of the Bering Strait at Gambell, Alaska on St. Lawrence Island (positions noted on Figure 3.2). The Aleutian Low is centered in the Gulf of Alaska from September (Figure 3.4A) to November (Figure 3.4C). It deepens during December (Figure 3.4D) and February (Figure 3.4F) before weakening in March (Figure 3.4G) and retreating to the Gulf of Alaska during April (Figure 3.4H) and May (Figure 3.4I). During December the Aleutian Low is forced to the northwest over the Bering Strait and Alaska by a blocking high located over the western Canadian coast and connects with a low located over the CAA (wintertime MSLP configuration type B) after [*Pickart et al.,* 2009]. During November (Figure 3.4C), we see the normal climatological development of the Siberian High over continental Siberia *Pickart et al.* [2009]. The Siberian High strengthens through December (Figure 3.4D) and January (Figure 3.4E) while

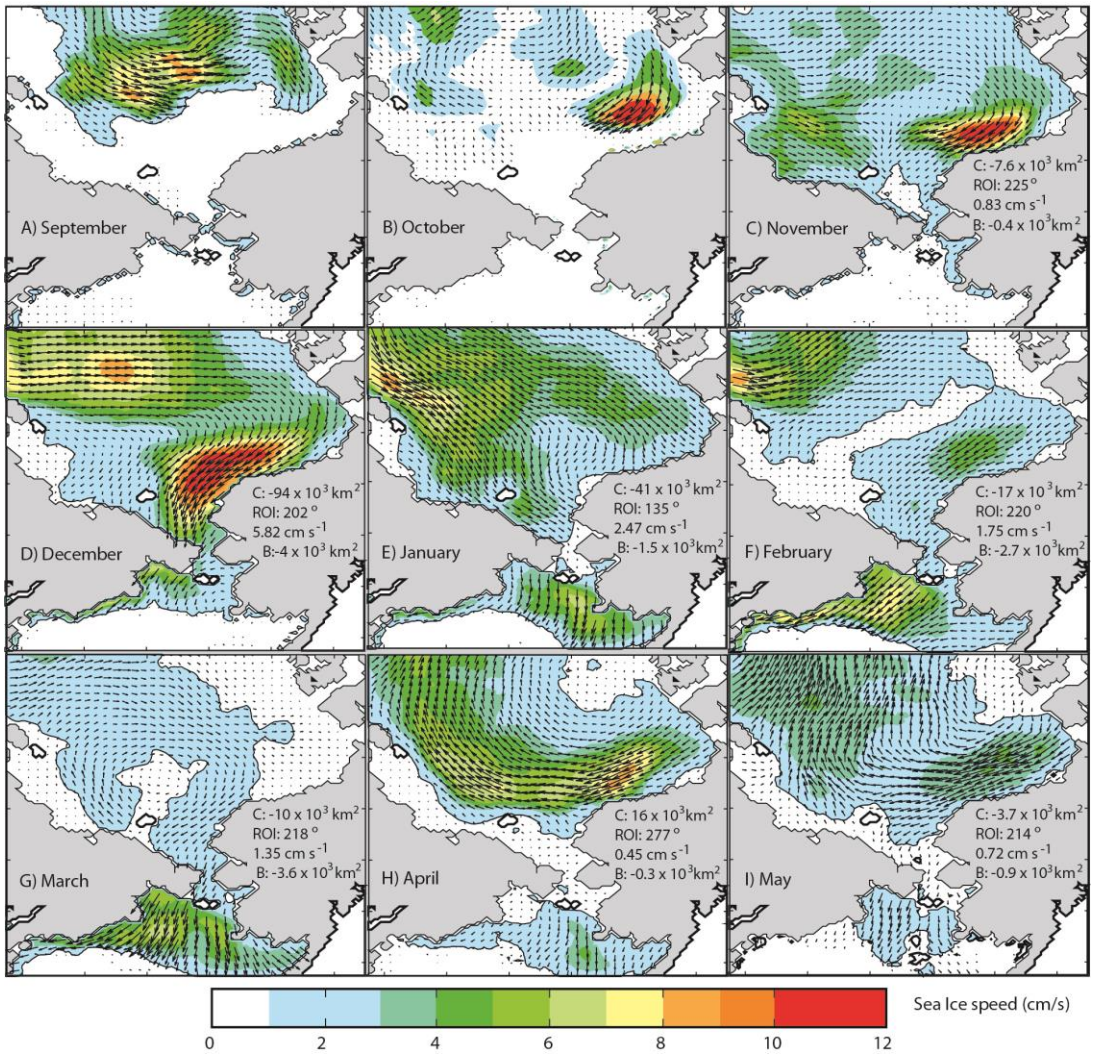

Figure 3.3: Monthly (September 2011 to May 2012) means of ice motion (NSIDC Polar Pathfinder 25km EASE grid vectors) are presented for the area encompassing the Bering Sea and Pacific Arctic. Vectors show mean direction of motion while colour contours show the speed (cm s^{-1}). Monthly mean speed and heading (°) of ice motion within the ROI and ice flux (km^2) across the Bering Strait and Chukchi Sea are provided for each month.

expanding across the East Siberian, Chukchi and Beaufort Seas as it approaches the CAA. By February (Figure 3.4F) the Siberian High covers the entire Pacific Arctic and subsequently strengthens through March (Figure 3.4G) and April (Figure 3.4H) as it transitions to the Beaufort High [*Overland* 2009; *Serreze and Barrett* 2011].

Collectively the Siberian High and Aleutian Low create a strong pressure gradient across the Bering Strait from September 2011 to May 2012 which is reflected in persistent northerly

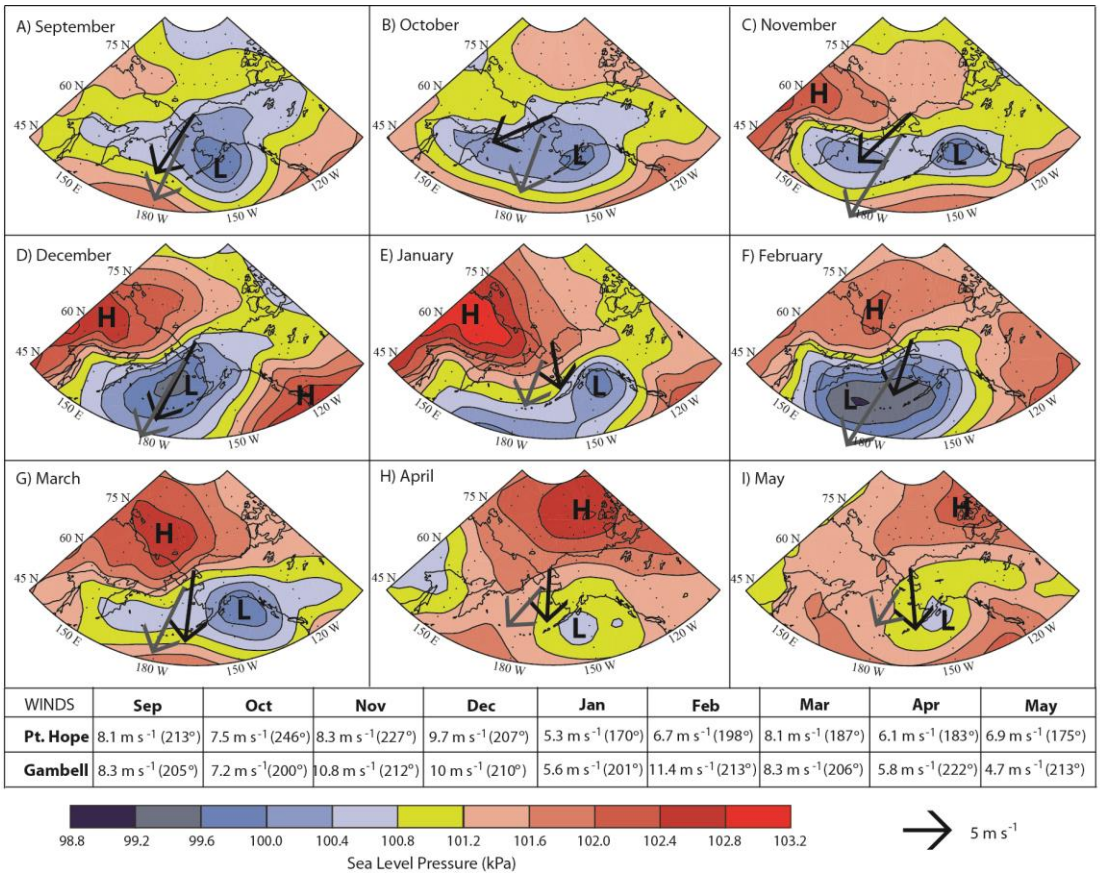

WINDS	Sep	Oct	Nov	Dec	Jan	Feb	Mar	Apr	May
Pt. Hope	8.1 m s^{-1} (213°)	7.5 m s^{-1} (246°)	8.3 m s^{-1} (227°)	9.7 m s^{-1} (207°)	5.3 m s^{-1} (170°)	6.7 m s^{-1} (198°)	8.1 m s^{-1} (187°)	6.1 m s^{-1} (183°)	6.9 m s^{-1} (175°)
Gambell	8.3 m s^{-1} (205°)	7.2 m s^{-1} (200°)	10.8 m s^{-1} (212°)	10 m s^{-1} (210°)	5.6 m s^{-1} (201°)	11.4 m s^{-1} (213°)	8.3 m s^{-1} (206°)	5.8 m s^{-1} (222°)	4.7 m s^{-1} (213°)

Figure 3.4: Monthly (September 2011 to May 2012) MSLP for the region surrounding the Bering Strait. Monthly mean wind vectors from the Pt. Hope (black arrow) and Gambell (grey arrow), Alaska NOAA weather stations are overlaid on these plots with monthly mean wind speed (m s^{-1}) and direction given in the table below the Figure.

monthly mean winds at Pt. Hope and Gambell, Alaska (Figure 3.4). Table 2 summarizes the monthly mean ROI ice speed and direction, monthly mean 10m wind speed and direction from Pt. Hope, and the ratio between ice and wind speeds and the turning angle. The comparison of coastal wind station data to offshore ice motion is not precise but the coastal winds do provide a sense of wind speed and direction that is complimentary to the MSLP analysis. When ice was present in the ROI (November 2011 – May 2012) the monthly mean wind direction was predominantly southward at both Pt. Hope (170° to 227°) and Gambell (201° and 222°). For all months but January monthly mean wind speeds were higher than the critical wind speed of 5.6 cm s^{-1} (Figure 3.4), which *Sodhi* [1977] found to be the fastest speed to allow ice arches to form

across the Bering Strait. Therefore, high wind speeds reduced the likelihood of ice arch formation, increasing the mobility of sea ice through the Bering Strait during 2011-2012. The fastest monthly mean wind speed for the Pt. Hope station was recorded during December 2011 (9.72 m s^{-1}) coinciding with peaks in ROI ice drift speed (5.82 cm s^{-1}), ice flux into the Chukchi Sea (103 x 10^3 km^2) and ice flux through the Bering Strait (4.8 x 10^3 km^2). In free drift ice will drift 45° to the right of surface winds with the geostrophic winds, however internal stresses within the ice pack can reduce the turning angle [*Kimura and Wakatsuchi,* 2000; *Vihma et al.,* 2012] which is what our analysis suggests. Sea ice turning angles were lowest during November and December and highest during April, with an anomalous negative turning angle during January (Table 3.2). The turning angle of -35° during January is attributed to high internal stresses within the ice pack resulting from the drift of ice from the East Siberian Sea into the Chukchi Sea (Figure 3E) along the isobars of the Siberian High (Figure 3.4E). Typical turning angles prevailed during February, March and May but a high turning angle of 74° in April (Table 3.2) shows that ice within the Chukchi Sea drifted west as part of the BG and not southwest as we would expect under persistent northerly winds at Pt. Hope. Overall ice within the ROI drifted between 0.07% and 0.60% of 10m wind speeds, lower than the typical 2% and likely due to

Table 3.2: ROI ice drift (Figure 3) and Pt. Hope 10m wind (Figure 4) comparison through the 2011-2012 event. Ice drift to the right of surface winds has a positive turning angle.

	ROI ice drift		**Pt. Hope 10m winds**		**Ice: Wind comparison**	
	Speed (cm s^{-1})	Heading (°)	Speed (m s^{-1})	Heading (°)	Speed ratio (%)	Turning angle (°)
Sep	----	----	8.05	213°	----	----
Oct	----	----	7.50	246°	----	----
Nov	0.83	225°	8.30	227°	0.10%	-2°
Dec	5.82	202°	9.72	207°	0.60%	-5°
Jan	2.47	135°	5.28	170°	0.47%	-35°
Feb	1.75	220°	6.67	198°	0.26%	22°
Mar	1.35	218°	8.05	187°	0.17%	31°
Apr	0.45	277°	6.10	183°	0.07%	74°
May	0.72	214°	6.94	175°	0.10%	39°

coastal constriction of the ice pack leading to increased internal stress. We also see a seasonal decrease from December to April as internal stresses increase within the ROI and reduce the responsiveness of ice to surface winds.

During winter 2011-2012 northerly winds at Gambell, Alaska and thus southward ice motion within the Bering Sea conveyor belt persisted from December (Figure 3.3D) to May (Figure 3.3I) and led to the second highest recorded sea ice extent in the Bering Strait [NSIDC 2012]. The conveyor belt [*Overland and Pease,* 1982] transported Beacon E and its associated MYI into the western Bering Sea and onto the Kamchatka Peninsula (Figure 3.2). The fastest monthly mean wind speed of 11.39 m s^{-1} was recorded at Gambell during February (Figure 3.4E) and caused a peak in Bering Sea ice drift speeds of 8 cm s^{-1}. During April and May ice drift slowed to ~2 cm s^{-1} under the force of 5.83 cm s^{-1} and 4.72 cm s^{-1} northerly winds at Gambell. Sea ice within the Bering Sea drifted between 0.3% (April) and 1.08% (January) of 10m wind speeds measured at Gambell. Ice consistently drifted to the right of the surface winds, indicative of an ice pack with low internal stress able to respond to the Coriolis force.

3.3.2 Historical Context

3.3.2.1 Sea Ice historical context

To set the historical context of this 2011-2012 sea ice export we use historic ice beacon data from the IABP and historic fields of ice motion from the Polar Pathfinder 25km-EASE grid data product provided by the NSDIC. For both datasets we examine the record from January 1979 to May 2012 to determine the timing and frequency of past export events.

Our analysis of the IABP dataset revealed that of the 910 ice beacons deployed in the Arctic between 1979 and 2012, 544 have passed through the our initial study region of the Beaufort Sea (70°N – 76°N, 140°W – 122°W), 31 of which have drifted past Pt. Barrow and

entered the Southern Chukchi Sea (Chukchi Sea ice flux gate – Figure 3.2) and none have passed southwards through the Bering Strait. In fact, no ice beacon deployed in the Arctic has ever been exported south through the Bering Strait. Instead ice beacons from the Beaufort Sea drift west through the Chukchi Sea and either continue to drift west into the East Siberian Sea or drift north into the central Arctic Basin as part of the BG [*Hutchings and Rigor*, 2012] (grey lines in Figure 3.5A and 3.5B).

In Figure 3.5A we highlight five IABP beacons which travelled southwards in the Chukchi Sea for prolonged periods. IABP beacons 3165 (yellow) and 3836 (red) were deployed on MYI [I. Rigor, personal communication, 2013] in August 1985 and drifted south in the Chukchi Sea between December 1985 and February 1986 when Beacon 3836 failed ~100 km north of the Bering Strait and 3165 began drifting north until it failed in the fall of 1986. IABP beacons 97800 (green) and 99800 (blue) were deployed in open water in the Chukchi Sea in October 2009 but were within 90-100% ice concentration (IABP website) by November 29th and are representative of the drift of young ice as of that date [I. Rigor, personal communication, 2013]. Beacons 97800 and 99800 drifted south-southwest towards the northeast coast of Siberia where they failed in late December 2009, ~300 km northwest of the Bering Strait. IABP beacon 83726 (purple) was deployed in the High Arctic (82°N, 150°W) in the fall of 2008. After two years in the BG it entered the Chukchi Sea and drifted near the Siberian coast during the winter of 2010-2011 before drifting north past Wrangel Island into the East Siberian Sea during spring 2011 (Figure 3.5A). This highlights the possible export of young first year ice during November and December 2009 and the possible export of MYI during December 1985, January 1986, and winter 2010-2011. However none of these beacons passed through the Bering Strait, instead

drifting to the southwest towards the Siberian coast (Figure 3.5A) instead of south like Beacon A (Figure 3.2).

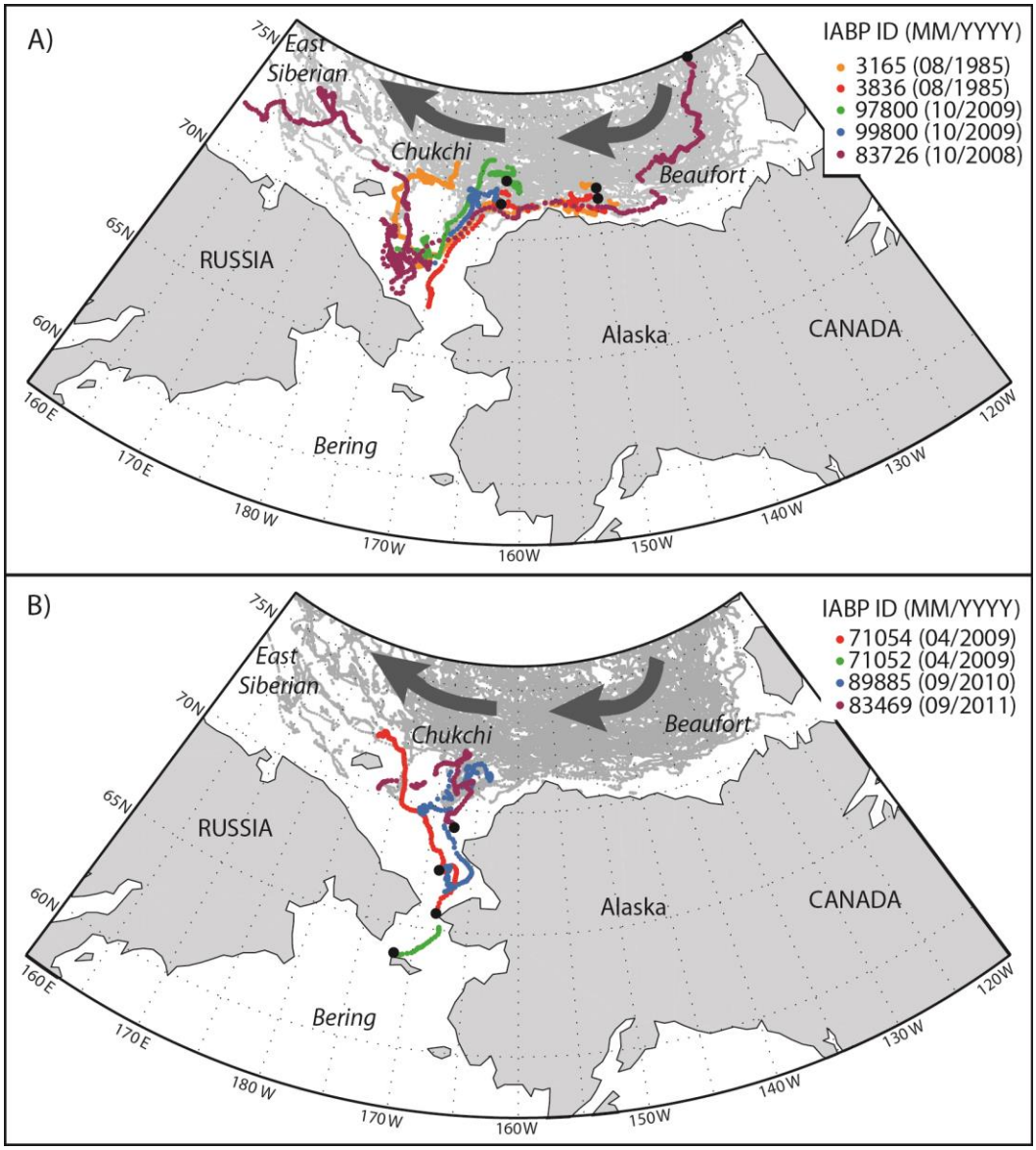

Figure 3.5: Historic IABP ice beacon data in our study region (grey lines - dark grey arrows show the prominent westward direction) with IABP ID and date (MM/YYYY) of deployment in the legend. Black dots represent the starting point of the beacons drift. Figure 5A highlights the drift of 5 ice beacons that drifted south in the Chukchi Sea towards the Bering Sea, though none passed through the Bering Strait. Figure 5B highlights the drift of 4 ice beacons deployed near the Bering Strait or in the southern Chukchi Sea near our ROI.

We also highlight four IABP ice beacons deployed in the southern Chukchi Sea near the Bering Strait, which drifted north during spring, summer and fall (Figure 3.5B). IABP beacons

71054 (red) and 71052 (green) were deployed in the Bering Strait in April 2009. Beacon 71052 drifted north for two weeks before failing and 71054 drifted north with the retreating ice pack until it failed in August 2009. IABP beacons 89885 (blue) and 83469 (purple) were deployed in the southern Chukchi Sea in September 2010 and September 2011, respectively, and both beacons drifted north during October and November. Beacon 89885 was in the Chukchi Sea during December 2011 and began drifting to the southwest as part of our export event, before it failed in late December. These four cases demonstrate that sea ice can be imported and advected northwards from the Bering Strait into the Arctic Ocean during spring, summer and fall. No IABP beacons have captured the northward advection of sea ice through the Bering Strait into the Arctic Ocean during winter.

We analysed historic satellite-derived ice motion fields to see if 2011-2012 patterns of ice motion have occurred previously. The monthly means of ice motion for the ROI (Figure 3.2) for November to May for 1979-2012 are presented in Table 3. Months with southward headings are shown in bold in Table 3.3. Southward motion is most frequent during December (11/33 years (33%)) and January (14/34 years (41%)), followed by a decline in the frequency of southward motion until May when southward motion has only been observed twice, in 1988 and in 2012. Between the winters of 1979-1980 and 1998-1999 southward ice motion within the ROI never occurred during consecutive months. Since the winter of 1999-2000 southward ice motion has occurred during December and January five times (1999-2000, 2001-2002, 2004-2005, 2005-2006 and 2011-2012) and in two of those years (2004-2005 and 2011-2012) southward ice motion persisted into February (Table 3.3). During the 2011-2012 export event southward ice motion continued into March, marking the first time in 34 years that southward ice motion had persisted for five straight months in the region. Not only was the event of 2011-2012 anomalous

in the duration of southward motion but the speed with which the ice drifted (Table 3.3) in December, January and February was significantly ($p < 0.01$) faster than the long term monthly means. Ice drift during April and May was significantly ($p < 0.01$) slower than the long term mean, a reflection of the increased internal stresses which opposed ice motion and forced ice drift to directionally vary from the geostrophic winds [e.g. *Vihma et al.,* 2012]. At no time since 1979 has ice in the southern Chukchi Sea drifted south towards the Bering Strait for as long a time or with the significantly higher speeds that we observed during the winter of 2011-2012 (Table 3.3).

Using the ice motion fields we quantify the area of ice (km^2) that was exchanged across the Bering Strait and between the Chukchi Sea and Arctic Ocean during our study period and the previous 34 years (Figure 3.6). The largest southward fluxes in 34 years occurred for each gate during 2011-2012 as 159 x 10^3 km^2 of sea ice entered the Chukchi Sea from the Arctic Ocean and 13.5 x10^3 km^2 of sea ice was exported through the Bering Strait into the Bering Sea (Figure 3.6). The exchange of ice between the Arctic Ocean and Chukchi Sea is highly variable as positive (northward) fluxes occurred during 19 of 33 years with negative (southward) fluxes during 14 of 33 years. Between 1979-1980 and 2010-2011 an annual average of 3.8 x 10^3 (±57 x 10^3) km^2 of sea ice entered the Arctic Ocean from the Chukchi Sea, with a peak positive (northward) flux of 175 x 10^3 km^2 in 2008-2009 and peak negative (southward) flux of -159 x 10^3 km^2 during 2011-2012 (Figure 3.6). On average 64.5% of the net (November to May) ice flux between the Arctic Ocean and Chukchi Sea occurs through the De Long Strait between Wrangel Island and Siberia. On average sea ice is exported from the Arctic Ocean into the Chukchi Sea during November, December and January, while the opposite occurs during February, March, April and May. December 2011 and January 2012 exported over four times

and three times their respective monthly mean ice fluxes from the Arctic Ocean into the Chukchi Sea During February, March and May 2012 ice was uncharacteristically exported from the Arctic Ocean into the Chukchi Sea.

*Table 3.3: Mean ice drift direction (°) and speed (cm s^{-1}) from the ROI for the months of November to May for each winter since 1979. Bold cells denote months with southern headings (between 135° and 225° from 0° North). Our export event from 2011-2012 is highlighted with an * in the last two rows of the table.*

	January	**February**	**March**	**April**	**May**		**November**	**December**
	Head (°) Spd (cm s^{-1})	**Head (°) Spd (cm s^{-1})**	**Head (°) Spd (cm s^{-1})**	**Head (°) Spd (cm s^{-1})**	**Head (°) Spd (cm s^{-1})**		**Head (°) Spd (cm s^{-1})**	**Head (°) Spd (cm s^{-1})**
1979	279 (0.68)	298 (0.40)	232 (0.66)	***215 (0.22)***	310 (1.06)		---	292 (0.35)
1980	258 (1.10)	292 (1.00)	235 (0.74)	295 (0.15)	278 (1.40)		---	17 (0.17)
1981	327 (0.13)	234 (0.13)	236 (0.32)	327 (0.66)	336 (0.58)		---	283 (1.97)
1982	269 (1.93)	116 (0.63)	257 (0.62)	240 (1.21)	291 (0.94)		---	262 (2.91)
1983	286 (0.71)	***200 (0.88)***	***224 (0.79)***	356 (0.56)	322 (0.88)		227 (1.54)	310 (2.37)
1984	126 (0.85)	132 (1.38)	***163 (0.38)***	345 (0.48)	347 (1.88)		---	277 (2.76)
1985	259 (0.48)	105 (0.45)	268 (1.04)	254 (0.40)	336 (0.43)		---	245 (4.24)
1986	***209(7.29)***	320 (0.56)	48 (0.43)	323 (3.24)	313 (2.94)		---	259 (3.81)
1987	***167 (2.17)***	286 (0.45)	316 (0.77)	235 (0.33)	299 (1.34)		---	250 (6.96)
1988	3 (2.00)	266 (1.61)	***193 (1.16)***	298 (1.22)	***206 (0.74)***		---	***198 (1.25)***
1989	72 (1.45)	331 (1.72)	240 (2.11)	289 (1.29)	287 (1.08)		---	244 (1.52)
1990	254 (1.82)	237 (0.21)	356 (0.35)	329 (0.56)	315 (0.49)		---	260 (2.10)
1991	***166 (0.91)***	251 (1.18)	***188 (0.61)***	256 (0.81)	317 (1.69)		---	***149 (2.23)***
1992	265 (2.16)	280 (0.61)	***189 (0.41)***	323 (0.48)	39 (1.86)		---	254 (1.88)
1993	***136 (0.85)***	300 (2.00)	56 (0.37)	261 (0.64)	307 (2.51)		---	***220 (3.42)***
1994	268 (2.62)	306 (1.50)	***146 (0.88)***	***204 (0.48)***	305 (1.54)		297 (0.61)	***154 (1.64)***
1995	337 (0.49)	309 (1.33)	334 (0.97)	340 (0.11)	284 (1.93)		---	292 (3.25)
1996	304 (1.27)	290 (1.37)	345 (2.92)	***220 (1.92)***	332 (1.38)		---	308 (3.01)
1997	***197 (2.23)***	239 (0.89)	308 (1.16)	313 (2.07)	304 (1.92)		---	***208 (1.59)***
1998	250 (1.71)	***201 (0.40)***	332 (1.48)	251 (0.72)	289 (1.23)		---	299 (2.51)
1999	***173 (1.27)***	278 (0.49)	231 (0.73)	307 (0.48)	337 (0.75)		---	***212 (1.40)***
2000	***170 (2.71)***	231 (1.05)	261 (0.85)	335 (0.27)	341 (1.40)		---	250 (2.70)
2001	***186 (1.67)***	316 (1.46)	***161 (0.39)***	279 (1.51)	308 (1.66)		287 (1.41)	***174 (3.36)***
2002	***158 (1.08)***	305 (1.59)	329 (5.25)	349 (1.18)	332 (1.18)		---	***189 (2.71)***
2003	323 (0.55)	***222 (0.92)***	329 (1.05)	322 (2.74)	337 (0.93)		---	291 (1.17)
2004	275 (3.42)	***217 (1.54)***	***208 (0.08)***	329 (0.99)	297 (2.68)		---	***178 (1.47)***
2005	***142 (0.62)***	***184 (1.07)***	292 (0.95)	308 (0.31)	287 (1.41)		---	***200 (2.70)***
2006	***162 (1.19)***	284 (0.32)	308 (2.02)	***192 (1.09)***	352 (0.80)		---	---
2007	265 (1.52)	317 (3.51)	66 (1.11)	279 (3.00)	332 (1.60)		---	247 (4.39)
2008	249 (2.09)	***154 (1.45)***	268 (2.33)	302 (2.54)	292 (2.60)		***204 (2.99)***	342 (4.83)
2009	***151 (3.74)***	22 (2.79)	265 (2.35)	341 (1.79)	358(4.41)		***183(2.86)***	265(4.33)
2010	***186 (2.11)***	***170 (1.58)***	312 (1.04)	***202 (0.27)***	292 (1.08)		250(0.09)	245 (1.68)
2011	302 (0.70)	25 (4.16)	340 (4.20)	249 (2.30)	324 (1.81)		***225(0.83)****	***202(5.82)****
2012	***135(2.47)****	***220(1.75)****	***218(1.35)****	277(0.45)*	***214(0.72)****		---	---

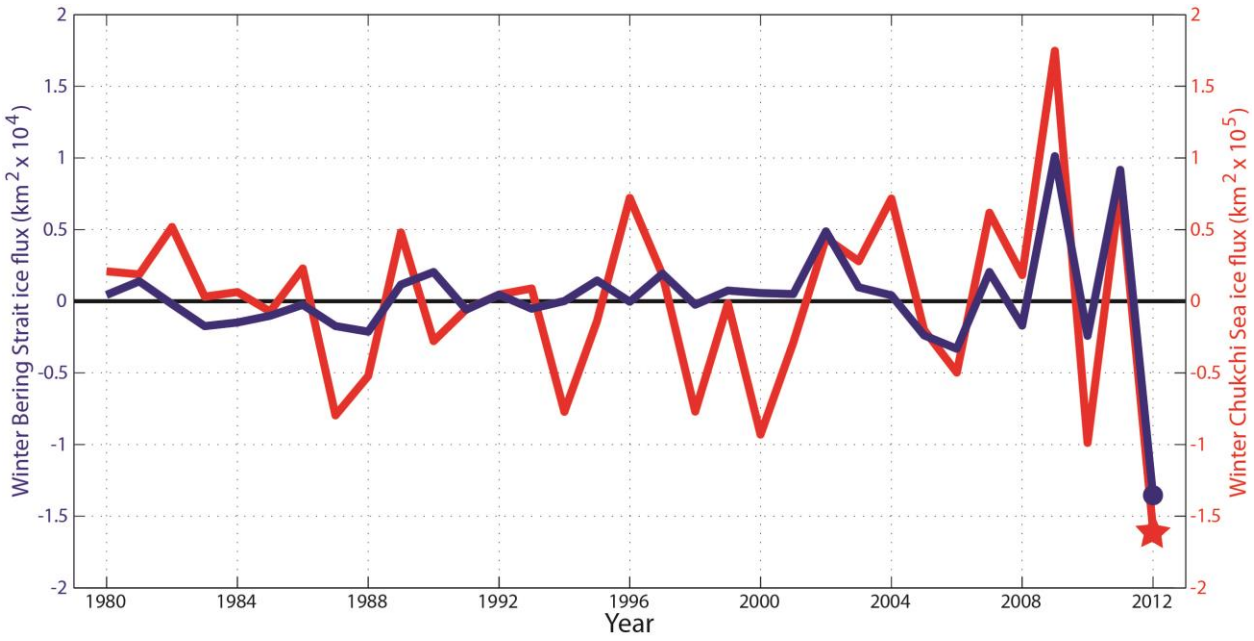

Figure 3.6: Net areal fluxes of sea ice (km^2) through the Bering Strait (blue) and into the southern Chukchi Sea (red) between November and May for the period of 1979-1980 to 2011-2012. Fluxes from 2011-2012 are highlighted with a circle (Bering Strait) and a star (Chukchi Sea). Positive fluxes represent positive meridional (northward) ice drift into the Arctic Basin, whereas negative fluxes represent negative meridional (southward) ice drift out of the Arctic Basin.

During 2011-2012 the Bering Strait exported four times as much sea ice as it had exported during its previous maximum in 2005-2006 (3.3 x 10^3 km^2), which we attribute to an overall reduction in the mechanical strength of the ice pack and the high wind speeds that prevented the formation of ice arches across the Bering Strait. Between 1979-1980 and 2007-2008 an average of 59 (±1.6 x 10^3) km^2 of sea ice was imported into the Chukchi Sea across the Bering Strait. However Since 2007-2008 the Bering Strait has become increasingly mobile, experiencing 3 of its 4 largest fluxes in the last three winters with a peak flux, prior to our event, of 10 x 10^3 km^2 of sea ice northwards through the Bering Strait into the Chukchi Sea (Figure 3.6). The recent increase in ice flux through the Bering Strait can be related to a weaker arctic ice pack that is no longer able to form ice arches across the Bering Strait and impede ice drift. *Kwok et al.,* [2010] found a similar change in Nares Strait, where a thinner and mechanically weaker ice pack is now unable to form seasonal ice arches through winter that oppose southward ice flow. The authors

state that Nares Strait has transitioned to a higher flow state and is acting to significantly deplete the remaining MYI from the Arctic. Under a warming climate and declining ice cover, the Bering Strait may be another example of a more mobile region susceptible to increased ice flux, in a fashion similar to Nares Strait [*Kwok et al.*, 2010].

3.3.2.2 MSLP Climatology

Expanding on the work of *Pickart et al.* [2009] we set the historical context of the monthly MSLP patterns from 2011-2012 by presenting the climatological (1979 to 2011) monthly MSLP patterns for September to May (Figure 3.7). The climatology shows the dominance of the Aleutian Low and the Siberian and Beaufort Highs in the MSLP patterns of this region in the long-term average (Figure 3.7). The Aleutian Low is present for the entire period between September and May. It is deepest between December (Figure 3.7D) and February (Figure 3.7F), and dissipates through the spring. The Siberian High develops over continental Siberia through November (Figure 3.7C) and December (Figure 3.7D) before deepening and extending a ridge of high pressure over the Pacific Arctic during January (Figure 3.7E) and February (Figure 3.7F). By March (Figure 3.7G) the Siberian High has moved over the Pacific Arctic as it transitions to the springtime Beaufort High [*Overland* 2009; *Serreze and Barrett* 2011]. MSLP gradients across the Bering Strait are greatest between December and February with isobars running east to west creating easterly geostrophic winds and westward ice drift that is typical of this region.

To determine how MSLP across the Bering Strait varied from the climatology during winter 2011-2012 we present monthly MSLP anomalies from winter 2011-2012 (Figure 3.8). Negative anomalies (blue) indicate below average MSLP and positive anomalies (red) indicate above average MSLP during winter 2011-2012. December 2011 (Figure 3.8D) was characterised by positive anomalies over the west coast of Canada, indicative of a blocking high, and negative

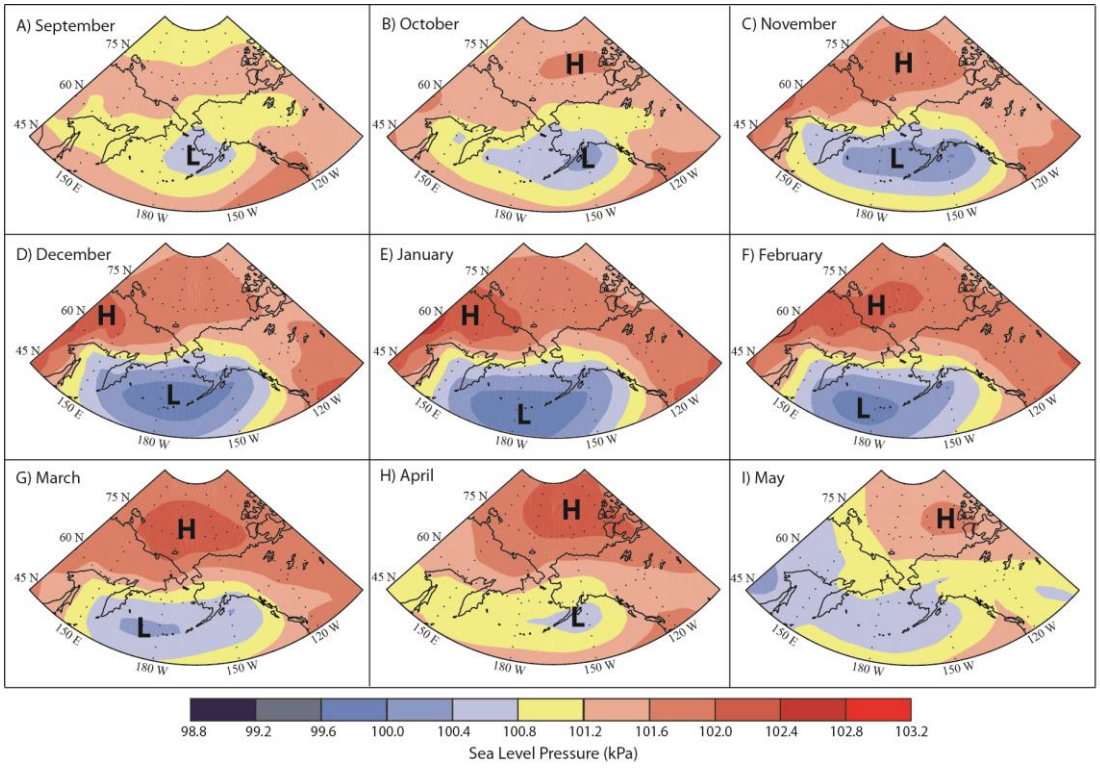

Figure 3.7: Climatological monthly means of MSLP for our study region from NCEP reanalysis-2 fields from 1979-2011

anomalies over the Bering Strait and Alaska indicative of the displaced Aleutian Low driven northwards by the blocking high. Negative MSLP anomalies over the Bering Strait, in conjunction with positive anomalies over Siberia, increased the MSLP gradient over this region. The increased MSLP gradient caused high wind speeds at Pt. Hope (9.72 m s^{-1}) (Figure 3.4D) which drove rapid southward ice motion in the ROI (5.82 cm s^{-1}) (Figure 3.3D and Table 3.3) and the largest southward ice fluxes of 2011-2012 across the two ice flux gates. This fed the export event of 2011-2012 by forcing over four times the average December ice flux into the southern Chukchi Sea, specifically it drove the MYI we were tracking into the Chukchi Sea thereby making it available for export. During January 2012 (Figure 3.8E) positive anomalies existed over the Siberian High as negative anomalies covered the Canada Basin. The strong Siberian High coupled with low pressure over the Canada Basin forced ice from the East

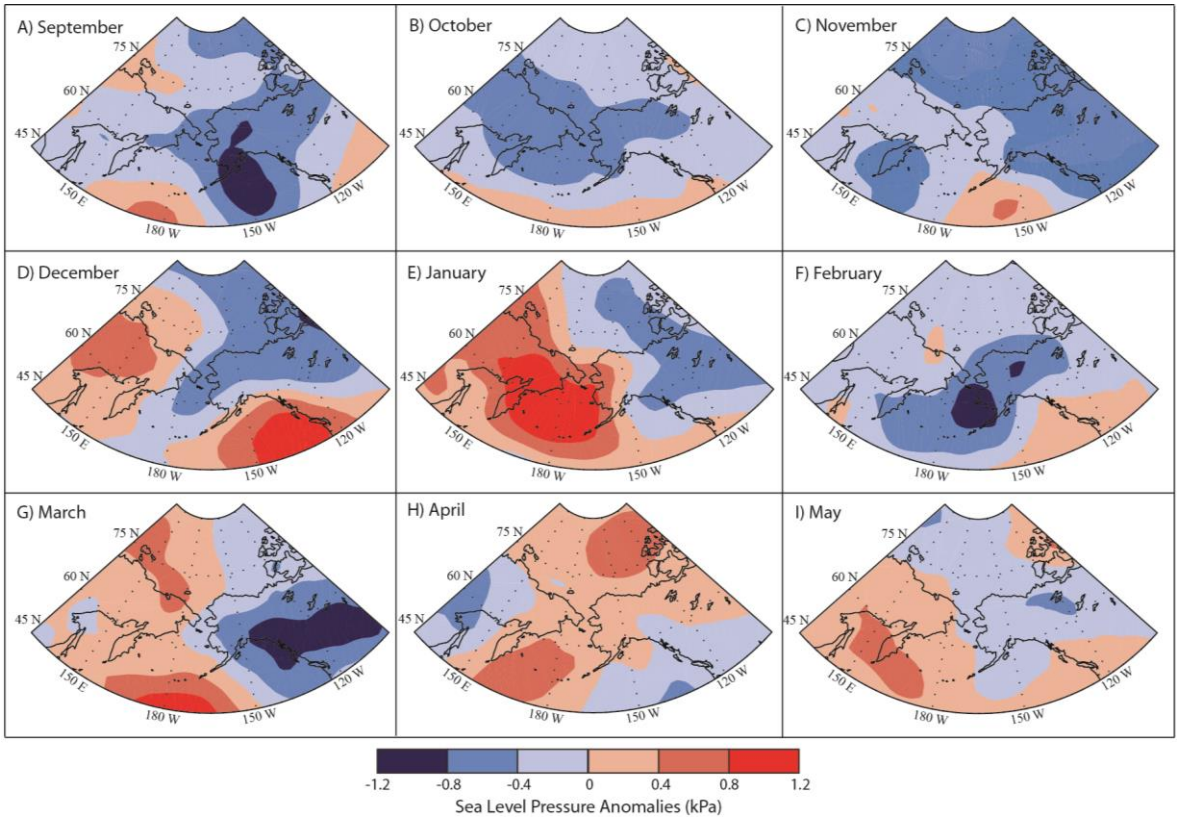

Figure 3.8: The MSLP anomalies of 2011-2012 from the 1979-2011 climatology. Red represents positive anomalies and blue represents negative anomalies.

Siberian Sea to the southeast along isobars into the Chukchi Sea, creating high internal stresses within the Chukchi Sea. Beyond the displaced Aleutian Low in December and small anomalies in January the MSLP anomalies from 2011-2012 do not indicate a large departure from climatological means. We therefore speculate that the 2011-2012 sea ice export event was predominantly driven by a change in the way that the arctic ice pack responds to typical forcing mechanisms.

In the long-term, the Aleutian Low is stable in the Bering Sea surrounded by a ridge of high pressure extending from the Siberian High, across the Pacific Arctic to high pressure located over North America (e.g. Figure 3.7E, type A after *Pickart et al.,* 2009). However type B which is characterized by a blocking high is not represented in the climatology, though the blocking high was present during December 2011 (Figure 3.4D) and played a significant role in

forcing ice into the Chukchi Sea. Therefore, we analyze MSLP for each December from 1979 to 2012 to assess how often the blocking high was present in the long-term. Between 1979 and 2012 the blocking high was present during 8 of 34 Decembers (24%), of which five experienced southward ice motion in the ROI. During some years the blocking high connected to the Siberian High across the Pacific Arctic, similar to type A MSLP, but during other years low pressure extends from the displaced Aleutian Low and joins a low located over the CAA, subsequently disrupting the ridge of high pressure across the Pacific Arctic. Including December 2011 this occurred during 11 of 34 Decembers (1988, 1991, 1993, 1994, 1997, 1999, 2001, 2002, 2004, 2005 and 2011), which were the 11 Decembers when ice moved southwards through the ROI (Table 3.3). However, December 2011 ice speeds were significantly ($p < 0.01$) faster and therefore forced more than twice the average amount of ice into the southern Chukchi Sea from the Arctic Ocean compared to the other 10 Decembers during which the Aleutian Low broke out. The increased ice flux resulted in vast amounts of ice entering the Chukchi Sea and increasing internal stresses while making this ice available for export through the Bering Strait. Southward motion also persisted beyond December 2011 which prolonged and increased the export event, whereas previous Decembers with southward motion were only followed by southward motion in January four times (Table 3.2). When the Aleutian Low is shifted north it creates a northwest-southeast MSLP gradient (e.g. Figure 3.4D) which drives sea ice to the south-southwest along the isobars. Theoretically under these conditions we would anticipate northwest surface winds but during December 2011 winds from the northeast blew through Pt. Hope and Gambell, Alaska, which explains the low turning angle (-5°) during December (Table 3.2).

3.4 Conclusions:

Six ice beacons deployed on multiyear sea ice in the Beaufort Sea during August 2011 tracked anomalous sea ice export through the Bering Strait into the Bering Sea between November 2011 and May 2012. One ice beacon tracked the drift of MYI onto the Kamchatka Peninsula in the western Bering Sea. These are the first observations of ice beacons within the IABP 34+ year dataset being exported out of the Arctic through the Bering Strait. Historically ice beacons drift either west or north from the Chukchi Sea. Only 31 of the 910 ice beacons within the dataset have drifted south into the Chukchi Sea, 5 of those have drifted to within 300km of the Bering Strait, and none have been exported. Using satellite-derived ice motion fields we find that between November 2011 and May 2012 13.5 x 10^3 km^2 of sea ice was exported through the Bering Strait, more than four times the previous maximum export of the 34 year dataset. Overall we find southward ice motion persisted through the Chukchi Sea for six of the seven months between November 2011 and May 2012 and that sea ice drift speeds were significantly ($p < 0.01$) greater than the 34 year climatology during four of these months. Southward ice motion is not uncommon to the Chukchi Sea, occurring during one in three Decembers and Januaries, but southward motion persisted for longer than any other period in the last 34 years during 2011-2012. Using 34 years of ice beacon data and satellite derived fields of ice motion we do not find evidence of similar prolonged export events occurring in the past, specifically we find no evidence of MYI export as we recorded in 2011-2012. We note that during 2011-2012 159 x 10^3 km^2 of sea ice entered the southern Chukchi Sea, the largest export of ice out of the Arctic Ocean into the Chukchi Sea in the 34 year record, which helped to supply and promote the export of sea ice. MSLP patterns for this region were characterized by the Siberian High and Aleutian Low which collectively created a pressure gradient that forced northerly winds and thus southward ice

drift through the Bering Strait for all months between September 2011 and May 2012. Wind speeds were greater than the critical speed of 5.6m s^{-1} which precludes the formation of ice arches during all months but January. This in combination with a well-documented reduction in the mechanical strength of the arctic ice pack and increased mobility allowed sea ice to drift relatively unimpeded through the Bering Strait. Similar climate induced weakening of ice arches leading to increased ice flux through a narrow channel has been documented in Nares Strait [*Kwok,* 2010].

In terms of the forcing of this event, the winter of 2011-2012 was characterized by typical winter conditions with minor MSLP anomalies. We note a northward displaced Aleutian Low over the Bering Strait and Alaska during December which along with a strong Siberian High created a northwest-southeast MSLP gradient that drove the highest ice flux of 2011-2012 southwards into the Chukchi Sea. This continued the export that began in November, but more importantly forced the MYI floes we were tracking into the Chukchi Sea and made them available for export through the Bering Strait. The displaced Aleutian Low merged with a low over the CAA and interrupted the ridge of high pressure which as per the climatology typically extends across the Pacific Arctic from Siberia to northern Canada. The Aleutian Low has broken out like this in 11 of 34 Decembers all of which were characterized by southward motion through the Bering Strait. However, southward sea ice drift was significantly faster during December 2011, indicating a change in the response of the ice pack to this typical forcing mechanism. In January positive anomalies over the Siberian High coupled with negative anomalies over the Canada Basin forced ice from the East Siberian Sea into the Chukchi Sea creating great internal stresses within the ice pack and forcing ice to the south-southeast through the Bering Strait. The duration of the export event was characterized by northerly winds and thus southward ice export

through the Bering Strait with only minor MSLP anomalies. MSLP anomalies played a role in this export event during December and January however these anomalies were within the variability of MSLP patterns of this region. We believe that the speed and persistence of the 2011-2012 export event is primarily attributable to the decreased mechanical strength and increased mobility of the arctic ice pack which is responding differently to typical forcing mechanisms as part of the dramatic sea ice reduction. The results presented here suggest ice flux through the Bering Strait is increasing under a warming climate and that the strait may present a new pathway for the export of multiyear sea ice from the Arctic basin thereby contributing to the ongoing reduction of the multiyear sea ice mass balance.

3.5 Acknowledgements

The Authors wish to extend their thanks to the Captain and crew of the *CCGS Amundsen* for their expertise and assistance during our field program. Thanks to ArcticNet, the Canada Research Chair program, the Canada Excellence Research Chair program, NSERC, and Aboriginal Affairs and Northern Development Canada for funding. This is a contribution to the Arctic Science Partnership (ASP) and ArcticNet. Thanks to industry partners at Imperial Oil Research Ventures Ltd. for funding and taking part in our field program. Thanks to P. Olsson from the Alaska State Climate Center at the University of Alaska Fairbanks for sharing weather station data. Thanks to C. Fowler from the National Snow and Ice Data Center for sharing the ice motion dataset and answering questions so freely. Thanks to S. Prinsenberg from the DFO Canada, M. Johnston from the NRC of Canada and K. Hochheim from CEOS for sharing ice thickness data collected during our field program. Thanks to J. Hutchings and an anonymous reviewer for their helpful feedback.

References

Aagaard, K. and E.C. Carmack (1989), The role of sea ice and other fresh water in the Arctic Circulation, *J. Geophys. Research*, 94, C10, 14,485-14,498.

Alekseev, G.V., O.I. Myaskoshin and N.P. Smirnov (1997), Variability of the ice transport through the Fram Strait. Available in English. *Meteorol Gidrol*, 9, 37-41.

Arfeuille, G., L.A. Mysak and L.-B. Tremblay (2000), Simulation of the interannual variability of the wind driven Arctic sea-ice cover during 1958-1998, *Climate Dynamics*, 16, 107-121.

Barber, D.G., R. Galley, M.G. Asplin, R. De Abreu, K. Warner, M. Pućko, M. Gupta, S. Prinsenberg, and S. Julien (2009), Perennial pack ice in the southern Beaufort Sea was not as it appeared in the summer of 2009, *Geophys. Res. Letters*, 36, L24501, doi: 10.1029/2009GL041434.

Bourke, R.H., and R.P. Garrett (1987), Sea ice thickness distribution in the Arctic Ocean, *Cold Regions Science and Technology*, 13, 259-280.

Cavalieri, D.J. and C.L. Parkinson (1987), On the relationship between Atmospheric Circulation and the Fluctuations in the Sea Ice Extents of the Bering and Okhotsk Seas, *J. Geophys. Research*, 92(7), 7141-7162.

Cavalieri, D.J., C.L. Parkinson, P. Gloersen and H. Zwally (1996, updated 2012), *Sea ice concentration from Nimbus-7 SMMR and DMSP SSM/I-SSMIS Passive Microwave Data* [1979-2012]. Boulder, Colorado USA: NASA DAAC at the National Snow and Ice Data Center.

Clement, J.L., L.W. Cooper and J.M. Grebmeier (2004), Late winter water column and sea ice conditions in the northern Bering Sea, *J. Geophys. Research*, 109, C03022, doi: 10.1029/2003JC002047.

Colony, R. and A.S. Thorndike (1980), The Horizontal Coherency of the Motion of Summer Arctic Sea Ice, *J. of Physical Oceanography*, 10, 1281-1289.

Colony, R. and A.S. Thorndike (1984), An Estimate of the Mean Field of Arctic Sea Ice Motion, *J. Geophys. Research*, 89(C6), 10,623-10,629.

Comiso, J.C. (2012), Large Decadal Decline of the Arctic Multiyear Ice Cover, *J. Climate*, 25, 1176-1193.

Fowler, C., 2003, updated 2010. Polar pathfinder daily 25 km EASE-grid sea ice motion vectors [1979-2012]. Boulder, Colorado, USA: NASA DAAC at the National Snow and Ice Data Center. Digital media.

Francis, J.A., and E. Hunter (2007), Drivers of declining sea ice in the Arctic winter: A tale of two seas, *Geophys. Res. Letters*, 34, L17503, doi:10.1029/2007GL030995.

Galley, R.J., B.G.T. Else, S.J. Prinsenberg, D. Babb, D.G. Barber (2013), Sea ice concentration, extent, age, motion and thickness in regions of proposed offshore oil and gas development near the Mackenzie Delta – Canadian Beaufort Sea, *Arctic*, 66(1), 105-116.

Gordienko, P.A. (1958), Arctic drift ice, in *Proceedings on the Conference of sea ice, Publ. 598,* edited by R.W. Thurston, pp 210-222, National Research Council, National Academy of Sciences, Washington D.C.

Gow, A.J. and W.B. Tucker III (1987), Physical Properties of Sea ice discharged from Fram Strait, *Science*, 236 (4800), 436-439.

Grebmeier, J.M., J.E. Overland, S.E. Moore, E.V. Farley, E.C. Carmack, L.W. Cooper, K.E. Frey, J.H. Helle, F.A. McLaughlin and S.L. McNutt (2006), A Major Ecosystem Shift in the Northern Bering Sea, *Science*, 311(5766), 1461-1464.

Hibler III, W.D., J.K. Hutchings, C.F. Ip (2006), Sea-ice arching and multiple flow states of Arctic pack ice, *Annals of Glaciology*, 44, 339-344.

Howell, S.E.L., A. Tivy, J.J. Yackel, B.G.T. Else and C.R. Duguay (2008), Changing sea ice melt parameters in the Canadian Arctic Archipelago: Implications for the future presence of multiyear ice, *J. Geophys. Research*, 113, C09030, doi:10.1029/2008JC004730.

Howell, S.E.K., A. Tivy, T. Agnew, T. Markus and C. Derksen (2010), Extreme low sea ice years in the Canadian Arctic Archipelago: 1998 versus 2007, *J. Geophys. Research*, 115, C10053, doi:10.1029/2010JC006155.

Howell, S.E.L, T. Wohlleben, M. Dabboor, C. Derksen, A. Komarov and L. Pizzolato (2013), Recent changes in the exchange of sea ice between the Arctic Ocean and the Canadian Arctic Archipelago, *J. Geophys. Research*, 118, 1-13, doi:10.1002/jgrc.20265.

Hutchings J.K. and I.G. Rigor (2012), Role of ice dynamics in anomalous ice conditions in the Beaufort Sea during 2006 and 2007, *J. Geophys. Research*, 117, C00E04, doi: 10.1029/2011JC007182.

Kalnay, E., *et al.*, (1996), The NCEP/NCAR 40-year Reanalysis Project, March 1996, *Bulletin of the American Meteorological Society*, 77(3), 437-471.

Kanamitsu ,M. W. Ebisuzaki, J. Woollen, S-K Yang, J.J. Hnilo, M. Fiorino, and G. L. Potter. (2002), NCEP-DEO AMIP-II Reanalysis (R-2), Nov 2002, *Bulletin of the American Meteorological Society*, 1631-1643.

Kimura, N. and M. Wakatsuchi (2000), Relationship between sea-ice motion and geostrophic wind in the Northern Hemisphere, *Geophys. Res. Letters*, 27(22), 3735-3738.

Kubat, I., M. Sayed, S.B. Savage and T. Carrieres (2006), Flow of ice through converging channels, *International Journal of Offshore and Polar Engineering*, 16 (4), 268-273.

Kwok, R. (2009), Outflow of Arctic Ocean Sea Ice into the Greenland and Barents Seas: 1979-2007, *J. of Climate*, 22, 2438-2457.

Kwok, R., A. Schweiger, D.A. Rothrock, S. Pang, and C. Kottmeier (1998), Sea ice motion from satellite passive microwave imagery assessed with ERS SAR and buoy motions, *J. Geophys. Research*, 103, C4, 8191-8214.

Kwok, R, G.F. Cunningham and S.S. Pang (2004), Fram Strait sea ice outflow, *J. Geophys. Research*, 109, C01009, doi: 10.1029/2003JC001785.

Kwok, R., G. F. Cunningham, M. Wensnahan, I. Rigor, H.J. Zwally and D. Yi (2009), Thinning and volume loss of the Arctic Ocean sea ice cover: 2003-2008, *J. Geophys. Research*, 114, C07005, doi:10.1029/2009JC005312.

Kwok, R. and G.F. Cunningham (2010), Contribution of melt in the Beaufort Sea to the decline in Arctic multiyear sea ice coverage: 1993-2009, *Geophys. Res. Letters*, 37, L20501, doi:10.1029/2010GL044678.

Kwok, R., G. Spreen, and S. Pang (2013), Arctic sea ice circulation and drift speed: decadal trends and ocean currents, *J. Geophysical Research – Oceans*, doi:10.1002/jgrc.20191.

Lukovich, J., and D. Barber (2006), Atmospheric controls on sea ice motion in the Southern Beaufort Sea, *J. Geophys. Research*, 111, D18103, doi: 10.1029/2005JD006408.

Maslanik, J., J. Stroeve, C. Fowler and W. Emery (2011), Distribution and trends in Arctic sea ice age through spring 2011, *Geophys. Res. Letters*, 38, L13502, doi: 10.1029/2011GL047735.

Melling, H. (2002), Sea ice of the northern Canadian Arctic Archipelago, *J. Geophys. Research*, 107, C11, doi: 10.1029/2001JC001102.

Melling, H. (1999), Exchanges of Freshwater through the shallow straits of the North American Arctic, in The Freshwater Budget of the Arctic Ocean, editors E.L. Lewis et al., pp. 479-502, Kluwer Academic Publishers, Netherlands.

Nansen, F. (1902), Norwegian North Polar Expedition 1893-1896, Scientific Results, vol. 3, The Oceanography of the North Polar Basin, 427 pp., Longmans, Green, London.

Overland, J.E., and C.H. Pease (1982), Cyclone Climatology of the Bering Sea and Its Relation to Sea Ice Extent, *Mon Wea. Rev.*, 110, 5-13.

Overland, J.E. and P.J. Stabeno (2004), Is the climate of the Bering Sea Warming and Affecting the Ecosystem?, *EOS Transactions of the American Geophysical Union*, 85(33), 309-316.

Overland, J.E. (2009), Meteorology of the Beaufort Sea, *J. Geophys. Research*, 114, C00A07, doi: 10.1029/2008JC004861.

Parkinson, C.L. and D.J. Cavalieri (2008), Arctic sea ice variability and trends, 1979-2006, *J. Geophys. Research*, 113, C07003, doi:10.1029/2007JC004558.

Parkinson, C.L. and J.C. Comiso (2013), On the 2012 record low Arctic sea ice cover: Combined impact of preconditioning and an August Storm, *Geophys. Res. Letters*, 40, 1-6, doi:10.1002/grl.50349.

Pease, C.H. (1980), Eastern Bering Sea Ice Processes, *Mon. Wea. Rev.*, 108, 2015-2023.

Perovich, D.K., Richter-Menge, J.A., Jones, K.F., and Light, B. (2008), Sunlight, water and ice: Extreme Arctic sea ice melt during the summer of 2007, *Geophys. Res. Letters*, 35, L11501, doi: 10.1029/2008GL034007.

Peterson, I.K., Prinsenberg, S.J. and Holladay, J.S., (2008) Observations of sea ice thickness, surface roughness and ice motion in Amundsen Gulf. *J. Geophys. Research*, 113, C06016, doi: 10.1029/2007JC004456.

Pickart, R.S., G.W.K. Moore, A.M. Macdonald, I.A. Renfrew, J.E. Walsh and W.S. Kessler (2009), *J. Phys. Oceanography*, 39, 1317-1339, doi: 10.1175/2008JPO3891.1.

Polyakova, A.M. (2007), Extreme supply of floating ice to the northwestern part of the Pacific Ocean, *Oceanology*, 47(1), 1-4.

Rampal, P., J. Weiss and D. Marsan (2009), Positive trend in the mean speed and deformation rate of arctic sea ice, 1979-2007, *J. Geophys. Research*, 114, C05013, doi: 10.1029/2008JC005066.

Rigor, I., J.M. Wallace and R. Colony (2002), Response of Sea Ice to the Arctic Oscillation, *J. of Climate*, 15, 2648-2663.

Serreze, M.C. and A.P. Barrett (2011), Characteristics of the Beaufort Sea High, *J. Climate*, 24, 159-182, doi: 10.1175/2010JCLI3636.1.

Sodhi, D.S. (1977), Ice arching and the drift of pack ice through restricted channels, Report 77-18, Cold Regions Research and Engineering Laboratory, Hanover, New Hampshire.

Stabeno, P.J., N.A. Bond and S.A. Salo (2007), On the recent warming of the southeastern Bering Sea shelf, *Deep-Sea Research II*, 54, 2599-2618.

Steele, M., J. Zhang, D. Rothrock and H. Stern (1997), The force balance of sea ice in a numerical model of the Arctic Ocean, *J. Geophys. Research*, 102(C9), 21,061-21,079.

Stroeve, J.C., J. Maslanik, M.C. Serreze, I. Rigor, W. Meier and C. Fowler (2011), Sea ice response to an extreme negative phase of the Arctic Oscillation during winter 2009/2010, *Geophys. Res. Letters*, 38, L02502, doi: 10.1029/2010GL045662.

Stroeve, J.C., V. Kattsov, A. Barrett, M. Serreze, T. Pavlova, M. Holland and W.N. Meier (2012), Trends in Arctic sea ice extent form CMIP5, CMIP3 and observations, *Geophys. Res. Letters*, 39, L16502, doi: 10.1029/2012GL052676.

Spreen, G., R. Kwok and D. Menemenlis (2011), Trends in Arctic sea ice drift and role of wind forcing: 1992-2009, *Geophys. Res. Letters*, 38, L19501, doi: 10.1029/2011GL048970.

Thorndike, A.S. and R. Colony (1982), Sea Ice Motion in Response to Geostrophic Winds, *J. Geophys. Research*, 87(C8), 5845-5852.

Vihma, T., P. Tisler and P. Uotila (2012), Atmospheric forcing on the drift of Arctic sea ice in 1989-2009, *Geophysical Research Letters*, 39, L02501, doi:10.1029/2011GL050118.

Woodgate, R.A., K. Aagaard and T.J. Weingartner (2006), Interannual changes in the Bering Strait fluxes of volume, heat and freshwater between 1991 and 2004, *Geophys. Res. Letters*, 33, L15609, doi: 10.1029/2006GL026931.

Zubov, N.N (1945), Arctic Ice, English Translation: U.S. Naval Oceanographic Office (1963), 506 pp.

CHAPTER FOUR: SEASONAL EVOLUTION OF SEA ICE MOTION AND FORCING MECHANISMS IN THE BEAUFORT SEA

This paper has been prepared for submission to the *Journal of Geophysical Research – Oceans*. The work represents a core chapter of my thesis that was conceived, analyzed and reported by me as the senior author.

Babb, D.G., J.V. Lukovich, K.U. Hochheim, G.G. McCullough, R. Scharien and D.G. Barber (in preparation), Seasonal evolution of sea ice motion and forcing mechanisms in the Beaufort Sea, *J. Geophys. Res. Oceans*.

Abstract:

The arctic ice pack within the Beaufort Sea undergoes a transition from a consolidated ice state in late winter to a less extensive, weaker ice pack in summer. Using an array of autonomous instruments deployed in early April 2012 along the periphery of the Beaufort Sea multiyear ice pack, we highlight the seasonal increase in ice drift speeds as ice floes enter a state of free drift. Hourly coincident *in situ* observations of ice drift, surface winds, and ice mass balance were collected between April and July, 2012. Monthly mean ice drift speeds nearly tripled between April and July as ice motion within the BREA array became less coherent and increasingly variable throughout the season. Monthly mean wind speeds remained around 4m/s throughout the study, indicating atmospheric forcing did not facilitate the increased ice drift speeds. We therefore ascribe the change in ice drift speeds to the mechanical weakening and gradual breakup of the Beaufort ice pack which reduced internal stresses within the ice pack and allowed ice to enter a state of free drift. Using a combination of *in situ* observations and remotely sensed observations, we highlight the declining flexural strength of the ice pack, the seasonal decline of ice concentrations, seasonal increase in the presence of open water and a declining floe size

distribution which collectively represent the seasonal decline in mechanical strength of the Beaufort ice pack that allowed ice speeds to increase as ice floes entered a state of free drift.

4.1 Introduction:

Sea ice motion is characterized by a strong annual cycle with maximum ice drift speeds around the September sea ice minimum, and minimum ice drift speeds during the annual March sea ice maximum [*Rampal et al.,* 2009; *Spreen et al.,* 2011]. The inverse relationship between sea ice drift speeds and the arctic ice state is attributed to the annual cycle in internal stresses that develop within the ice pack and oppose ice motion [*Steele et al.,* 1997]. *Spreen et al.,* [2011] show that the annual cycle in sea ice drift speeds is not driven by a similar trend in wind speed, and instead follows the annual melt/freeze cycle. *Spreen et al.* [2011] note that ice speeds begin to increase in April with the onset of the melt season and continue to increase through to the September sea ice minimum. The seasonal increase of ice drift speeds and attendant governing factors comprise the focus of this paper as we use a unique dataset of coincident *in situ* ice drift and surface wind observations to quantitatively analyze the balance of forces as the ice pack evolves from a compact, mechanically strong ice pack in late winter to a fractured set of discrete ice floes in a state of free drift during summer.

Sea ice motion is the realization of five forces acting on an ice floe. The exchange of momentum across the ocean-sea ice-atmosphere system is represented by the following equation,

$$\mathrm{M}\, a = \tau_a + \tau_w + F_c + F_i + F_t \qquad (1)$$

where the ice floe mass (M) times the acceleration (a) is equal to the sum of the air drag (τ_a), water drag (τ_w), Coriolis force (F_c), internal ice stress (F_i) and the force due to sea surface tilt (F_t) [*Wadhams,* 2000]. Surface winds are the dominant forcing factor whereas ocean currents can

either exert an accelerative or decelerative force [*Leppäranta,* 2005]. The Coriolis force is the result of the earth's rotation and acts 90° to the right of the direction of motion in the northern hemisphere thereby deflecting ice floes to the right of the surface wind direction. Internal stresses within the ice pack arise due to floe-floe interactions which oppose motion and dampen ice drift speeds. When internal stresses are absent sea ice enters a state of free drift, in which ice drift is controlled by the atmospheric, oceanic and Coriolis forces, with the latter creating inertial oscillations along the ice floes trajectory [*McPhee,* 1978]. *Leppäranta* [2005] defines three states of ice drift according to increasing levels of internal stress; free drift, drift in the presence of internal stresses and stationary ice. The latter indicates a compact, mechanically strong ice pack in which internal forces oppose all external forcing and lock up the ice pack [*Steele et al.,* 1997]. The sea surface height force arises due to horizontal gradients in sea surface height, however this term is negligible on short time scales [*Hibler and Tucker* 1979; *Thorndike and Colony*, 1982; *Wadhams*, 2000].

Air drag and water drag represent the transfer of momentum across the air-ice and ice-ocean interfaces, respectively. Both are dependent on surface roughness, which is represented by a surface drag coefficient (C) that represents both the skin drag (small scale roughness) and form drag (large scale roughness; e.g. ridges and keels) [*Wadhams,* 2000; *Leppäranta,* 2005]. The surface roughness of sea ice is dependent on the age and deformation state of the ice pack [*Guest and Davidson,* 1991]. C is highly variable though C_a and C_w are related due to the high correlation of surface and bottom ice roughness [*Wadhams,* 2000; *Leppäranta,* 2005]. C is higher for multiyear sea ice (MYI) than first year sea ice (FYI) [*Wadhams,* 2000; *Leppäranta,* 2005]. Seasonally C_a increases as the ice pack breaks up through spring, thereby exposing sides of ice floes that increase the form drag of the ice floe as well as the skin drag by increasing turbulence

within the near surface wind field [*Wadhams,* 2000]. C_a is dependent on ice concentration, with a maximum value at 8/10 ice cover [*Anderson,* 1987]. Seasonally C_w decreases as melt water increases the density stratification of the oceanic boundary layer which reduces vertical momentum transfer and reduces drag by creating 'slippery ice' [*McPhee,* 1979; *Wadhams,* 2000]. Theoretically the seasonal decline of C_w is compounded by the preferential melt of keels by the turbulent ocean heat flux [*Wadhams,* 1992; S*chramm et al.,* 2000] which reduces the form drag of the ice pack.

Surface winds are the dominant forcing factor of sea ice motion over short (daily to weekly) time scales and explain up to 70% of the variation in ice drift [*Thorndike and Colony,* 1982]. The relation between ice drift and surface or geostrophic winds is described by a scaling factor (F) (%) and a turning angle (θ) (°). For sea ice in the northern hemisphere it is a rule of thumb that F = 2% and that θ = 30° - 45° to the right of wind direction [*Nansen,* 1902, *Colony and Thorndike,* 1980]. However, both F and θ vary seasonally and spatially according to the internal stresses within the ice pack [*Steele et al.,* 1997; *Kimura and Wakatsuchi,* 2000]. Spatially, F is greatest in the seasonal ice zone which is covered by thin FYI that is mechanically weaker than thicker MYI and is therefore subject to less internal stresses; conversely F is lowest along the north flank of the Canadian Arctic Archipelago and Greenland where the thickest sea ice in the Arctic [*Bourke and Garret,* 1987; *Melling,* 2002] creates the greatest internal stresses within the Arctic [*Kimura and Wakasutchi*, 2000]. Seasonally F is greatest during summer, when the ice pack is weakest and ice floes enter free drift, and lowest during winter when internal stresses are so great that they may 'lock-up' the arctic ice pack and render it motionless [*Steele et al.,* 1997; *Thomas,* 1999]. Internal stresses within the ice pack also cause θ to vary from a winter minimum to a summer maximum [*Thorndike and Colony,* 1982; *Thomas,* 1999]. During winter θ

decreases as the Coriolis force is nullified by internal stresses within the compact ice pack and conversely, θ increases during summer when the ice pack weakens and ice floes enter a state of free drift [*Thorndike and Colony,* 1982; *Thomas,* 1999]. *Thomas* [1999] used monthly mean values of *F* (|*A*| by the authors notation) and θ to define a winter ice drift regime from November to April, characterized by low *F* and θ values, and a summer ice drift regime from June to September, characterized by higher *F* and θ values. May and October are defined as transition months in which ice drift responds to seasonal changes in the ice pack that drive seasonal changes in internal stresses that dictate ice motion [*Thomas,* 1999]. Therefore, as the arctic ice pack deteriorates from a consolidated, mechanically strong ice pack in late winter to a less extensive, weaker ice pack in summer the internal stresses decline, allowing ice to approach a state of free drift in which *F* and θ increase.

The mechanical strength of the arctic ice pack provides a limit to ice drift speeds on both the seasonal scale [*Spreen et al.,* 2011; *Zhang et al.,* 2012] and on the longer decadal scale, during which a reduction in mechanical strength has fostered a positive trend in ice drift speeds over the last 30 years [*Hakkinen et al.,* 2008; *Rampal et al.,* 2009; *Spreen et al.,* 2011; *Kwok et al.,* 2013]. *Zhang et al.,* [2012] compared model runs from 1979-2006 to 2007-2011 and found a 33% reduction in sea ice volume that resulted in a 37% decline in ice mechanical strength and 31% decline in internal stresses, which collectively fostered a 13% increase in ice drift speeds. The mechanical strength of sea ice is a broadly used term that generally reflects the temperature, flexural strength and thickness of individual ice floes, and the local sea ice concentration, thickness distribution and floe size distribution. The temperature and salinity of an ice floe control the brine volume which influences the flexural strength of an ice floe [*Timco and O'Brien* 1994; *Timco and Johnston,* 2002]. Colder floes with lower brine volumes are more

resilient to fracturing as the ice lattice is more complete and therefore stronger, conversely warm, isothermal floes have greater brine volumes and a less complete ice lattice which weakens the ice and makes it more susceptible to fracturing [*Timco and O'Brien* 1994; *Timco and Johnston,* 2002]. The mechanical strength of sea ice is highly dependent on ice thickness as thicker floes are stronger and more resilient to deformation, thereby allowing internal stresses to be transmitted great distances through the ice pack [*Hibler,* 1979].Recent increases in ice drift speeds [*Rampal et al.,* 2009; *Spreen et al.,* 2011; *Kwok et al.,* 2013] have been attributed to a gradual thinning of the Arctic ice pack since initial measurements were made in 1958 [*Rothrock et al.,*1999; 2008; *Kwok and Rothrock,* 2009]. Sea ice concentration limits the floe-floe interactions which create internal stresses within the ice pack and strengthen the ice pack by removing areas of weak ice through dynamic processes [*Wadhams,* 2000]. A highly concentrated ice pack, such as the arctic ice pack during late winter, experiences greater internal stresses than an area of low sea ice concentrations such as the marginal ice zone during summer, where ice floes experience little to no internal stresses and may enter a state of free drift [*Thorndike and Colony,* 1982; *Wadhams,* 2000]. The floe size distribution within an ice pack affects its response to dynamic and thermodynamic forcing [*Steer et al.,* 2008]. Floes are fractured by waves and swells near the ice edge and throughout the ice pack by winds, currents, isostatic imbalances and thermal cracking [*Rothrock and Thorndike,* 1984]. At any given time the floe size distribution is in flux [*Steer et al.,* 2008]. Generally the floe size distribution declines during summer, when isothermal floes become more susceptible to breaking up [i.e. *Asplin et al.,* 2012; 2014] and more resilient floes are liberated from large aggregate floes that form during winter. Conversely, floe size distributions increase during winter when floes aggregate and 'weld' together into a larger aggregate ice pack [*Rothrock and Thorndike,* 1984]. Smaller ice floes are more susceptible

to lateral melt, which further weakens the ice pack, and atmospheric forcing, which along with low ice concentrations and a mechanically weak ice pack will allow ice drift speeds to increase [*Toyota et al.*, 2006; *Asplin et al.*, 2012].

Inertial oscillations are characteristic of free drift conditions in which no internal stresses are present and an individual ice floe is able to respond to atmospheric and oceanic forcing, and the Coriolis force. Inertial oscillations are excited by atmospheric forcing, though they are generally opposed by internal stresses and dampened by water drag [*Thorndike and Colony*, 1982]. Therefore inertial oscillations generally occur during summer when ice floes enter free drift, and are less common during winter when internal stresses are present within the ice pack [*McPhee*, 1978; *Colony and Thorndike*, 1980; *Gimbert et al.*, 2012]. *McPhee* [1978] ascribed the difference between summer and winter ice drift at the inertial frequency to the percentage of open water during summer. As the arctic ice pack has mechanically weakened over recent decades there has been a significant positive trend in the magnitude of inertial oscillations which reflects a reduction in internal stresses within the ice pack [*Gimbert et al.*, 2012]. The frequency and period of inertial oscillations are dependent on latitude and occur on a near diurnal cycle in the polar regions [*McPhee*, 1978; *Geiger and Perovich*, 2008].

Sea ice concentrations within the Beaufort Sea are subject to a large annual cycle; with a historic (1979-2004) late winter maximum of 98% and summer minimum of 46% [*Galley et al.*, 2008]. However since 2004 the Beaufort ice pack, like the rest of the Arctic, has gone through a significant decline that is highlighted by a transition to a younger ice pack [*Maslanik et al.*, 2011; *Comiso*, 2012]. A younger ice pack is susceptible to increased melt rates as a result of a prolonged melt season [*Stroeve et al.*, 2014], presence of rotten ice [*Barber et al.*, 2009], a reduction in albedo [*Perovich et al.*, 2008] and an increase in the ocean heat flux [*Steele et al.*,

2008]. Collectively these factors contribute to the ice-albedo feedback loop, and preconditioned the Beaufort ice pack for a large reduction during the record 2012 September sea ice minimum (3.41×10^6 km^2) when sea ice in the Beaufort Sea retreated north of Banks Island, leaving the entire Beaufort Sea (south of 75°N) ice free [NSIDC, September 2012].

During winter the Beaufort Sea is characteristically composed of two sea ice regimes: 1) a band of landfast sea ice along coastal regions, and 2) high concentrations of mobile ice within the Beaufort ice pack [*Galley et al.,* 2008]. The mobile ice pack is composed of both FYI and MYI [*Galley et al.,* 2008], though there has been a trend towards younger ice types as less MYI now survives the summer melt [*Stroeve et al.,* 2011]. Historically (1979-2000) the spring breakup of the Beaufort ice pack began in early April with the development of two flaw leads along Banks Island and near the Mackenzie Shelf [*Barber and Hanesiak,* 2004]. By mid-May these flaw leads have typically opened and span from the west coast of Banks Island to the western Beaufort Sea along the Beaufort shelf [*Barber and Hanesiak,* 2004]. The flaw lead may open as early as 1 May [*Barber and Hanesiak,* 2004] though the mean time is closer to the end of May [*Galley et al.,* 2008]. Once the flaw lead opens breakup progresses northward and typically the Beaufort Sea breaks up between late-July and late-August [*Galley et al.,* 2008].

The ice pack within the Beaufort Sea has become of particular interest in recent years as it poses considerable hazards to the development of northern transportation routes and offshore resource activities [*Barber et al.,* 2014]. As a result the Government of Canada developed the Beaufort Regional Environmental Assessment (BREA; www.beaufortrea.ca) which funded a large multidisciplinary study of the chemical, physical and biological systems of the Beaufort Sea. The University of Manitoba led the sea ice component of BREA, with a focus on the detection, tracking and forcing of extreme sea ice features in the Beaufort Sea. A portion of our

BREA work comprises the focus of this paper, with future papers to come from the extensive BREA dataset. Central to this study is the use of coincident sea ice state, drift, and surface wind measurements to quantify the role of atmospheric forcing during the transition from a consolidated to a fractured MYI ice regime in the Beaufort Sea. Examined in particular is the i) decline in the ice pack and ii) seasonal evolution in ice drift and surface winds from April to July, 2012. A forecast (2012-2027) of offshore development in the Beaufort Sea completed as part of the BREA program predicts there are 1.7 x 10^9 m^3 of recoverable oil resources and 1.6 x 10^{12} m^3 of marketable gas resources in the Beaufort Sea and Mackenzie Delta [BREA 2012]. Subsequently the Northern Oil and Gas 2012 Annual Report (2013), published by Aboriginal Affairs and Northern Development Canada, stated that current estimates could more than double once undiscovered deep water resources within the Beaufort Sea become available. As of 31 December, 2012 the Canadian Government had sold 18 exploration licenses and 38 significant discovery licenses in the Beaufort Sea, covering a combined 3.3 x 10^6 hectares of offshore area [Northern Oil and Gas Annual Report, 2012], with the first well predicted to be drilled in 2018 [BREA, 2012]. Before offshore development proceeds it is important to understand the Beaufort ice pack, specifically sea ice drift and the ice packs response to external forcing mechanisms so that potential risks may be mitigated and managed.

4.2 Methods:

High sea ice concentrations were present throughout the Beaufort Sea in April 2012 as the ice pack reached its annual peak ice state. As part of the anticyclonic Beaufort Gyre, a large area of old ice had drifted southwards from the high arctic into the Beaufort Sea, creating a tongue of MYI which was surrounded by and separated from the coast by thinner FYI (Figure 4.1A). Our study area was located along the periphery of this MYI tongue, roughly 100km northeast of the

town of Sachs Harbour, NWT. Potential MYI study sites were identified on a March 21, 2012 Radarsat image, 12 of which were ultimately surveyed (Figure 4.1B). Study sites were identified as potentially thick MYI floes that were of particular interest to the BREA project and would provide suitable, long lasting sites for our autonomous equipment. Due to differences in surface roughness MYI appears lighter and FYI appears darker in Figure 4.1B. Each of the 12 study sites was outfitted with an ice beacon and extensively surveyed for ice thickness, yielding mean floe thicknesses between 4.8m (S3) and 7.48m (S5) with a maximum point thickness of >12m. During the two week field program an array of thirteen ice beacons, one ice mass balance buoy (IMB) and one under ice acoustic doppler current profiler (ADCP) were deployed on MYI floes along the periphery of the MYI tongue. The array of autonomous equipment collected a spatially and temporally coincident dataset of *in situ* observations of the ocean-sea ice-atmosphere system.

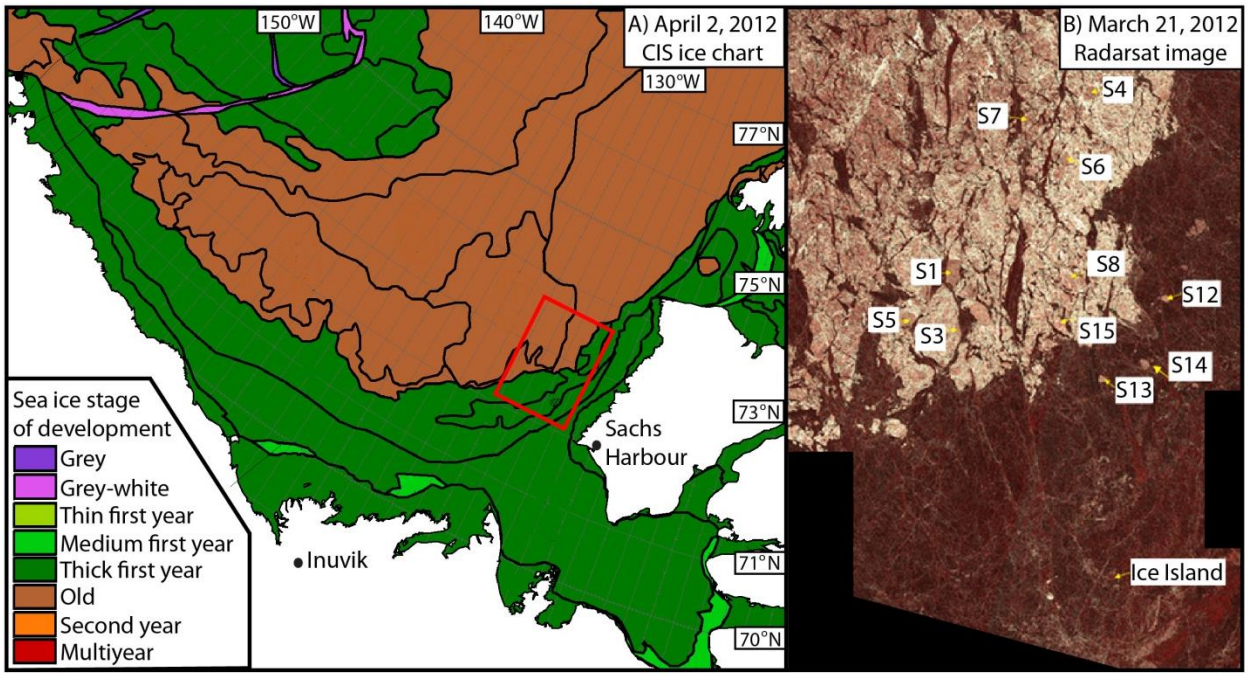

Figure 4.1: A) Canadian Ice Service stage of development ice chart for the Beaufort Sea from April 2, 2012. Helicopter surveys were based out of Sachs Harbour and study sites were located along the periphery of the MYI pack (red box). B) Radarsat scene from March 21 of our study area which covered the area encompassed within the red box in A. Study sites are depicted in the Radarsat scene where lighter coloured ice represents MYI and darker colored ice represents FYI.

Ice beacons are housed in a weather/waterproof cylinder and deployed in an auger (8" diameter) hole drilled 18" deep into the ice in order to keep the Iridium and GPS antennae facing upwards. Ice beacons provided their location every hour and operate until they sink, lose power or are destroyed by wildlife. Given that the ice beacons were powered for over one year of continuous operation we believe they failed throughout the summer of 2012 as the ice pack melted and broke up, causing the equipment to sink. Monthly meander coefficients were calculated for each ice beacon and are used to assess the variability in motion through spring across the BREA array. Meander coefficients are the ratio of overall translation of an ice floe to its net displacement over a period of time and describe its deviation from linear drift [*Heil et al.*, 2009; 2011]. A meander coefficient of 1 indicates direct linear drift, whereas higher values indicate increasingly variable drift where reversals and inertial loops increase the value.

The IMB measured ice mass balance, air temperature, air pressure and ice drift every 30 minutes. The IMB was outfitted with a Campbell Scientific Marine Wind Monitor, which recorded surface winds at a height of 2m every 30 minutes. To correct wind direction for ice floe rotation we deployed the IMB, ADCP and an ice beacon in a triplet formation (sides of 380, 280 and 230m) on the BREA primary floe (S3) and used the three independent GPS positions to correct wind direction for floe rotation. Surface winds were corrected for ice drift and used to calculate the scaling factor (F) and turning angle (θ) between the ice drift vector and surface wind vector. Ice temperature was recorded every 10cm through the 523cm vertical section of the MYI floe and used to infer bottom ablation and surface melt, as well as to calculate the flexural strength of the primary ice floe. Flexural strength equations from *Timco and O'Brien* [1994] were solved using a constant salinity of 2.1 [*Eicken et al.*, 1995]. The under ice sounder failed

shortly after being deployed, hence we are unable to determine ice thickness after the instrument was deployed.

The flexural strength of sea ice is dependent on the brine volume, or total porosity of sea ice where strength declines as porosity increases [*Timco and O'Brien*, 1994]. Flexural strength has a strong seasonal cycle with a peak during winter (0.6-0.7 MPa), when the ice is cold and brine volumes are lowest, and a minimum during summer (< 0.2 MPa), when sea ice becomes isothermal and the brine volume increases as brine networks expand within the ice floe [*Timco and O'Brien,* 1994; *O'Brien and Johnson,* 2000]. *Timco and O'Brien* [1994] compiled 2500 sea ice strength tests and found a strong relationship between the flexural strength (σ_f) (MPa) and the brine volume (v_b) of sea ice that is described by the following equation,

$$\sigma_f = 1.76e^{-5.88\sqrt{v_b}} \quad (2)$$

Where v_b is expressed as a brine volume fraction, which is dependent on the ice temperature (T_i) and salinity (S_i). Using a relationship developed by *Frankenstein and Garner* [1967] *Timco and O'Brien* [1994] estimated the brine volume fraction with the following equation,

$$v_b = S_i \left[\frac{49.185}{|T_i|} + 0.532\right] \text{ for } -0.5°C \geq T_i \geq -22.9°C \quad (3)$$

A Nortek Z-Cell 600kHz ADCP was outfitted with a Nortek iridium communications module and deployed facing downwards through 4m of sea ice on the BREA primary site. The ADCP recorded near surface ocean currents in 30 separate 2m bins every 30 minutes. Ocean currents were corrected for ice drift using the iridium modules GPS, and magnetic declination using an online calculator maintained by Natural Resources Canada (http://geomag.nrcan.gc.ca/calc/mdcal-eng.php).

Daily mean sea ice concentrations within the Beaufort Sea (70°N – 76°N; 125°W – 155°W) were calculated from the National Snow and Ice Data Centers dataset "Sea ice concentrations from Nimbus-7 SMMR and DMSP SSM/I-SSMIS Passive Microwave" which has a spatial resolution of 25km.

Radarsat-2 ScanSAR wide scenes were collected over the BREA array throughout the drift of the autonomous equipment. ScanSAR scenes have a spatial resolution of 100m and a swath width of 500 km. Boxes 150 x 150 km centered on the BREA primary site were extracted from available scenes and used to extract local ice concentrations and floe size statistics.

4.3 Results

BREA ice beacon trajectories for the period between 7 April and 1 August, 2012 are presented in Figure 4.2A and are coloured by date. Initial beacon locations (Figure 4.1) are denoted with a black dot on the tracks in the eastern Beaufort Sea near Banks Island. Overall the ice drifted west towards the Chukchi Sea as part of the Beaufort Gyre [*Rigor et al.*, 2002; *Lukovich et al.,* 2011; *Babb et al.,* 2013]. *Nghiem et al.,* [2014] state that westward ice drift in the Beaufort Sea during spring 2012 facilitated divergence within the ice pack, causing it to fracture and become increasingly susceptible to the intrusion of warm water from the Mackenzie River. Ice drift during April and July are plotted separately in Figure 4.2B and 4.2C, respectively, and are coloured by beacon ID which corresponds to the study sites presented in Figure 4.1. Ice drift during April (Figure 4.2B) was near linear with very few reversals which gave the BREA array a low monthly meander coefficient of 1.30 (Table 4.1). Ice drift during May was similar with a meander coefficient of 1.63 (Table 4.1) and minimal variability in the values across the BREA array. In June ice continued to drift westward though reversals and random walks began to occur more often, causing meander coefficients to increase for all ice beacons with a monthly mean of

2.02 (Table 4.1) and a peak value of 2.46 (S4). During July (Figure 4.2C) ice drift became increasingly variable with large reversal events and inertial oscillations present along ice beacon trajectories. Inertial oscillations became evident in mid-July and are characteristic of ice drifting in free drift conditions; they therefore indicate a mechanically weak ice pack. As a result meander coefficients increased for all 10 ice beacons raising the monthly mean to 3.17 with two beacons (S3 and S8) exceeding a value of 4.

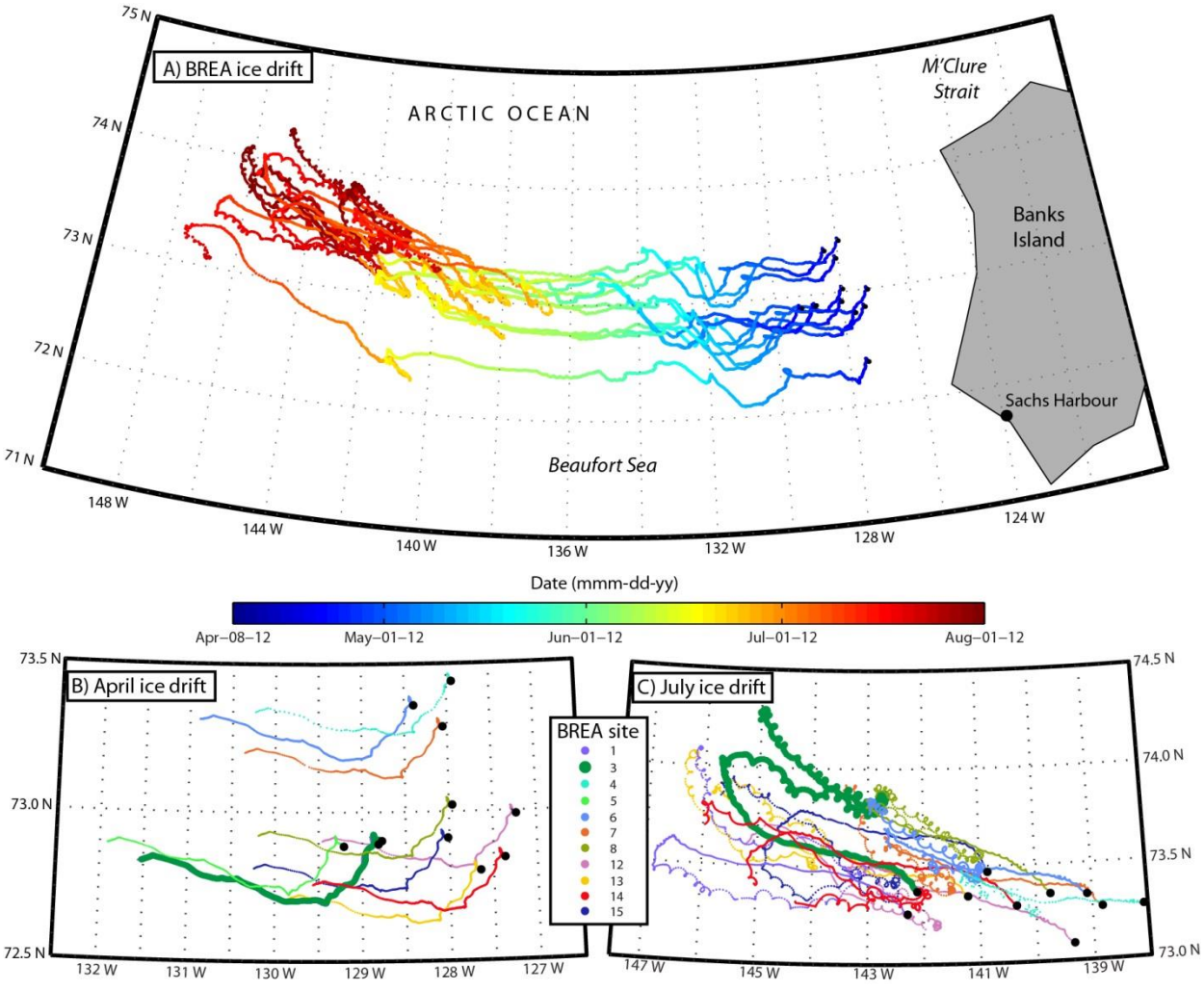

Figure 4.2: A) BREA ice beacon drift between 8 April and 1 August, 2012 coloured by date. BREA ice drift during April (B) and July (C), coloured by BREA study site. In B and C the BREA primary site (3) is enlarged.

Table 4.1: Monthly meander coefficients for each ice beacon and the overall monthly mean meander coefficient

ID	Site	Apr MC	May MC	Jun MC	Jul MC
244410	1	1.26	1.56	1.77	3.68
936500	3 (P)	1.27	1.56	1.82	4.03
130040	4	1.28	1.92	2.46	3.82
530480	5	1.28	1.57	---	---
424340	6	1.32	1.86	2.34	3.90
124720	7	1.3	1.85	2.26	3.03
243400	8	1.30	1.61	1.94	4.41
247410	12	1.33	1.53	2.16	2.53
535480	13	1.30	1.47	1.74	3.00
523940	14	1.35	1.49	2.01	3.13
123720	15	1.32	1.56	1.70	3.31
Mean		1.30	1.63	2.02	3.17

Monthly correlation coefficients of ice drift speeds between the BREA primary site and other sites are presented in Table 4.2. High correlation coefficients ($r > 0.90$) during April and May indicate cohesive motion within the ~70 km wide BREA array, as the ice drifted westward (Figure 4.2A and 4.2B). Cohesive drift during late winter is the result of a compact ice pack in which ice floes are constrained to drift in concert with neighboring ice floes [*Colony and Thorndike,* 1980]. As ice drift became increasingly variable during June the inter-beacon correlations declined (Table 4.2), indicating a considerable reduction in the cohesive nature of the ice pack. Inter-beacon correlations increased slightly during July, though the increase was small compared to the large decrease observed between May and June. S4 was furthest away (70 km at deployment) from the primary site (Figure 4.1B) and routinely had the lowest correlation coefficients, including a negative correlation in the V-component of motion during July (not shown). S6 and S7 were deployed ~60 km north of the primary site near S4 and routinely had the second and third lowest correlation coefficients, though the values of these sites were more aligned with the other sites rather than those of S4. S5 and S1 were located nearest to S3, 13km

Table 4.2: Monthly correlations of ice drift speeds between each ice beacon and the ice beacon at the primary site. Monthly mean correlations are presented at the bottom.

Beacon	Site	April	May	June	July
244410	1	1.0	1.0	0.97	0.85
130040	4	0.88	0.75	0.49	0.49
530480	5	0.99	0.99	0.97	--
424340	6	0.93	0.88	0.60	0.79
124720	7	0.89	0.83	0.57	0.73
243400	8	0.90	0.90	0.68	0.83
247410	12	0.90	0.88	0.60	0.75
535480	13	0.89	0.91	0.84	0.81
523940	14	0.88	0.89	0.76	0.75
123720	15	0.90	0.92	0.82	0.80
Mean		**0.92**	**0.90**	**0.73**	**0.76**

and 2km away respectively and showed very high correlations (> 0.97) through April, May and June. Subsequently in July the beacon at S5 failed, likely due to dynamic breakup of the floe, and the correlation between S3 and S1 declined considerably. Both these events are ascribed to the breakup of the Beaufort ice pack in which floes entered a state of free drift and drifted less coherently over short scales of several kilometers. Overall inter-beacon correlations within the BREA array highlight the seasonal loss of coherent motion within the ice pack. This combined with the seasonal increase in meander coefficients reveals the seasonal evolution from a consolidated ice pack drifting cohesively to a deteriorating ice pack entering a state of free drift.

4.3.1 Seasonal decline of the Beaufort ice pack

The seasonal decline of the arctic ice pack through spring is driven by the return of solar energy after the long polar night. Solar energy increases air temperatures and warms the snow pack, thereby initiating surface melt which reduces the albedo and increases the penetration of solar energy which ultimately leads to surface melt and bottom ablation [*Perovich et al.,* 2002; 2007]. *In situ* IMB observations of air temperature, ice temperature profiles and surface water

temperature from 7 April to 30 July, 2012 are presented in Figure 4.3. Gaps in the data are due to failed transmissions from the IMB during which it was unable to connect to the iridium satellite communications system. Air temperatures (Figure 4.3A) were between -10°C and -30°C during April, increased through May and varied between -4°C and 10°C from 27 May to 29 July, when the IMB failed. Once temperatures reached 0°C the surface would have quickly transitioned from

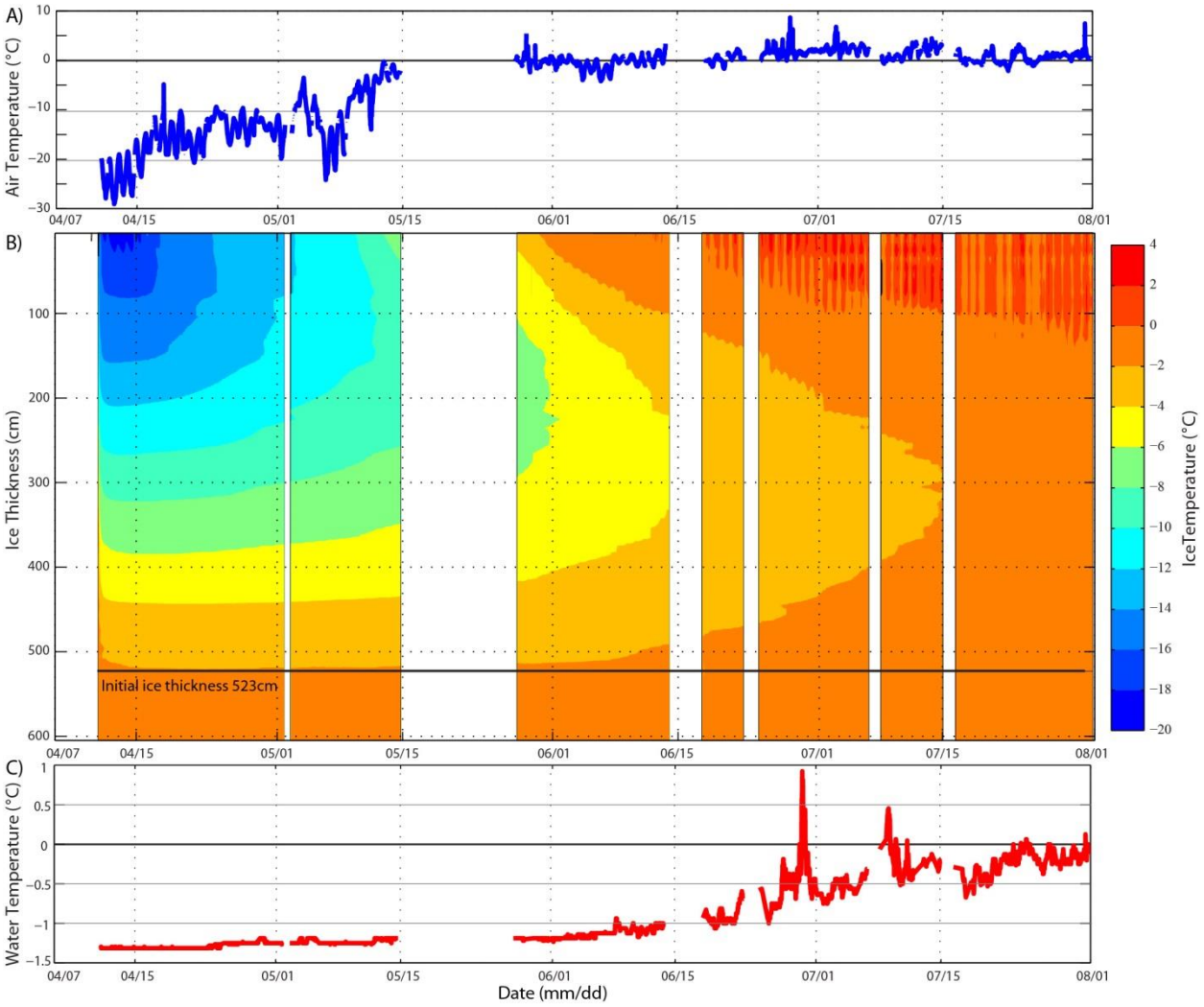

Figure 4.3: IMB observations on air temperature (A), ice temperature profile (B) and near surface (2.8m below the ice-ocean interface) water temperatures (C). All temperatures are presented in °C with black lines denoting 0°C in the top and bottom panel. The black line in the middle panel denotes the initial ice thickness of 523cm on 10 April, 2012.

'dry snow' to 'melting snow' to 'pond formation' with a coincident decline in surface albedo [*Perovich et al.,* 2008]. As the albedo declined seasonally more incident solar energy would have penetrated the ice pack, thereby warming the ice floe and initiating surface melt.

Initially there was a very strong vertical temperature gradient through the 523cm thick ice floe, with temperatures of -21°C near the ice-snow interface and -1.9°C at the ice-ocean interface (Figure 4.3B). As air temperatures increased throughout spring, so too did temperatures within the ice floe. Temperatures at the ice-snow interface increased through May and were routinely above 0°C by June 3rd, indicating that surface melt began around this time. In mid-June near surface temperature sensors began recording temperatures above 0°C with a diurnal cycle which we believe indicates the ice had melted out around these temperature sensors and they were recording air temperatures. When the IMB failed on 29 July, the temperature sensor ~130cm below the initial ice surface was recording temperatures above 0°C with diurnal cycles, indicating considerable surface melt had occurred during spring. *Perovich and Elder* [2001] showed that thick ice floes may never become isothermal as the middle portion is insulated from the warming atmosphere and ocean by several meters of ice. The BREA primary floe became isothermal on 15 July, though the middle portion (~300cm below the initial ice-snow interface) only became warmer than -2.0°C after air temperatures had exceeded 0°C for two months and considerable surface warming/melt had occurred within the top 100 cm of the ice floe. As the ice floe became isothermal its internal temperature gradient disappeared, causing the conduction of energy away from the ice-ocean interface to cease, thereby allowing the ocean heat flux to dominate the energy balance at the ice-ocean interface and force bottom ablation. Due to the malfunction of our under ice acoustic sounder we cannot measure bottom ablation and the daily melt rate, though *Perovich et al.,* [2008] show that once an ice floe has become isothermal

bottom melt can occur rapidly (2-4 cm day^{-1}). Therefore as the ice floe warmed considerably throughout spring 2012 (Figure 4.3B) it would have become much thinner via considerable rates of surface melt and bottom ablation.

Near surface water temperatures measured at the end of our 8 m long temperature string, or ~2.8m below the initial ice-ocean interface, are presented in Figure 4.3C. Overall water temperatures increased throughout the season from -1.3°C in April to between -0.5°C and 0.1°C in late July. The maximum water temperature of 0.9°C was recorded on 29 June two days after the peak air temperature of 8.9°C was recorded (Figure 4.3A). As near surface water temperatures increased seasonally so too would the ocean heat flux, which warms the ice from below and drives bottom ablation [*Perovich et al.,* 2008]. *Perovich et al.,* [2008] present observations of near surface water temperatures which increase seasonally with abrupt increases that can temporarily double daily bottom melt rates. We note a similar pattern in our near surface water temperatures which increased seasonally with episodic increases on 29 June and 9 July when temperatures increased to 0.9°C and 0.5°C, respectively. Spikes in water temperatures would have temporarily increased the ocean heat flux and either initiated or increased the rate of bottom ablation. The latter peak occurred shortly after a large discharge of warm river water entered the Beaufort Sea from the Mackenzie River between 14 June and 5 July, which caused an average increase of 6.5°C in open water surface temperatures throughout the Beaufort Sea [*Nghiem et al.,* 2014]. The authors note that this heat did not immediately penetrate the ice pack, though the IMB was located along the periphery of the ice pack that bordered the large expanse of open water (316 000 km^2; *Nghiem et al.,* 2014), and therefore may have been subject to increased heat content in the upper ocean. Beyond heat input from the Mackenzie river, it has been shown that the entire Arctic had a large amount of heat content in the near surface waters

that drove the record 2012 September sea ice minimum [*Zhang et al.,* 2013]. Bottom ablation weakens the ice pack by thinning it but also reduces C_w and the transfer of momentum across the ice-ocean interface. Bottom ablation creates a smoother ice-ocean interface by preferentially melting keels [*Wadhams,* 1992] and increases the density stratification of the oceanic boundary layer by adding fresh melt water, thereby reducing vertical momentum transfer and reducing drag by creating 'slippery ice' [*McPhee,* 1979; Wadhams, 2000].

Using *in situ* IMB ice temperature profiles and an assumed MYI salinity of 2.1 [*Eicken et al.,* 1995], we calculated the daily flexural strength of the BREA primary floe. Between April and July 2012 the flexural strength of the BREA primary site declined by 85% (Figure 4) from 0.97 MPa on 7 April to 0.15 MPa on 31 July. These results agree with the seasonal decline of flexural strength outlined by *Timco and O'Brien* [1994] that occurs as the ice floe warms and brine volumes increase, thereby reducing the completeness and strength of the ice lattice. The daily flexural strength declined at a rate of -0.0019 MPa day^{-1} during April and -0.0051 MPa day^{-1} during May as the ice floe began to warm. By June the rate doubled to -0.011 MPa day^{-1} as the ice began to weaken rapidly. During July the rate remained high at -0.0098 MPa day^{-1}, though we note a decrease in the rate of decline during the last few days of the record as the ice floe had become isothermal and couldn't weaken much further. *Asplin et al.,* [2012] calculated the flexural strength of a well-drained, isothermal MYI floe in the Beaufort Sea during September to be 0.04 MPa, one quarter of our MYI floes final flexural strength value. The floe *Asplin et al.,* [2012] sampled subsequently fractured due to a storm induced long period swell that penetrated and broke up the ice pack. A warmer and therefore weaker ice floe is more susceptible to fracturing which reduces the floe size distribution and makes ice floes more susceptible to lateral melt and dynamic forcing [*Toyota et al., 2006; Asplin et al.,* 2012].

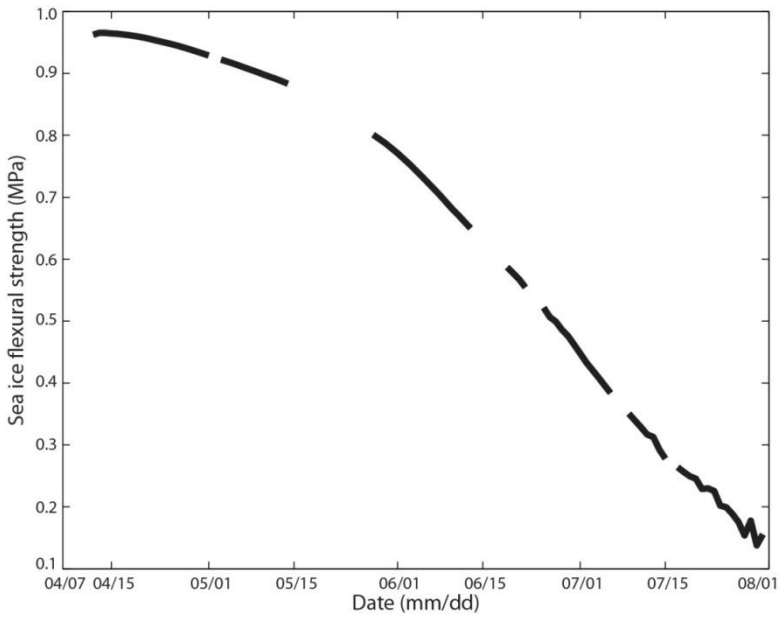

Figure 4.4: Daily sea ice flexural strength (MPa) of the BREA primary floe (S3). Ice strength is derived from ice temperatures measured from the IMB and a standard salinity value of 2.1 [Eicken et al., 1995].

Beyond the strength and thickness of individual ice floes, the mechanical strength of the ice pack is dependent on the local sea ice concentration and floe size distribution. Using Radarsat ScanSAR wide scenes we analyze local ice conditions (150km x 150km) around the BREA array during three separate days of the study (Figure 4.5). During late winter (9 April; Figure 4.5A) the local sea ice concentration was 100% with 26% coverage of MYI and 74% coverage of FYI. Note that during winter it is possible to distinguish between MYI (lighter pixels) and FYI (darker pixels), though once surface melt begins this is no longer possible due to the influence of melt water on the microwave signatures. Within Figure 4.5A there are discrete MYI floes, several of which we sampled, however they are 'welded' together by FYI into a large aggregate ice pack that drifted coherently (Figure 4.2B; Table 4.1; Table 4.2). Two months later (16 June; Figure 4.5B) the ice pack had broken up and the local sea ice concentration had declined to 82%. Notably the ice pack had broken up between April and June, liberating discrete floes from the aggregate ice pack and freeing them to drift independently with some internal

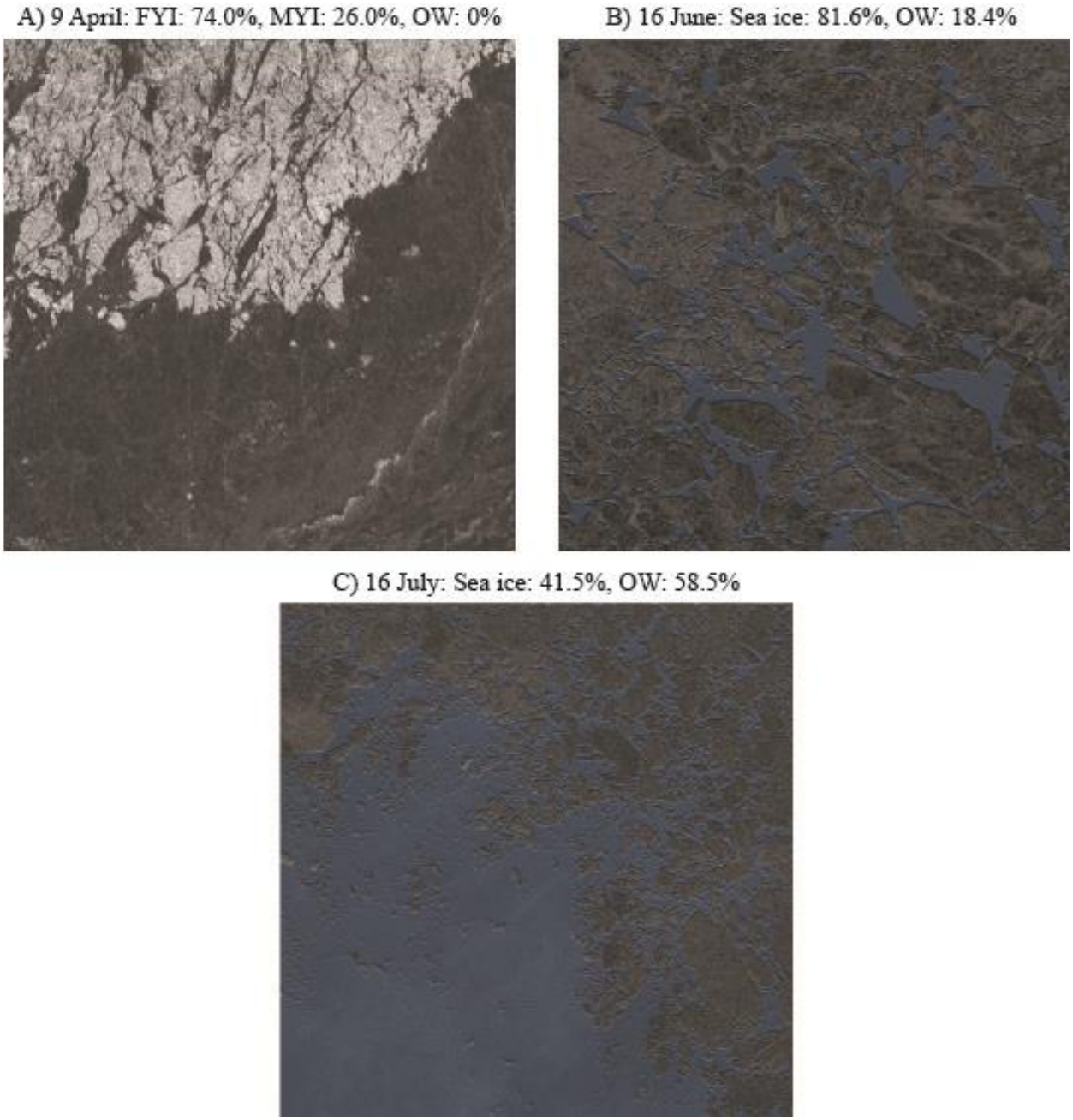

Figure 4.5: 150km x 150km Radarsat ScanSAR scenes from 9 April (A), 16 June (B) and 16 July (C) centered on the BREA primary site. Sea ice concentration is derived from each image. Blue represents open water. Images are rotated so North is to the top of the scene.

resistance to motion present due to floe-floe interactions. By liberating discrete floes and exposing their edges, which in turn increase turbulent momentum flux, the C_a of the ice pack would have increased and approached its maximum value which occurs at 80% sea ice

concentration [*Anderson*, 1987]. One month later (16 July; Figure 4.5C) local sea ice conditions had changed dramatically with a reduction in sea ice concentration to 42% and a corresponding increase in open water to 58%. Coincidentally the floe size distribution declined considerably, with a majority of the ice existing as small discrete ice floes. As a result C_a would have decreased from its seasonal peak in mid-June, though in terms of ice drift the reduction in C_a would have been offset by the reduction in internal stresses. With reduced sea ice concentrations solar penetration into the upper ocean would have increased and fostered a dramatic rise in the bottom and lateral melt rates that would act to further weaken the ice pack [e.g. *Steele*, 1992; *Perovich et al.,* 2008]. Figure 4.5 highlights the seasonal evolution of the sea ice surrounding the BREA array as it transitioned from a compact ice pack in late winter to a fractured but still compact ice pack in June before becoming a broken up set of independent ice floes in a state of free drift in July.

On a regional scale, daily sea ice concentrations in the Beaufort Sea (70°N – 76°N; 125°W – 155°W; 21 450 km^2) for the duration of the BREA study are presented in Figure 4.6A. Overall mean daily sea ice concentrations in the Beaufort Sea declined from a late winter peak of 99% to an early summer minimum of 15%. This reduced the mechanical strength of the Beaufort ice pack and contributed to ice floes entering a state of free drift. Daily sea ice concentrations declined at a rate of -0.1% day^{-1}, -0.7% day^{-1}, -1.3% day^{-1} and -0.7% day^{-1} during April, May, June and July respectively. The dramatic retreat of sea ice during June (-1.3% day^{-1}) was not limited to the Beaufort Sea as *Parkinson and Comiso* [2013] showed that Arctic sea ice retreated faster than normal during June 2012 because the ice pack was preconditioned towards younger and thinner sea ice. Subsequently *Zhang et al.,* [2013] showed that preconditioning and ocean

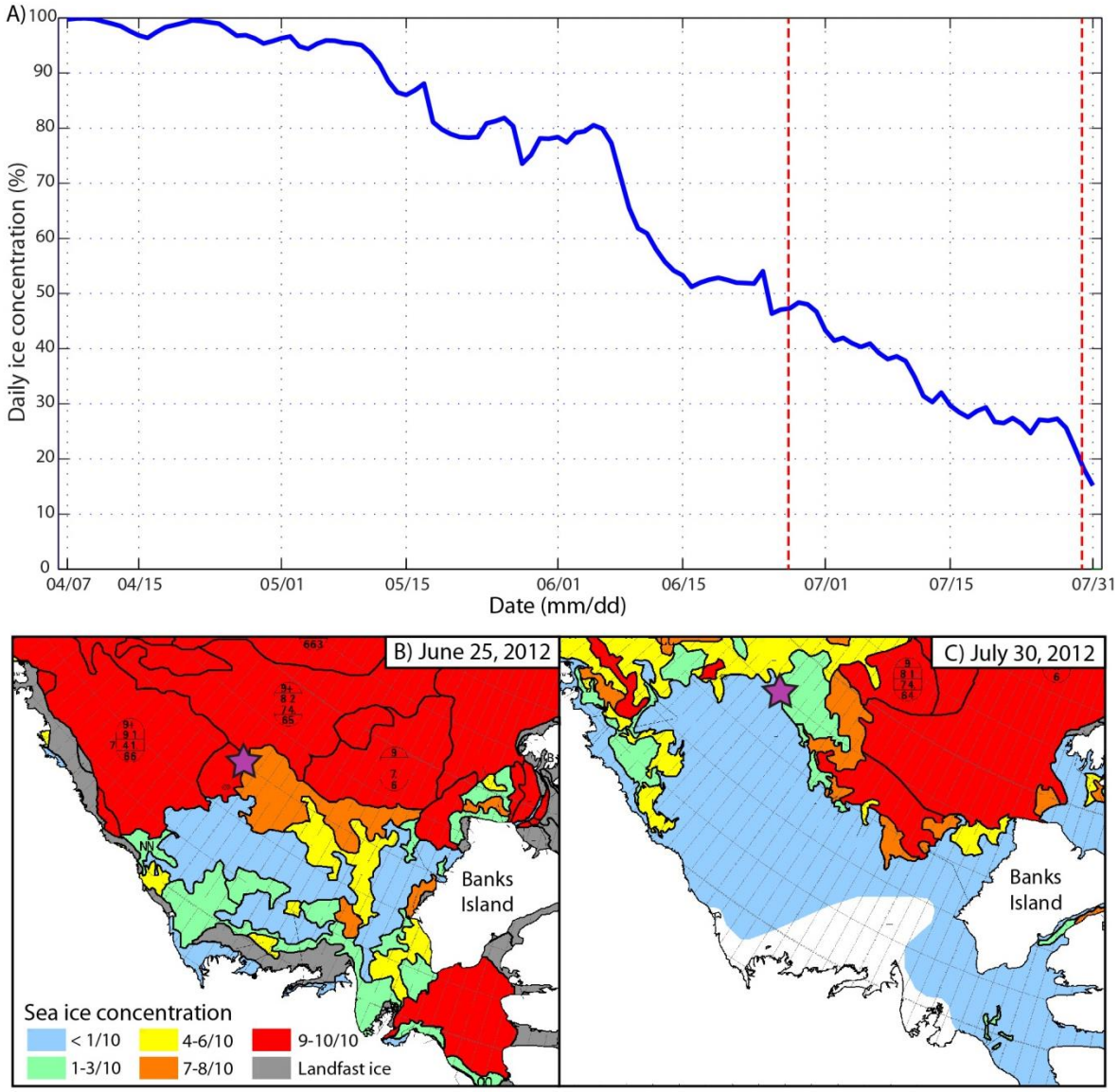

Figure 4.6: A) Daily mean ice concentration (%) in the Beaufort Sea (70°N to 76°N, 125°W to 155°W). B) and C) weekly Canadian Ice Service sea ice concentration ice charts for 25 June and 30 July, 2012, respectively. Ice chart dates are denoted in A) by dashed red lines. The location of the BREA primary site in B) and C) is denoted by the purple star.

heat in the near surface temperature maximum were significant enough to cause a 2012 record September sea ice minimum, though the 'great arctic cyclone of 2012' [*Simmonds and Rudeva,*, 2012] did further reduce the minimum by 4.4% to a record low of 3.41 x 10^6 km^2 on 16 September 2012 [NSIDC, 2012]. Of note, sea ice concentrations within our defined area of the Beaufort Sea declined below 1% on September 6 and 7 and remained below 15% from 1 August

to 11 October, allowing considerable amounts of solar energy to penetrate and warm the upper ocean, which in turn would have delayed the onset of freeze up [e.g. *Stroeve et al.*, 2014].

Figure 4.6B and 4.6C provide context for the sea ice decline in the Beaufort Sea relative to the location of the BREA primary site (purple star). Note there may be a discrepancy in sea ice concentrations between Figures 4.6A, which was derived from satellite based passive microwave sensors, and 4.6B and 4.6C which were produced by experienced sea ice forecasters at the Canadian Ice Service who integrate real time information from various satellite sensors, aerial reconnaissance, ship reports and operational model results. The BREA array was within an area of 9/10 sea ice concentration until early June when the ice pack began to decline rapidly. By 25 June the BREA primary site was located in an area of 7-8/10 sea ice concentration (Figure 4.6B). By 30 July, the day the IMB and ADCP failed, the BREA primary site was along the periphery of the ice pack in an area of 1-3/10 sea ice concentrations that bordered the vast expanse of open water in the Beaufort Sea (Figure 4.6C). This would have made the floes susceptible to waves penetrating the ice pack [e.g. *Asplin et al.*, 2012; 2014] and exposed ice floes to greater melt rates as the vast area of open water would have promoted the ice-albedo feedback loop and fostered further bottom and lateral melt.

As solar radiation returned to the Beaufort Sea during spring 2012 the Beaufort ice pack declined seasonally, becoming thinner, weaker and less concentrated with a tendency towards smaller floe sizes. Collectively these changes reduced the mechanical strength of the Beaufort ice pack, thereby reducing internal stresses and permitting ice floes to enter a state of free drift.

4.3.2 Seasonal evolution of ice drift and wind speeds

Daily mean ice drift speeds for the period of 8 April – 31 July, 2012 are presented in Figure 4.7A and show an increasing trend. Monthly mean ice drift speeds (black lines) increased

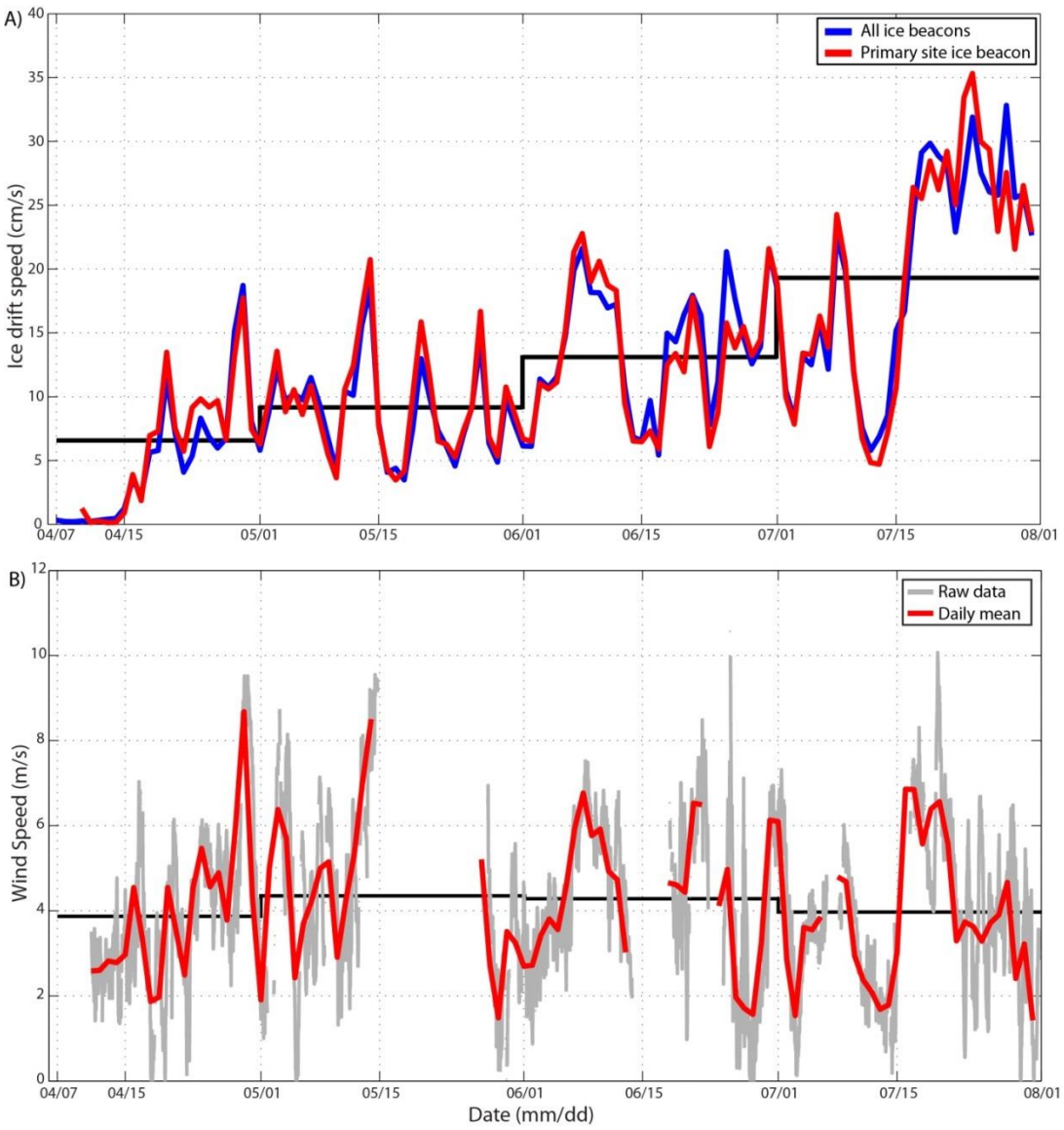

Figure 4.7: A) BREA in situ ice drift speeds (cm/s) for all ice beacons (blue) and for the primary site (red). B) In situ surface wind speeds (m/s) for the raw 30-minute data (grey) and the daily mean (red). Black lines in both plots denote the monthly means.

295% during spring from 6.56 cm/s in April to 19.36 cm/s in July. Ice drift speeds increased during all four months with intermediate monthly means of 9.23 cm/s in May and 13.16 cm/s in June. The seasonal increase in ice drift speeds was not accompanied by a similar increase in surface winds which remained around 4 m/s (Figure 4.7B). Overall there is a high level of coherence between ice drift speeds and wind speeds, as indicated by significant ($p < 0.05$)

positive correlations during all four months (Figure 4.8). Correlations of 0.73 and 0.78 for April and May, respectively, indicate a relatively strong relationship between ice and wind speeds during early spring (Figure 4.8A and 4.8B). The slightly lower correlation during April is attributed to observations of stationary ice (0 cm/s) which occurred under wind speeds as high as 4.7 m/s. Stationary ice occurs when external forces are collectively less than the strength of the ice [*Leppäranta,* 2005]. Such conditions existed during April when the mechanically strong Beaufort ice pack became locked up and unresponsive to external forcing. There are no other observations of stationary ice after April. As ice drift speeds increased during June and July the correlation with wind speeds declined to monthly values of 0.60 and 0.51, respectively (Figure 4.8C and 4.8D). The decline in July is ascribed to the loss of coherence that occurred after 15 July when wind speeds increased to 6.8 m/s, thereby forcing ice drift speeds to increase to a seasonal peak of 28 cm/s. Subsequently wind speeds declined steadily to a daily mean of 1.7 m/s on 30 July whereas ice speeds remained at their seasonal peak between 23 and 35 cm/s. The loss of coherence between ice and wind speeds during late July is ascribed to the onset of free drift conditions which are revealed by the presence of inertial oscillations along the ice beacon trajectories around this same time (Figure 4.2C).

Monthly frequency distributions of hourly ice speed (blue) and wind speed (red) are presented in Figure 4.9. The modal ice drift speed for April, May and June was 5-10 cm/s though the frequency of observations in the 10-15 cm/s bin increased during all four months until it was the modal speed in July (Figure 4.9D). Conversely the frequency of observations between 0-5 cm/s decreased during all four months, highlighting the tendency towards higher ice drift speeds. Higher ice drift speeds caused the right tail of the ice speed distribution to increase, which is reflected by a decrease in the kurtosis values of each month from a mesokurtic (bell shaped)

value of 2.97 in April to platykurtic (flat) values of 2.47 and 2.55 in June and July, respectively. In terms of wind speed all four distributions are fairly equal with monthly means near 4 m/s and modes of 3-4 m/s. In fact monthly mean wind speeds were statistically equal ($p < 0.05$) during April and July, and May and June.

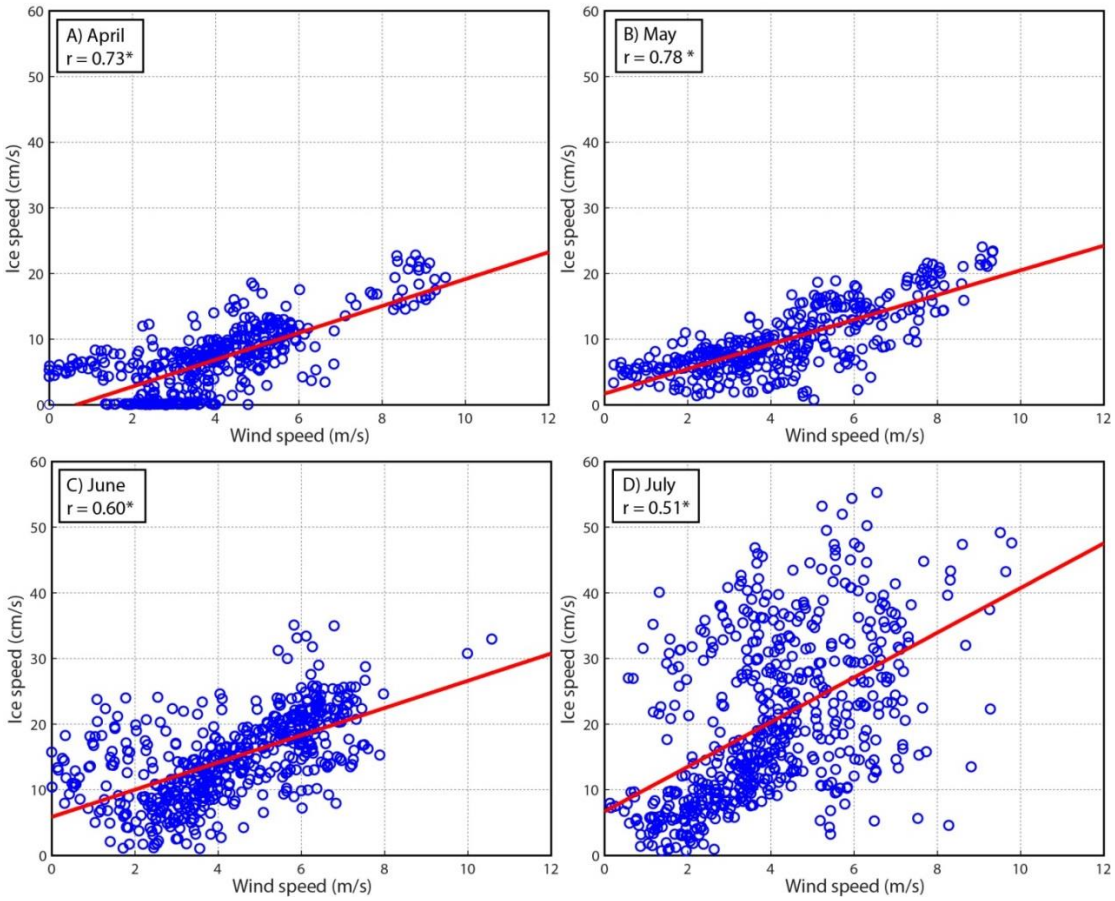

Figure 4.8: Monthly scatterplots of wind speed (m/s) and ice speed (cm/s) for hourly in situ observations. The red line is the line of best fit, with the correlation coefficient presented. Note all correlations are significant at the 95% confidence level.

Monthly distributions of *F* (speed reduction factor) are presented in Figure 4.10 with bin widths of 0.5%. The monthly mean *F* increased by 3.65% during spring from 2.06% in April to 5.71% in July. At the same time the right tail of the distribution expanded and the monthly mode of *F* increased from 0-0.5% in April to 2 - 2.5% in May, 3 - 3.5% in June and 3.5 – 4% in July. This indicates a tendency towards higher *F* factors as ice drift transitioned from a winter regime

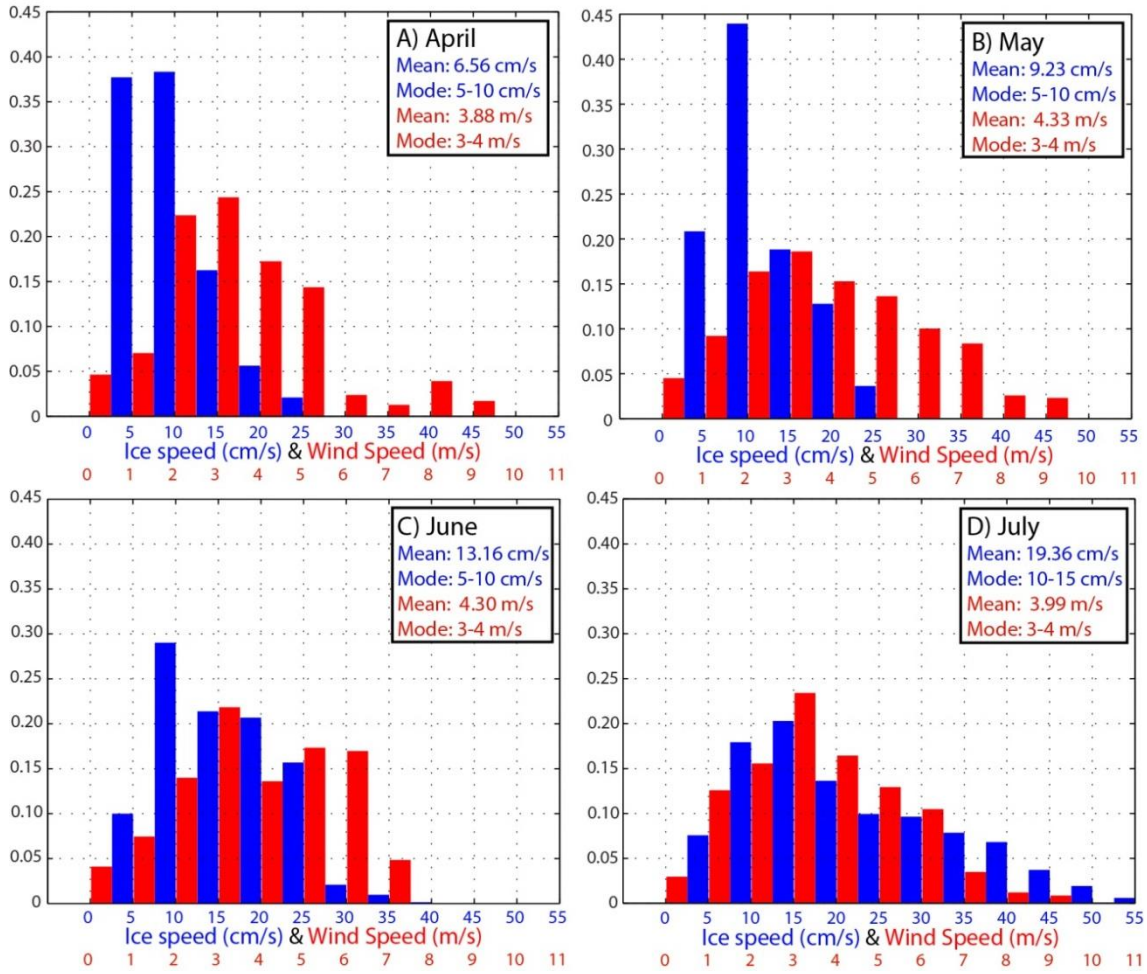

Figure 4.9: Monthly PDF's of the hourly ice speed (blue) and wind speed (red) measured at the BREA primary site. Monthly means and modes are presented for both.

in April, through the transition month of May into the summer regime during June and July [*Thomas*, 1999]. *Leppäranta* [2005] shows that *F* is related to the ratio of the air-ice and ice-ocean drag coefficients and notes that a higher *F* may be associated with a lower ice-water drag coefficient due to the preferential melt of keels, thereby reducing the form drag of the ice floe [*Wadhams* 1992; *Schramm et al.*, 2000], and the release of meltwater from bottom ablation into the upper ocean, thereby stratifying the ocean boundary layer and creating 'slippery ice' [*McPhee*, 1979]. Conversely the air drag increases seasonally as the ice pack breaks up and exposes the above water faces of the ice floe to surface winds [*Wadhams*, 2000]. Higher *F* values

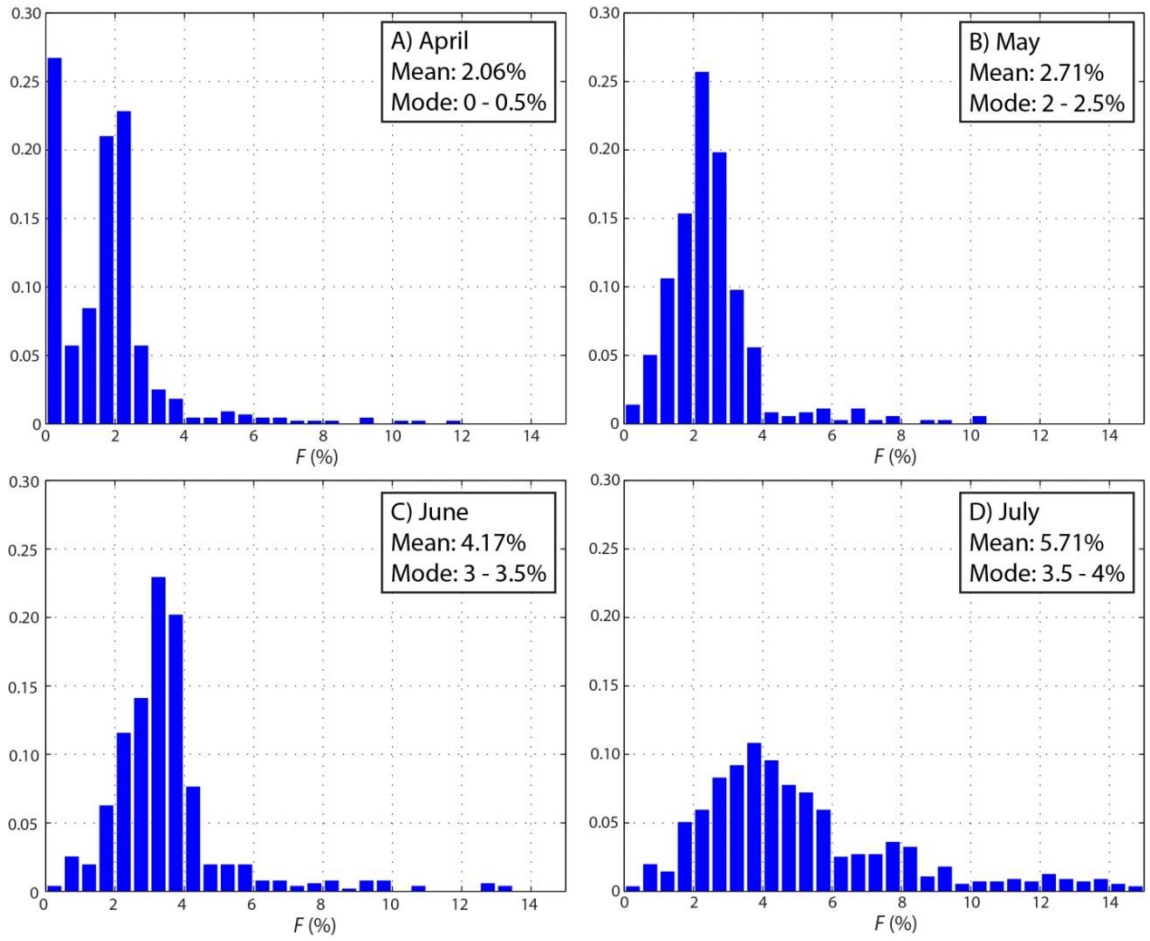

Figure 4.10: Monthly PDF's of the hourly F (speed reduction) factor between surface winds and ice drift at the BREA primary site. Bins are 0.5% wide. Monthly means and modes are presented.

in July relative to April, the observed increase in bottom ablation shown by the IMB results (Figure 4.3), and transition to smaller floes (Figure 4.5), are consistent with these results. From Figure 4.9 it is apparent that the 2% rule of thumb [*Nansen*, 1902; *Thorndike and Colony*, 1982] best applies to late winter conditions when the consolidated ice pack is mechanically strong. Conversely the rule of thumb does not correspond with ice drift in the marginal ice zone during spring and summer when floes enter a state of free drift and become increasingly responsive to atmospheric forcing.

Ice direction (blue) and wind direction (red) are presented in Figure 4.11 where angles rotate from 0° north clockwise to 360° north. Note that ice direction represents the direction in which the ice drifted whereas wind direction, as per general convention, is the angle at which the

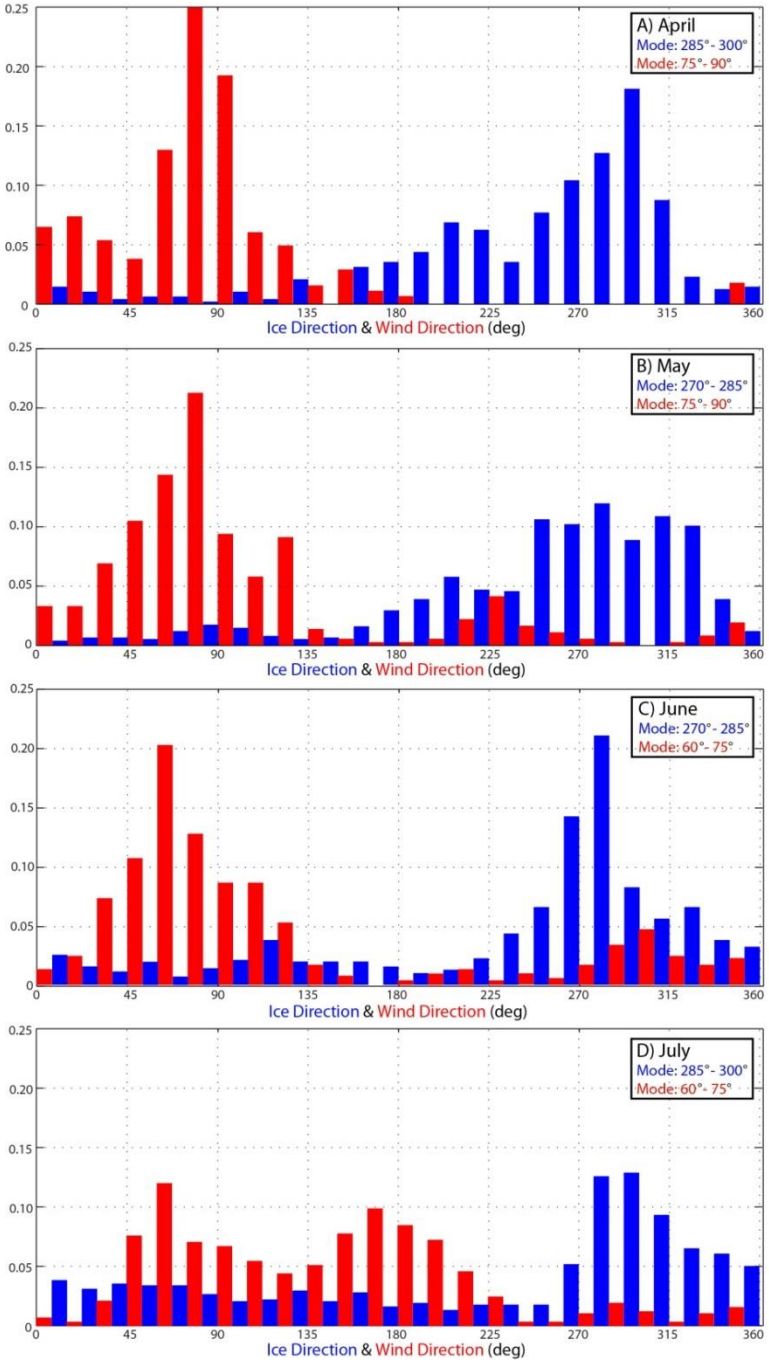

Figure 4.11: Monthly PDFs of hourly ice drift direction (blue) and wind direction (red) measured at the BREA primary site. Monthly modes are presented.

wind blew from. Predominantly winds blew from the east with monthly modes of 75°-90° during April and May (Figure 4.11A and 4.11B), and 60°-75° during June and July (Figure 4.11C and 4.11D). Accordingly ice drifted predominantly to the west, as in Figure 4.1, with monthly modes of 285°-300° in April and July (Figure 4.11B and 4.11H), and 270°-285° in May and June (Figure 4.11D and 4.11F). In July the wind direction distribution was more variable with a bimodal distribution that drove the large scale reversal events present in July ice trajectories (Figure 4.2C). Interestingly the bimodal distribution of winds is not accompanied by a comparable bimodal distribution in the ice direction distribution. The first peak in wind direction at 60°-75° (east-north-easterly winds) forced the peak in ice drift direction between 285°-300° (west-northwestward drift). Therefore we would anticipate the second peak in wind direction at 165°-180° (southerly winds) to force a second peak in ice drift directions around 0°/360° (northward drift). However there is no secondary peak in the ice drift direction distribution, instead there is a broad plateau of observations between 0° and ~90° (northward-eastward drift). This plateau is ascribed to internal stresses that may arise in response to on-ice winds which compress the marginal ice zone against the remaining arctic ice pack. Under such conditions ice may be prevented from drifting with the surface winds, thereby precluding a corresponding northward peak in the July ice drift direction distribution.

Monthly distributions of the turning angle between the ice direction and wind heading are presented in Figure 4.12 and highlight an increasing trend in turning angles through spring. It should be noted wind heading is the direction in which the wind blew and is rotated 180° from the wind direction presented in Figure 4.11. Negative turning angles indicate ice drift to the left of surface winds, whereas positive turning angles indicate ice drift to the right of surface winds which is the result of the Coriolis force. Monthly mean turning angles increased from -0.80° in

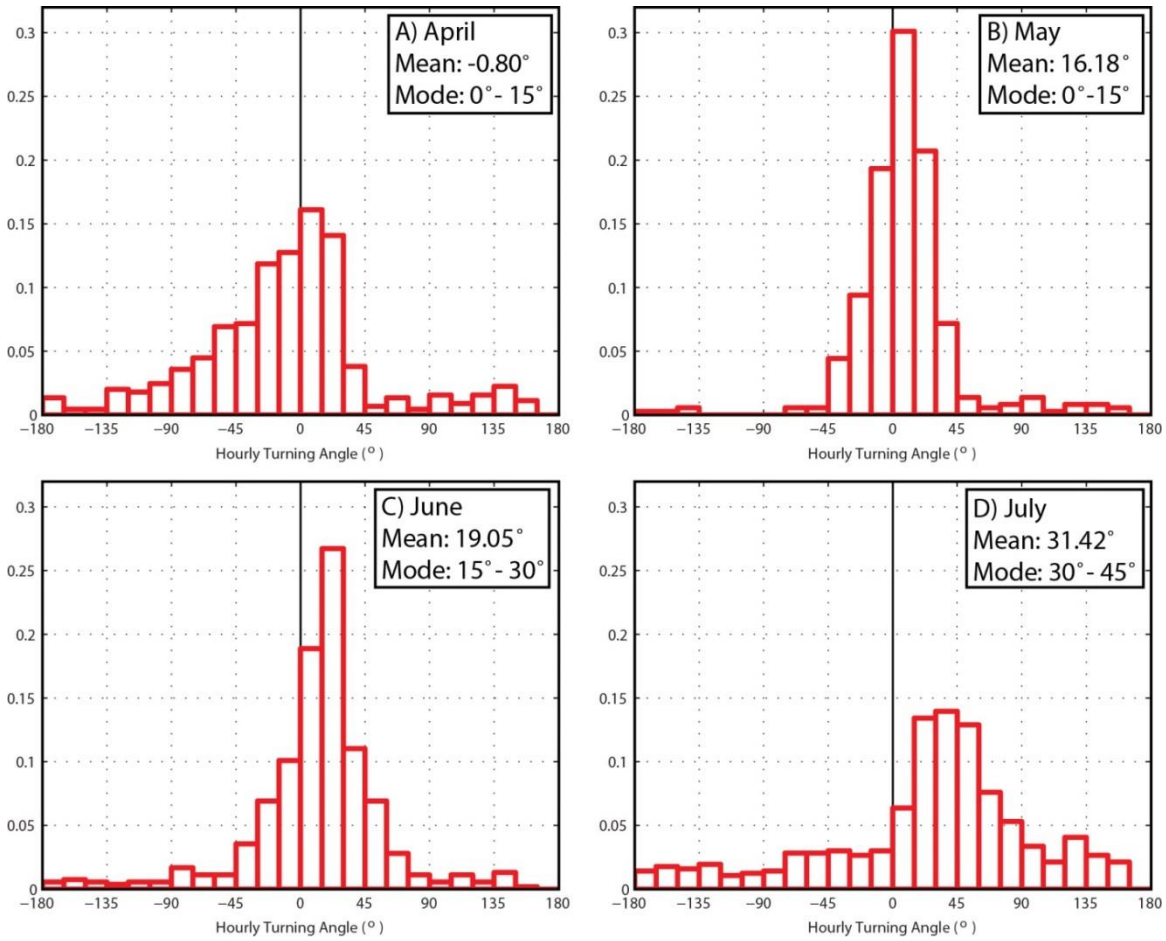

Figure 4.12: Monthly PDFs of hourly turning angles between the ice drift and surface wind at the BREA primary site. Note Positive values indicate ice drift to the right of the wind and negative values indicate ice drift to the left of the wind.

April to 16.18°, 19.05° and 31.42° during May, June and July, respectively (Figure 4.12). Likewise the monthly mode increased from 0-15° in April and May to 15-30° in June and 30-45° in July. Overall we see a transition to increasingly positive turning angles as during each month the net frequency of negative turning angles declined and the frequency of turning angles between 30° and 45° increased. Again we note the change in ice drift from a characteristically winter regime in April, through the transition month of May into the summer regime of June and July [*Thomas*, 1999]. The negative turning angles during April (Figure 4.12A) are attributed to the dynamic effects of a consolidated late winter ice pack which became locked up and therefore

less responsive to surface winds. *Thomas* [1999] showed that turning angles near 0° are characteristic of ice drift during the winter ice drift regime (November to April). Turning angles in April were limited as the Coriolis force was dampened out by internal stresses. This specifically occurred along the MYI edge where under easterly winds there theoretically should have been a northward component to the westward ice drift. However this was not the case, and ice instead drifted directly with the winds giving rise to very low and even negative turning angles. Only once the MYI edge weakened would easterly winds force westward ice drift with positive turning angles, like we recorded during May, June and July. The seasonal increase in turning angles is attributed to the mechanical weakening and degradation of the arctic ice pack which allowed ice floes to enter free drift conditions, in which ice characteristically drifts between 30° and 45° to the right of surface winds [*Nansen,* 1902; *Thorndike and Colony,* 1982].

4.4 Conclusions:

Through spring 2012 the Beaufort ice pack mechanically weakened as local and regional sea ice concentrations declined, floe size distributions declined, and ice floes warmed, became thinner, and increasingly susceptible to fracturing. Collectively these changes broke up a large aggregate ice pack into discrete ice floes which reduced internal stresses and fostered free drift conditions for the remaining ice floes. As a result ice speeds increased nearly 300%, F increased by 3.65%, turning angles increased by 32°, meander coefficients increased 2.5 times and ice drift within the BREA array became less cohesive across increasingly small length scales. All this occurred despite the fact that monthly mean wind speeds were statistically ($p < 0.05$) equal during April and July. Indicating that the ice pack became increasingly responsive to atmospheric forcing in a manner consistent with the mechanisms that have fostered a pan arctic increase in ice drift speeds over the past three decades [*Rampal et al.,* 2009; *Spreen et al.,* 2011;

Zhang et al., 2012; *Kwok et al.,* 2013]. Therefore monitoring the seasonal evolution of sea ice, both in terms of dynamics and thermodynamics, may provide an ideal setting for predicting future scenarios of ice drift in the Arctic as the ice pack continues to decline.

The seasonal decline of the ice pack shown in the present study promoted the ice-albedo feedback loop which fostered further reductions and ultimately led to the Beaufort ice pack south of 75°N almost melting out entirely. The observational record from our autonomous equipment ended in late July 2012 when the ice pack broke up to the point where all of our equipment failed and likely sank. One month later the Beaufort Sea was ice free south of 75°N and the entire arctic ice pack reached a record minimum extent of 3.41 million km^2. It has been shown that the 2012 minimum was driven by preconditioning towards a younger ice pack that was more susceptible to the thermodynamic effects of increased ocean heat content, and the dynamic effects of the great Arctic cyclone of 2012. Our results corroborate other works and highlight the feedback between dynamics and thermodynamics within a seasonally declining ice pack. The role of the ice albedo feedback loop has been well defined [*e.g. Perovich et al.,* 2008], though our results here suggest that there is a dynamic impact of the feedback loop that increases the responsiveness of the ice pack to external forcing and thus causes an increase in ice drift speeds.

This work quantifies the evolution of ice drift and its response to forcing mechanisms from late winter conditions to early summer conditions in the Beaufort Sea. It also improves our understanding of the natural evolution of both the dynamic and thermodynamic nature of the ice pack during this period, which is necessary as it is the seasonal evolution of these factors that determine when the risk of ice hazards declines to an acceptable level for offshore economic activity to commence safely. *Stroeve et al.,* [2014] show that melt onset is occurring earlier in the Beaufort Sea, which theoretically would allow for earlier access to offshore resources. However,

Barber et al., [2014] discuss the counterintuitive situation where a declining ice pack may in fact create more dangerous and less predictable ice conditions. Within this paper we show how this counterintuitive situation occurs on a seasonal scale, during which large MYI floes enter a state of free drift, drift at higher speeds and become less predictable, thereby increasing the risk associated with early season offshore activity.

4.5 Acknowledgements:

We dedicate this paper to the memory of our friend and colleague Dr. Klaus Hochheim who was the leader of our BREA program. He will be remembered for his passion and dedication to Arctic research. Thanks to the BREA and those involved in administering and running the program. Thanks to the town of Sachs Harbour for hosting us for two weeks and to our helicopter pilots for safely flying us to our offshore study sites. Thanks to A. Crawford from Carleton University for taking part and assisting in our field program. This is a contribution to the Arctic Science Partnership (ASP) and ArcticNet. Thanks to Dr. R. Galley and Dr. M. Asplin for useful discussion as this paper was written.

References:

Andersen, R.J. (1987), Wind stress measurements over rough ice during the 1984 Marginal Ice Zone Experiment, *J. Geophys. Res.*, 92 (C7), 6933-6941, doi:10.1029/JC092iC07p06933.

Asplin, M.G., R. Galley, D.G. Barber and S. Prinsenberg (2012), Fracture of summer perennial sea ice by ocean swell as a result of Arctic storms, *J. Geophys. Res. Oceans*, 117, C06025, doi: 10.1029/2011JC007221.

Asplin, M.G., R. Scharien, B. Else, S. Howell, D.G. Barber, T. Papakyriakou and S. Prinsenberg (2014), Implications of fractured Arctic perennial ice cover on thermodynamic and dynamic sea ice processes, *J. Geophys. Res. Oceans*, 119, doi: 10.1002/2013JC009557.

Babb, D.G., R.J. Galley, M.G. Asplin, J.V. Lukovich and D.G. Barber (2013), Multiyear sea ice export through the Bering Strait during winter 2011-2012, *J. Geophys. Res. Oceans*, 118, 5489-5503, doi:10.1002/jgrc.20383.

Barber, D.G., G.M. McCullough, D.G. Babb, A.S. Komarov, L.M. Candlish, J.V. Lukovich, M. Asplin, S. Prinsenberg, I . Dmitrenko and S. Rysgaard (2014), Climate change and ice hazards in the Beaufort Sea, *Elementa*, 2:000025, doi:10.12952/journal.elementa.000025.

Barber, D.G., R. Galley, M.G. Asplin, R. De Abreu, K.A. Warner, M. Pucko, M. Gupta, S. Prinsenberg and S. Julien (2009), Perennial pack ice in the southern Beaufort Sea was not as it appeared in the summer of 2009, *Geophys. Res. Lett.*, 36, L24501, doi: 10.1029/2009GL041434.

Bourke, R.H., and R.P. Garrett (1987), Sea ice thickness distribution in the Arctic Ocean, *Cold Regions Science and Technology*, 13, 259-280.

BREA (2012), Oil and Gas Exploration and Development Activity Forecast – Canadian Beaufort Sea 2012-2027, Prepared for BREA – Aboriginal Affairs and Northern Development Canada.

Colony, R. and A.S. Thorndike (1980), The Horizontal Coherency of the motion of Summer Arctic Sea Ice, *J. of Physical Oceanography*, 10, 1281-1289.

Comiso, J.C. (2012), Large Decadal Decline of the Arctic Multiyear Ice Cover, *J. Climate*, 25, 1176-1193.

Eicken H., M. Lensu, M. *Leppäranta*, W.B. Tucker III, A.J. Gow and O. Salmela (1995), Thickness, structure and properties of level summer multiyear ice in the Eurasian sector of the Arctic Ocean, *J. Geophys. Res.* 100 (C11), 22,697-22,710.

Galley, R.J., B.G.T. Else, S.J. Prinsenberg, D. Babb, D.G. Barber (2013), Sea ice concentration, extent, age, motion and thickness in regions of proposed offshore oil and gas development near the Mackenzie Delta – Canadian Beaufort Sea, *Arctic*, 66(1), 105-116.

Geiger, C.A. and D.K. Perovich (2008), Springtime ice motion in the western Antarctic Peninsula, *Deep-Sea Research II*, 55, 338-350.

Hakinen, S., A. Proshutinsky and I. Ashik (2008), Sea ice drift in the Arctic since the 1950s, *Geophys. Res. Lett.*, 35, L19704, doi:10.1029/2008GL034791.

Heil, P., R. A. Massom, I. Allison and A. Worby (2011), Physical attributes of sea-ice kinematics during spring 2007 off East Antarctica, *Deep-Sea Research II*, 28, 1158-1171.

Heil, P., R.A. Massom, I. Allison, A.P. Worby and V. I. Lytle (2009), Role of off-shelf to on-shelf transitions for East Antarctica sea ice dynamics during spring 2003, *J. Geophys. Res.* 114, C09010, doi: 10.1029/2008JC004873.

Hutchings J.K. and I.G. Rigor (2012), Role of ice dynamics in anomalous ice conditions in the Beaufort Sea during 2006 and 2007, *J. Geophys. Research*, 117, C00E04, doi: 10.1029/2011JC007182.

Kimura, N. and M. Wakatsuchi (2000), Relationship between sea-ice motion and geostrophic wind in the Northern Hemisphere, *Geophys. Res. Letters*, 27(22), 3735-3738.

Kwok, R., and D.A. Rothrock (2009) Decline in Arctic sea ice thickness from submarine and ICESat records: 1958-2008, *Geophysical Research Letters*, 36, L15501, doi:10.1029/2009GL039035.

Kwok, R., G. Spreen and S. Pang (2013), Arctic sea ice circulation and drift speed: Decadal trends and ocean currents, *J. Geophys. Res. Oceans*, 118, 2408-2452, doi: 10.1002/jgrc.20191.

Maslanik, J., J. Stroeve, C. Fowler and W. Emery (2011), Distribution and trends in Arctic sea ice age through spring 2011, *Geophys. Res. Letters*, 38, L13502, doi: 10.1029/2011GL047735.

McPhee, M.G. (1979), The effect of the Oceanic Boundary Layer on the Mean Drift of Pack Ice: Application of a Simple Model, *J. Physical Oceanography*, 9, 388- 400.

McPhee, M.G. (1978), A simulation of inertial oscillations in drifting pack ice, *Dynamics of Atmospheres and Oceans*, 2, 107-122.

Melling, H. (2002), Sea ice of the northern Canadian Arctic Archipelago, *J. Geophys. Research*, 107, C11, doi: 10.1029/2001JC001102.

Nansen, F. (1902), Norwegian North Polar Expedition 1893-1896, Scientific Results, vol. 3, The Oceanography of the North Polar Basin, 427 pp., Longmans, Green, London.

Nghiem, S.V., D.K. Hall, I.G. Rigor, P. Li and G. Neumann (2014), Effects of Mackenzie River discharge and bathymetry on sea ice in the Beaufort Sea, *Geophys. Res. Lett.*, 41, 873-879, doi:10.1002/2013GL058956

Parkinson, C.L. and J.C. Comiso (2013), On the 2012 record low Arctic sea ice cover: Combined impact of preconditioning and an August Storm, *Geophys. Res. Letters*, 40, 1-6, doi:10.1002/grl.50349.

Perovich, D.K., Richter-Menge, J.A., Jones, K.F., and Light, B. (2008), Sunlight, water and ice: Extreme Arctic sea ice melt during the summer of 2007, *Geophys. Res. Letters*, 35, L11501, doi: 10.1029/2008GL034007.

Perovich, D.K., S. V. Nghiem, T. Markus and A. Schweiger (2007), Seasonal evolution and interannual variability of the local solar energy absorbed by the Arctic sea ice-ocean system, *J. Geophys. Res.* 112, C03005, doi: 10.1029/2006JC003558.

Perovich, D.K., T.C. Grenfell, B. Light and P.V. Hobbs (2002), Seasonal evolution of the albedo of multiyear Arctic sea ice, *J. Geophys. Res.* 107 (C10), doi: 10.1029/2000JC000438.

Perovich, D.K., B. C. Elder (2001) Temporal evolution of Arctic sea-ice temperature, *Annals of Glaciology*, 33, 207-211.

Rampal, P., J. Weiss and D. Marsan (2009), Positive trend in the mean speed and deformation rate of arctic sea ice, 1979-2007, *J. Geophys. Research*, 114, C05013, doi: 10.1029/2008JC005066.

Rothrock, D.A., Y. Yu and G.A. Maykut (1999), Thinning of the Arctic Sea-Ice cover, *Geophysical Research Letters*, 26(23), 3469-3472.

Rothrock, D.A., D.B. Percival and M. Wesnahan (2008), The decline in arctic sea-ice thickness: Separating the spatial, annual, and interannual variability in a quarter century of submarine data, *Journal of Geophysical Research*, 113, C05003, doi:10.1029/2007JC004252.

Rothrock, D.A., A.S. Thorndike (1984), Measuring the Sea Ice Floe Size Distribution, *J. Geophys., Research*, 89 (C4), 6477-6486.

Rigor, I., J.M. Wallace and R. Colony (2002), Response of Sea Ice to the Arctic Oscillation, *J. of Climate*, 15, 2648-2663.

Schramm, J.L., G.M. Flato and J.A. Curry (2000), Toward the modeling of enhanced basal melting in ridge keels, *J. Geophys. Research*, 105 (C6), 14,081-14,092.

Simmonds, I. and I. Rudeva (2012), The great Arctic cyclone of August 2012, *Geophys. Res. Lett.*, 39, L23709, doi:10.1029/2012GL054259.

Steele, M. (1992), Sea Ice Melting and Floe Geometry in a Simple Ice-Ocean Model, *J. Geophys. Res.*, 97 (C11), 17,729-17,738.

Steele, M., J. Zhang, D. Rothrock and H. Stern (1997), The force balance of sea ice in a numerical model of the Arctic Ocean, *J. Geophys. Research*, 102(C9), 21,061-21,079.

Stroeve, J.C., T. Markus, L. Boisvert, J. Miller and A. Barrett (2014), Changes in Arctic melt season and implications for sea ice loss, *Geophys. Res. Lett.*, 41, doi: 10.1002/2013GL058951.

Stroeve, J.C., J. Maslanik, M.C. Serreze, I. Rigor, W. Meier and C. Fowler (2011), Sea ice response to an extreme negative phase of the Arctic Oscillation during winter 2009/2010, *Geophys. Res. Letters*, 38, L02502, doi: 10.1029/2010GL045662.

Spreen, G., R. Kwok and D. Menemenlis (2011), Trends in Arctic sea ice drift and role of wind forcing: 1992-2009, *Geophys. Res. Letters*, 38, L19501, doi: 10.1029/2011GL048970.

Thorndike, A.S. and R. Colony (1982), Sea Ice Motion in Response to Geostrophic Winds, *J. Geophys. Research*, 87(C8), 5845-5852.

Thomas, D. (1999), The quality of sea ice velocity estimates, *J. Geophys. Res.* 104 (C6), 13,627-13,652.

Toyota, T., S. Takatsuji and M. Nakayayma (2006), *Geophs. Res. Lett*., 33, L02616, doi: 10.1029/2005GL024556.

Vihma, T., P. Tisler and P. Uotila (2012), Atmospheric forcing on the drift of Arctic sea ice in 1989-2009, *Geophysical Research Letters*, 39, L02501, doi:10.1029/2011GL050118.

Wadhams, P. (1992), Sea ice thickness distribution in the Greenland Sea and Eurasian Basin, *J. Geophys. Research*, 97, 5331-5348.

Zhang, J., R. Lindsay, A. Schweiger and I. Rigor (2012), Recent changes in the dynamic properties of declining Arctic sea ice: A model study, *Geophys. Res. Lett.*39, L20503, doi:10.1029/GL053545.

Zhang, J.,R. Lindsay, A. Schweiger and M. Steele (2013), The impact of an intense summer cyclone on 2012 Arctic sea ice retreat, *Geophys. Res. Lett.*, 40 (4), doi: 10.1002/grl.50190.

Zubov, N.N (1945), Arctic Ice, English Translation: U.S. Naval Oceanographic Office (1963), 506 pp.

CHAPTER FIVE: CONCLUSIONS AND RECOMMENDATIONS

5.1 Summary

The overall purpose of this study was to improve our understanding of sea ice motion in the Beaufort Sea and its response to external forces with a focus on how climate change is affecting the dynamic characteristics of the ice pack. Due to anthropogenic forcing the Beaufort ice pack has become younger, thinner, less extensive, mechanically weaker and therefore more mobile over the last few decades. Understanding the response of the Beaufort ice pack to these large scale changes is of interest to both scientific and industrial groups. In Chapter 1 we outlined the two objectives of this thesis as follows:

1) To analyze the export of multiyear sea ice through the Bering Strait during winter 2011-2012 and assess the forcing that caused this event. Subsequently, set the 34 year historical context of ice transport through the Bering Strait and the atmospheric forcing that drove this event.

2) To quantitatively analyze the seasonal evolution of ice drift and its response to external forcing mechanisms in the Beaufort Sea during the spring transition. Specifically highlighting how the dynamic nature changes as the ice pack transforms from a compact ice pack in late winter to a mechanically weak ice pack in early summer.

The first objective arose opportunistically as we captured the anomalous export of multiyear sea ice through the Bering Strait during winter 2011-2012 with three ice beacons that were deployed during the previous summer in the Beaufort Sea. Ice export through the Bering Strait was traditionally thought of as being episodic in nature and occurring over short periods of days. Overall small quantities of sea ice were thought to enter the Arctic through the Bering

Strait, and were negligible in terms of the Arctic ice mass balance. Using the 34 year long IABP ice beacon archive we found that between 1979 and 2012 no ice beacon had been exported through the Bering Strait, in fact no ice beacon deployed in the Arctic had come within roughly 100km of the Strait. Using spaceborne derived fields of ice motion and concentration we calculated a total sea ice export of 13.5 x 10^3 km^2 through the Bering Strait between November 2011 and May 2012. This was more than four times the previous maximum export that we calculated for the period from 1979 to 2011.Of note ice drifted southward through the Strait during six of the seven months and southward ice drift speeds were statistically significantly faster than the 34 year climatology during four of these months. During 2011-2012 159 x 10^3 km^2 of sea ice entered the southern Chukchi Sea, the largest export of ice out of the Arctic Ocean into the Chukchi Sea in the 34 year record, which helped to supply and promote the export event. During the export event, MSLP for the Bering Strait region was characterized by the Siberian High and Aleutian Low which collectively created a pressure gradient that forced northerly winds and thus southward ice drift through the Bering Strait for all months between September 2011 and May 2012. Wind speeds were greater than the critical speed of 5.6m s^{-1} which precludes the formation of ice arches during all months but January. This in combination with a well-documented reduction in the mechanical strength of the arctic ice pack and increased mobility allowed sea ice to drift relatively unimpeded through the Bering Strait. Similar increases in ice flux as a result of climate induced weakening of the arctic ice pack have been documented for Nares Strait [*Kwok,* 2010] and through interisland straits of the Canadian Arctic Archipelago [*Howell et al.,* 2013].

The second objective was to quantitatively analyze ice drift and external forcing mechanisms through the spring transition of the Beaufort ice pack using spatially and temporally

coincident *in situ* observations of ice drift, surface winds and ice mass balance. The study was spurred by growing industrial interest in the Beaufort Sea, and completed as part of the Canadian Governments Beaufort Regional Environmental Assessment. Through spring 2012 the Beaufort ice pack declined seasonally, becoming thinner, weaker and less concentrated with a tendency towards smaller floe sizes. Collectively these changes reduced the mechanical strength of the Beaufort ice pack, thereby reducing internal stresses and permitting ice floes to enter a state of free drift. As a result ice speeds increased nearly 300%, F increased by 3.65%, turning angles increased by 32°, meander coefficients increased 2.5 times and ice drift within the BREA array became less cohesive across increasingly small length scales. All this occurred despite the fact that monthly mean wind speeds were statistically ($p < 0.05$) equal during April and July. Indicating that the ice pack became increasingly responsive to atmospheric forcing in a manner consistent with the mechanisms that have fostered a pan arctic increase in ice drift speeds over the past three decades [*Rampal et al.,* 2009; *Spreen et al.,* 2011; *Zhang et al.,* 2012; *Kwok et al.,* 2013]. These observations from spring 2012 are unique and highlight a tendency towards increasing dynamic activity within the Beaufort ice pack as it approached the record 2012 September sea ice minimum during which Arctic sea ice extent dropped to 3.41 million km^2 and the Beaufort Sea became ice free south of 75°N. It has been shown that the 2012 minimum was driven by preconditioning towards a younger ice pack that was more susceptible to the thermodynamic effects of increased ocean heat content, and the dynamic effects of the great Arctic cyclone of 2012. Our results corroborate other works and highlight the feedback between dynamics and thermodynamics within a seasonally declining ice pack. The role of the ice albedo feedback loop has been well defined [*e.g. Perovich et al.,* 2008], though our results here suggest

that there is a dynamic impact of the feedback loop that increases the responsiveness of the ice pack to external forcing and thus causes an increase in ice drift speeds.

The results presented within this thesis highlight how multi-decadal and seasonal changes to the arctic ice pack affect sea ice dynamics and the ice packs response to external forcing mechanisms. They provide insight into new pathways of sea ice export, with both social and industrial implications for the area surrounding the Bering Strait and Bering Sea. They also provide insight into the seasonal evolution of the Beaufort ice pack and how external and internal forcing influences the dynamic nature of the ice pack. This thesis provides analysis that is pertinent to both the scientific community as well as the industrial community which has the objective of developing offshore resources.

5.2 Future Recommendations

As the arctic ice pack continues to evolve towards younger ice types and becomes mechanically weaker, the dynamic nature of the ice pack will continue to change. Increasing ice drift speeds [*Rampal et al.,* 2009; *Spreen et al.,* 2011; *Kwok et al.,* 2013] and increasing ice transport [*Kwok et al.,* 2010; *Babb et al.,* 2013; *Howell et al.,* 2013] in response to the mechanical weakening of the ice pack have been well documented. However further analysis of ice motion on a smaller scale is required, particularly in the Beaufort Sea where economic activity is bound to occur soon even though ice hazards continue to pose a significant threat [*Barber et al.,* 2014]. Based on this, some recommendations for future research include:

- Quantitative analysis similar to that presented in Chapter 4, on the seasonal evolution of ice drift and external forcing during the fall transition. Specifically examining how ice drift and the ice packs response to external forcing change as the ice pack transitions from summer conditions to winter conditions. This transition is highlighted by the

seasonal aggregation of ice floes from discrete floes to large aggregate floes that are subject to internal stresses and there respond differently to external forces.

- Improved techniques for quantifying floe size distributions, specifically the evolution of floe sizes over time and how this relates back to sea ice dynamics and drift characteristics. An automated system for extracting floe size characteristics from satellite imagery around a region of interest would be ideal and allow for analysis of floe sizes over a long temporal scale.
- Further analysis of surface roughness coefficients at both the air-ice and ice-ocean interfaces. Specifically looking at the seasonal evolution of these coefficients and how they contribute to the seasonal change in ice drift characteristics.

These recommendations would significantly increase our understanding and ability to model ice drift and the role of external forcing on both the decadal and annual time scales. This work would further our scientific understanding of sea ice drift while also mitigating the risk of offshore activity through enhanced forecasting of ice drift and improved decision making capabilities regarding potential ice hazards.

Literature Cited:

Barber, D.G., G.M. McCullough, D.G. Babb, A.S. Komarov, L.M. Candlish, J.V. Lukovich, M. Asplin, S. Prinsenberg, I . Dmitrenko and S. Rysgaard (2014), Climate change and ice hazards in the Beaufort Sea, *Elementa*, 2:000025, doi:10.12952/journal.elementa.000025.

Babb, D.G. R.J. Galley, M.G. Asplin, J.V. Lukovich and D.G. Barber (2013), Multiyear sea ice export through the Bering Strait during winter 2011-2012, *Journal of Geophysical Research – Oceans*, 118, 5489-5503, doi:10.1002/jgrc.20383.

Howell, S.E.L, T. Wohlleben, M. Dabboor, C. Derksen, A. Komarov and L. Pizzolato (2013), Recent changes in the exchange of sea ice between the Arctic Ocean and the Canadian Arctic Archipelago, *J. Geophys. Research*, 118, 1-13, doi:10.1002/jgrc.20265.

Kwok, R. L. Toudal Pedersen, P. Gudmandsen and S.S. Pang (2010), Large sea ice outflow into the Nares Strait in 2007, *Geophys. Res. Lett*,37, L03502, doi:10.1029/2009GL041872.

Kwok, R., G. Spreen and S. Pang (2013), Arctic sea ice circulation and drift speed: Decadal trends and ocean currents, *J. Geophys. Res. Oceans*, 118, 2408-2452, doi: 10.1002/jgrc.20191.

Perovich, D.K., Richter-Menge, J.A., Jones, K.F., and Light, B. (2008), Sunlight, water and ice: Extreme Arctic sea ice melt during the summer of 2007, *Geophys. Res. Letters*, 35, L11501, doi: 10.1029/2008GL034007.

Rampal, P., J. Weiss and D. Marsan (2009), Positive trend in the mean speed and deformation rate of arctic sea ice, 1979-2007, *J. Geophys. Research*, 114, C05013, doi: 10.1029/2008JC005066.

Spreen, G., R. Kwok and D. Menemenlis (2011), Trends in Arctic sea ice drift and role of wind forcing: 1992-2009, *Geophys. Res. Letters*, 38, L19501, doi: 10.1029/2011GL048970.

Zhang, J., R. Lindsay, A. Schweiger and I. Rigor (2012), Recent changes in the dynamic properties of declining Arctic sea ice: A model study, *Geophys. Res. Lett.*39, L20503, doi:10.1029/GL053545.

Zhang, J.,R. Lindsay, A. Schweiger and M. Steele (2013), The impact of an intense summer cyclone on 2012 Arctic sea ice retreat, *Geophys. Res. Lett.*, 40 (4), doi: 10.1002/grl.50190.

APPENDIX A: ABBREVIATIONS

Arctic Oscillation ..... AO

Beaufort Gyre ..... BG

Beaufort Regional Environmental Assessment ..... BREA

Canadian Arctic Archipelago ..... CAA

First-year sea ice ..... FYI

Helicopter-mounted Electromagnetic Induction System ..... HEMI

International Arctic Buoy Program ..... IABP

Mean Sea Level Pressure ..... MSLP

Multiyear sea ice ..... MYI

National Center for Environmental Prediction ..... NCEP

National Oceanic and Atmospheric Administration ..... NOAA

National Snow and Ice Data Center ..... NSIDC

Ocean-Sea ice-Atmosphere ..... OSA

Queen Elizabeth Islands ..... QEI

Sea level pressure ..... SLP

Transpolar Drift Stream ..... TDS